Fatigue and fracture assessment of butt welds

Georgios Moraitis

Master Thesis

presented in partial fulfillment
of the requirements for the double degree:
“Advanced Master in Naval Architecture” conferred by University of Liege
"Master of Sciences in Applied Mechanics, specialization in Hydrodynamics, Energetics and Propulsion” conferred by Ecole Centrale de Nantes

developed at West Pomeranian University of Technology, Szczecin
in the framework of the

“EMSHIP”
Erasmus Mundus Master Course
in “Integrated Advanced Ship Design”

Ref. 159652-1-2009-1-BE-ERA MUNDUS-EMMC

Supervisors: Prof. Maciej Taczala,
West Pomeranian University of Technology, Szczecin

Dr. Hubertus von Selle, Germanischer Lloyd SE

Reviewer: Prof. Patrick Kaeding, University of Rostock

Szczecin, February 2014

ABSTRACT

Fatigue and fracture assessment of butt welds

By **Georgios Moraitis**

The specific project is inspired by the general trend of investigating the effects of various parameters in the sensitive area of structural fatigue, which nowadays has become one of the most important design aspects in the ship and ocean structures building industry. The size of vessels, especially the container ships, has increased significantly during the past years, a development which leads to intensive use of high tensile steels in combination with plates of big thickness. This work has tried to deal with the above matters, i.e. the performance of high tensile steel and the plate thickness effect on fatigue strength of butt welded joints.

In the first part, an evaluation of fatigue test results takes place. The fatigue tests were carried out by Germanischer Lloyd in co-operation with shipyards for butt welded specimens of various thicknesses made of specific high tensile steel, called YP47. The purpose is to investigate the plate thickness effect and the overall performance of YP47. Following the recommendations of International Institute of Welding (IIW), the S – N curves for each series of data were designed and useful statistical information were extracted regarding the scatter of the results and the FAT class of each series. Influence of misalignments was investigated and additionally the results were compared with previous experiments. Generally, a good performance of YP47 was observed, while, in contrast to the relevant rules and guidelines, there was no clear thickness effect, mainly because of the large scatter of the results.

The second part is an assessment based on fracture mechanics concept. Specifically, the parameters C and m of the Paris crack growth equation were investigated. The numerical analysis was performed by the software VERB (failure assessment software), based on experimental results of fatigue tests from a joint development project between GL and Korean shipyards. The specimens used were butt welded 80 mm plates made of higher tensile steel and they were tested under a special two – level load history which resulted in creation of beachmarks on the fatigue crack surfaces. These beachmarks gave valuable information regarding the crack initiation location and the crack propagation phase that was used for the numerical assessment. The obtained results were compared with the recommended values from literature (IIW).

Finally in the third part, the thickness effect of butt welds is investigated in terms of the notch stress approach and fracture mechanics. Specimens of various thicknesses and different weld geometries from the first part are modeled and the notch stress distribution through the thickness is calculated using the software ANSYS. The influence of meshing, the thickness of the plate, the geometry of weld as well as the concept of fictitious notch rounding and undercut on the notch are examined. Moreover, crack propagation calculations are performed using the software FRANC2D (a 2dimensional crack propagation simulation) by initiating cracks of various lengths to the weld toe. Similar calculations are done by VERB, using the notch stress distribution obtained from ANSYS and the results are compared. Finally, the thickness effect in the total life time predicted by notch stress approach and fracture mechanics is investigated and compared with the values given in the references.

DECLARATION OF AUTHORSHIP

I declare that this thesis and the work presented in it are my own and has been generated by me as the result of my own original research.

Where I have consulted the published work of others, this is always clearly attributed.

Where I have quoted from the work of others, the source is always given. With the exception of such quotations, this thesis is entirely my own work.

I have acknowledged all main sources of help.

Where the thesis is based on work done by myself jointly with others, I have made clear exactly what was done by others and what I have contributed myself.

This thesis contains no material that has been submitted previously, in whole or in part, for the award of any other academic degree or diploma.

I cede copyright of the thesis in favour of the West Pomeranian University of Technology, Szczecin.

Date: Signature

ACKNOWLEDGEMENTS

This thesis was developed in the frame of the European Master Course in “Integrated Advanced Ship Design” named “EMSHIP” for “European Education in Advanced Ship Design”, Ref.: 159652-1-2009-1-BE-ERA MUNDUS-EMMC.

The main part of the work presented here was performed during my internship at the Research and Rule Development Department of Germanischer Lloyd SE in Hamburg, Germany. My special thanks go to Dr. Hubertus von Selle, my supervisor, who provided me with valuable help and support. I would also like to thank all other employees in Germanischer Lloyd, who were always by my side answering every question I had and giving me helpful guidance.

I would also like to thank Prof. Maciej Taczala, my supervisor from West Pomeranian University of Technology, Szczecin.

Finally, I would like to express my gratefulness to my family for their encouragement and unconditional support throughout my whole life and education.

CONTENTS

1 INTRODUCTION

1.1 Background and Motivation of the Research

Conventionally, the strength calculations for the safety of a structure take into account a specific static maximum load, also known as the design load.

Ships and ocean structures, however, due to the characteristics and nature of their loading environment, are largely exposed to stresses which are not static, but vary over time. The causes of this alternating stress pattern are the forces generated principally by the sea waves, but also by the propulsion system of the vessel and by the changes in the cargo loading of the ship, from fully loaded to ballast loaded. Each of the above causes creates forces of various frequencies which are repeated for thousands of cycles through the lifetime of the structure. These fluctuating stresses, though usually much lower than the stress required to cause failure in a single application, create in each circle a small but irreversible damage within the material and, conceptually, after many cycles the accumulated damage reduces the ability of the structural member to withstand loading.

The above described failure behavior is known as Fatigue and is one of the basic types of failure modes, along with others which are caused by static loading such as tensile or compressive yield of the material (plasticity), compressive instability (buckling) and brittle fracture which occur under a single extreme load.

It has been estimated that fatigue contributes to approximately 90% of all mechanical service failures and it is a problem that can affect any part or component that moves. It was initially recognized as a problem in the early 1800s when investigators in Europe observed that bridge and railroad components were cracking when subjected to repeated loadings (ASM International, 2008). As the century progressed and the use of metals expanded with the increasing use of machines, more and more failures of components subjected to repeated loads were recorded.

So, although at first it was assumed that fatigue resistance is implicitly included in the conventional safety factors or acceptable stress margins based on past experience, today and due to the combination of high strength materials, thick plates and high cyclic loads, structural fatigue becomes one of the most important parameters, especially for the design of details such as hatch corners and welded joints.

1.2 Objectives

It is a fact that nowadays the size especially of container ships has increased significantly, approaching capacities close to 20,000 TEU. This trend inevitably leads to extensive use of high tensile strength steels in combination with plates of great thicknesses, which in some cases, such as the upper hull girder area, can be up to 100mm. Fatigue has become one of the most important design aspects due to this combination of high tensile strength steels and big plate thicknesses, together with high cyclic loads induced by the sea waves and the presence of welded joints.

Hence, the main objective of the present study is to investigate the fatigue behavior of butt welds made of high tensile steel. The fatigue performance of the YP47 steel, a new material class with minimum yield strength of 460 N/mm^2 is examined. Moreover, further investigation of the well known phenomenon of the decrease of the fatigue strength with an increasing plate thickness, the so – called plate thickness effect, takes place. The investigation is being carried out by evaluating test results of butt welds, as well as by applying the notch stress approach with FEM program.

Additionally, deeper investigation takes place by applying fracture mechanic approach. The objective is at one hand to explore a potential development of the recommended values given by International Institute of Welding regarding the parameters C and m of the Paris equation by performing crack growth simulations based on experimental results.

On the other hand, fracture mechanics methods are applied by using 2-Dimensional crack propagation simulator. The objective is to determine with accuracy fatigue properties of the butt welds regarding the crack propagation, such as initial and final length of the crack, the stress intensity factors during the propagation and the total propagation life time of the specimen. The main final goal is to explore the thickness effect and how this is affected by various parameters such as the geometry of the weld.

The importance of deep investigation and understanding of the mechanisms of fatigue failure and crack initiation and propagation is indisputable. Such is the context in which the present study will try to examine the impact of various parameters in this failure mode.

1.3 Outline of the Thesis

The present work consists of seven chapters in total.

In the Chapter One, a brief introduction to the general topic is given and the objectives of the study are presented.

In Chapter Two, the basic principles and the theoretical background involved in the study is presented. The concepts of fatigue, stress concentration, S-N curves and fracture mechanics are briefly explained and principles of the butt welds are described.

Chapter Three deals with the evaluation of butt weld tests carried out by Germanischer Lloyd. The technical background is initially given, followed by the description of the butt weld tests. The test results are presented and finally the conclusions of the specific investigation are summed up.

In Chapter Four an investigation of parameters C and m of Paris crack growth equation takes place, based on fracture mechanics concept. A numerical analysis is performed, using data from butt weld fatigue tests. The obtained results are compared with the recommended values from literature.

Deeper investigation takes place in Chapter Five. In the first part the notch stress is applied. Specifically, specimens of various thicknesses and different weld geometries from the tests described in Chapter Three are modeled and the notch stress distribution through the thickness is calculated using the software ANSYS. In the second part of the chapter, the fracture mechanics concept is used and crack propagation calculations are performed in order for the propagation life time of the specimens to be estimated.

The overall conclusions of the present study, together with suggestions for further investigation are presented in Chapter Six and finally the references are given in Chapter Seven.

2 BASIC PRINCIPLES

2.1 Fatigue

As mentioned before, fatigue failures occur as a result of a cumulative effect in a structural member that is subjected to cyclic fluctuating loading, a stress pattern alternating from tension to compression through many cycles.

Two categories of fatigue damage are recognized (Rigo Ph.,Rizzuto En.) and they are known as high-cycle and low-cycle fatigue. The first category involves a large number of cycles ($N>10^5$) of relatively low stress (elastic), such as this induced by the sea waves. In this occasion, small cracks initiate the failure and they grow slowly and may often be detected and repaired. In low-cycle fatigue the level of stresses is higher (up to and beyond yield) which may create cracks after only several thousand cycles.

Fatigue crack nucleation and growth occurs in the following stages (ASM International,2008):

Stage I. The initiation of a crack usually occurs at a notch or other surface discontinuity, where stress concentration is observed. Crack will eventually initiate even if there is no surface defect, due to the formation of persistent slip bands (PSBs), so called because traces of the bands persist even when the surface damage is polished away. Slip bands are a consequence of the regular increase of fine slip movements on the order of only 1 nm. Nevertheless, the plastic strain within the PSB can be as much as 100 times greater than that in the surrounding material. The formation of intrusions and extrusions at the surface, which eventually leads to a crack, is the result of the back-and-forth movement of the PSBs (Figure 2.1). The initial crack propagates in a direction parallel to the PSBs and at approximately 45^o to the principal stress direction. The propagation of the crack during the first stage has a rate on the order of 1 nm per cycle, and produces a practically featureless fracture surface. After some time, the crack has a length which is adequate for the stress field at the tip to become dominant and as a result the direction of the crack propagation becomes perpendicular to the principal stress, and the crack enters stage II.

At Stage II the crack growth proceeds by a continual process of crack sharpening followed by blunting, as shown in the Figure 2.2 illustration. Crack propagation usually creates fatigue striations (Figure 2.3), with each of them representing one cycle of fatigue. Although striations are indicative of fatigue, fatigue failures can occur without the formation of them.

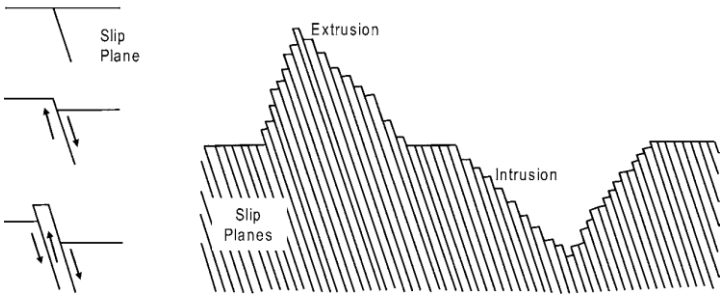

Figure 2.1.Development of extrusions and intrusions during fatigue (ASM International, 2008)

Striations are microstructural details, not visible to the naked eye, which can be examined with a scanning electron microscope (SEM). Frequently, visible examination of a fatigued surface will reveal a series of concentric markings on the surface, referred to as beach marks. These are present as a result of stress changes during fatigue and each of them can contain thousands or even tens of thousands of fatigue cycles.

Stage III. Ultimate failure occurs when the fatigue crack becomes long enough that the remaining cross section can no longer support the applied load (ASM International, 2008).

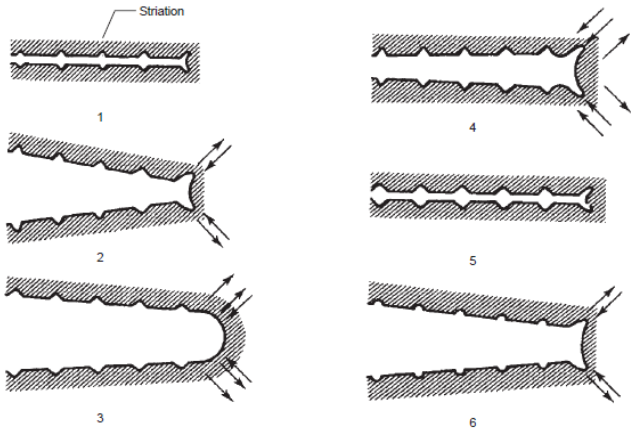

Figure 2.2. Fatigue crack propagation, (ASM International, 2008)

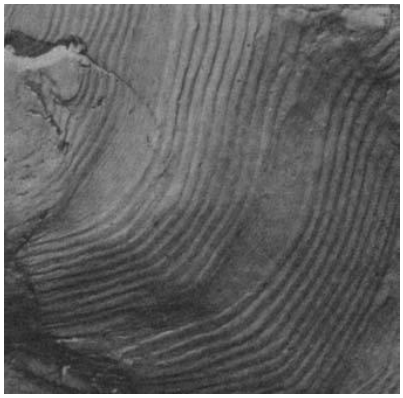

Figure 2.3. SEM image showing fatigue striations, (ASM International, 2008)

2.2 Stress Concentration and Determination of Stresses

There are various possible causes for stress increases and when calculating the stress, it is necessary to determine exactly which of them are present in order to be analyzed in depth.

In most structures, fatigue cracking usually initiates at a stress concentration. The stress concentration may by inherent in the design, such as a fillet, hole, thread, or other geometrical feature (Figures 2.4 and 2.5), or the stress concentration can result from a manufacturing process, such as a rough surface finish or residual stresses introduced by heat treatment.

In this sense, there are critical areas in a ship which can possibly face problems of fatigue. Hot Spots are the locations where fatigue cracking may occur. In order to correctly determine the stresses to be used in fatigue analyses, it is particularly important to clearly define the different stress categories to be calculated and assessed (ASM International, 2008).

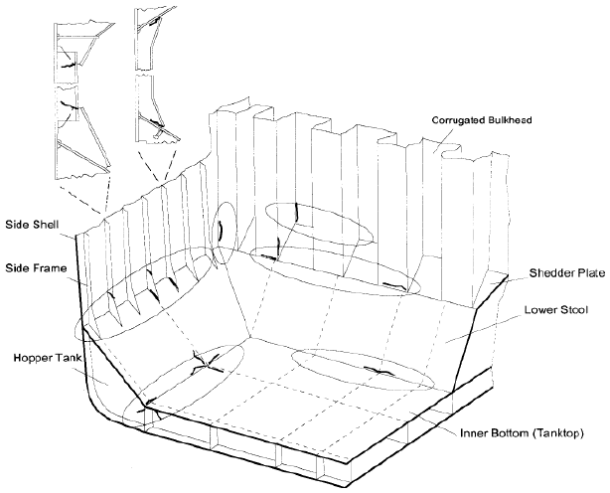

Figure 2.4. Fatigue crack locations and orientations in typical bulk carrier structure (Amrane, A. 2012)

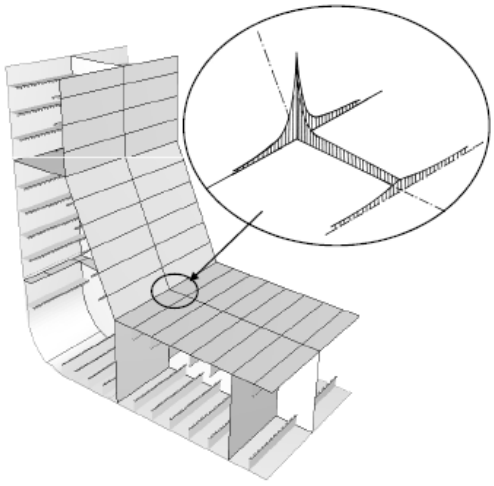

Figure 2.5. Stress concentration due to geometry of the detail (Amrane, A. 2012)

The stress types and categories (Figure 2.6) generally applied are the following (Radaj, 1990 and Niemi, 1995):

- Nominal Stress is this typically calculated by beam theory or coarse mesh FE models. It is the stress in a structural component taking into account macro-geometric effects and is usually taken to denote the stress that can be determined elementarily from the sectional forces and moments and the sectional properties of a structure or a component. It disregards structural discontinuities and weld effects.
- Structural Stress (Hot – Spot Stress) is that stress which, apart from the nominal one, also includes increases of stress caused by the structural discontinuities due to the geometry of the detail. It excludes the effects of the weld, because it can be very time consuming. This subdivision of stress increases is particularly meaningful for welded joints at which local stress peaks occur at weld toes. The structural stress acting there is also known as geometric stress.

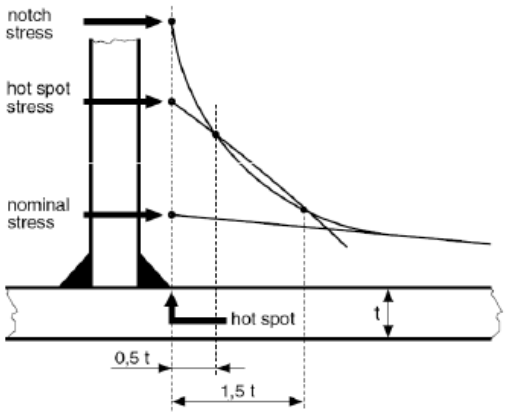

Figure 2.6. Stress types (Amrane, A.2012)

- Notch Stress is the locally increased stress in a notch such as the root of a weld or the edge of a cut – out. The stress components of the notch stress (σ_k) are the membrane stress σ_m, the shell bending stress σ_b and a non – linear stress peak σ_{nl} (Figure 2.7).

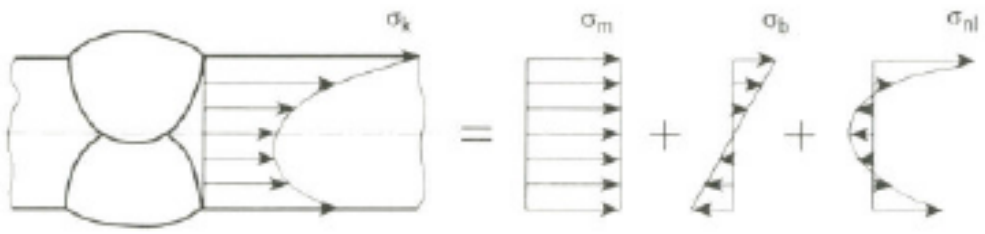

Figure 2.7. Notch stress at weld toe (Fricke, W., Petershagen, H., Paetzold, H., 1997)

2.3 Fatigue Loading and S – N Curves

The time – dependant loading in a component is characterized by the (Fricke, W., Petershagen, H., Paetzold, H., 1997):

- upper stress σ_{max} and lower stress σ_{min}
- stress amplitude σ_a, or stress range $\Delta\sigma$ and the mean stress σ_m

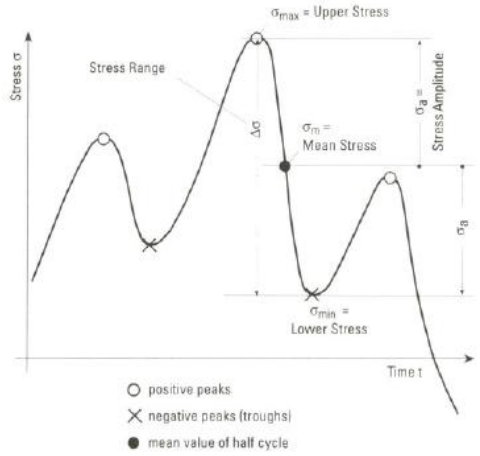

Figure 2.8. Stress History (Fricke, W., Petershagen, H., Paetzold, H., 1997)

To describe the position of the stress cycle, the stress ratio R is often used:

$$R = \frac{\sigma_{min}}{\sigma_{max}} \tag{2.1}$$

For a constant amplitude loading, the relationship between stress amplitude σ_a or stress range $\Delta\sigma$ and fatigue life N (number of cycles) is reflected in the S - N (Wöhler) curve. The axes are usually plotted with a log - log scale. For the lifetime up to crack initiation, corresponding S - N curves can be drawn up accordingly.

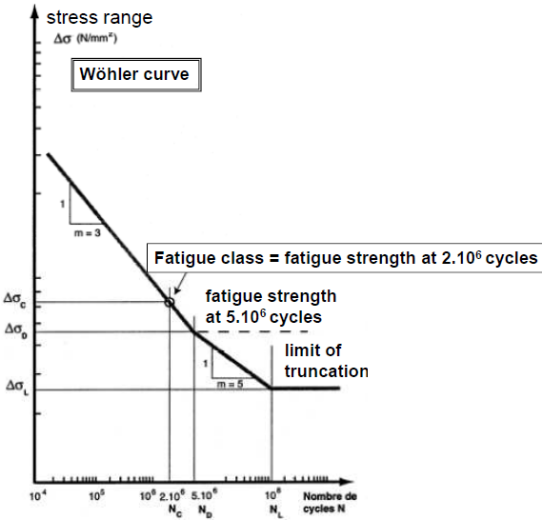

Figure 2.9. S-N curve for welded joints (Amrane, A.2012)

The fatigue life N can thus be calculated by the following formula:

$$logN = logC - mlog\Delta\sigma_R \text{ or } N = C\Delta\sigma_R^{-m} \quad (2.2)$$

With:

$\Delta\sigma_R$: fatigue strength at N cycles

m: curve slope (3 or 5)

N: number of cycles to failure of stress range $\Delta\sigma$

C: constant in equation of S – N curve with exponent m

As it can be seen by the S - N curve, fatigue failure no longer occurs below certain stress amplitude (endurance limit).

The parameters for the fatigue behavior under constant amplitude loading are (Fricke, W., Petershagen, H., Paetzold, H., 1997):

- stress amplitude σ_a or stress range $\Delta\sigma$
- mean stress σ_m or stress ratio R
- local stress peaks (notch effects)
- type and condition of the material
- environmental influences (corrosion)

On the other hand, for variable amplitude loading, the same influencing parameters must be taken into account, plus the additional factors of the shape of the loading spectrum and the load sequence.

In that case of variable amplitude loading and in order to calculate the fatigue life, the Miner model of cumulative damage hypothesis can be applied, which makes the assumption of linear accumulation of damage:

$$D = \sum_i \frac{n_i}{N_i} < 1, \quad (2.3)$$

Where,

n_i: number of cycles of stress range $\Delta\sigma_i$

N_i: number of cycles to failure of stress range $\Delta\sigma_i$.

Figure 2.10 shows the designed S - N curves for welded joints, which correspond to 97.5% survival probability. They are characterized by a reference value $\Delta\sigma_R$ at $2 \cdot 10^6$ stress cycles, which is referred to as the detail category or fatigue class (FAT). The slope exponent, denoted by m, amounts to m_0=3 for high – cycle fatigue. Past the knee point at 10^7 load cycles, a slope exponent of m=5 must be used for variable stress ranges. The stress range must be constant

and the environment non-corrosive in order for an endurance limit with a horizontal course to be assumed.

The S-N curves or detail categories $\Delta\sigma_R$ are assigned to the notch conditions by means of a catalogue of details, of which Figure 2.11 shows an extract. (Fricke, W., Petershagen, H., Paetzold, H., 1997).

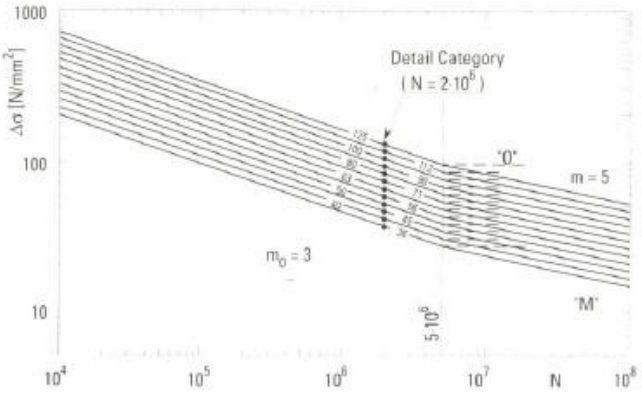

Figure 2.10. Recommendations for fatigue design of welded joints and components (Hobbacher A., 2008)

Butt welds, transverse loaded (A)				
Type No.	Joint configuration showing mode of fatigue cracking and stress σ considered	Description of joint	FAT class $\Delta\sigma_R$ Steel	Al
A1		Transverse butt weld ground flush to plate, 100 % NDT (Non-Destructive Testing)	112	45
A2		Transverse butt weld made in shop in flat position, max. weld reinforcement 1 mm + 0.1 x weld width, smooth transitions, NDT	90	36
A3		Transverse butt weld not satisfying conditions for joint type No. A2, NDT	80	32
A4		Transverse butt weld on backing strip or three-plate connection with unloaded branch	71	25
		Butt weld, welded on ceramic backing, root crack	80	28
A5		Transverse butt welds between plates of different widths or thickness, NDT		
		as for joint type No. A2: slope 1 : 5	90	32
		slope 1 : 3	80	28
		slope 1 : 2	71	25
		as for joint type No. A3: slope 1 : 5	80	25
		slope 1 : 3	71	22
		slope 1 : 2	63	20
		For the third sketched case the slope results from the ratio of the difference in plate thicknesses to the breadth of the welded seam. Additional bending stress due to thickness change to be considered, see also B.1.3.		
A6		Transverse butt welds welded from one side without backing bar, full penetration root:		
		• controlled by NDT	71	28
		• not controlled by NDT	36	12
		For tubular profiles $\Delta\sigma_R$ may be lifted to the next higher FAT class.		
		Laser (t ≤ 8 mm) and laser hybrid (t ≤ 12 mm) butt welds	80	28

Figure 2.11. Catalogue of details (extract, Germanischer Lloyd, 2013)

2.4 Fatigue Crack Propagation – Fracture Mechanics

Linear elastic fracture mechanics (LEFM) assumes that all structures contain flaws (ASM International, 2008). Cracks grow from an initial size, a_{in}, to a critical size, a_c, (or final crack size a_f) corresponding to failure as a function of the number of load cycles (Figure 2.12). At first, the crack growth rate da/dn (where a is the flaw or crack size; n is the number of cycles), which can be determined from the slope of the curve and it is relative to the applied stress, is slow but increases as the crack length gets larger. In the fracture mechanics approach, the crack growth rate, i.e. the amount of crack extension per loading cycle, is correlated with the stress-intensity factor (SIF), K and more precisely the stress – intensity factor range, ΔK, which describes the fatigue action at a crack tip in terms of crack propagation. It can be expressed in terms of Δσ:

$$\Delta K = \Delta K_{max} - \Delta K_{min} = Y \Delta\sigma \sqrt{\pi\alpha} \tag{2.4}$$

where Y is a correction function that depends on the specific specimen geometry.

An idealized da/dn versus ΔK curve is shown in Figure 2.13. In the first region, there is no actual crack propagation (crack growth rates approach zero), since the applied ΔK is less or near the ΔK_{th}, the lower end of the ΔK range. In region II, the crack growth rate is stable and essentially linear and can be modeled by power law equations, such as the Paris equation:

$$da/dn = C(\Delta K)^m \tag{2.5}$$

where: C and m are constant parameters and are related to material variables, environment, temperature, and fatigue stress conditions; and ΔK is the stress-intensity parameter range. The constants C and m are material parameters that must be determined experimentally. There are typical values for these parameters that can be found in literature (e.g. International Institute of Welding, Table 2.1).

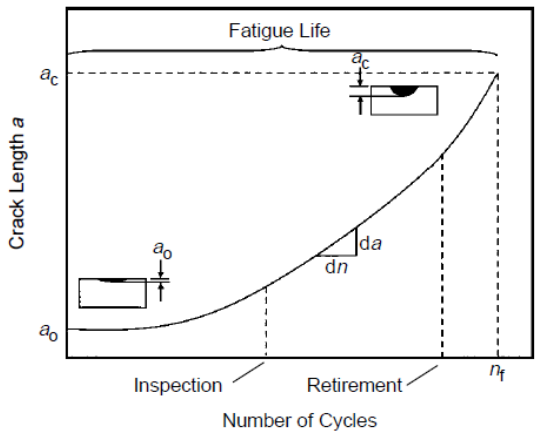

Figure 2.12. Crack length as a function of cycles (Meyers and Chawla, 1984)

Table 2.1. Parameters of the Paris power law and threshold data for steel (Hobbacher A., 2008)

Units	Paris power law parameters	Threshold values ΔK_{th}			
		R≥0.5	0≤R≤0.5	R<0	surface crack depth <1 mm
K [N·mm$^{-2/3}$] da/dN [mm/cycle]	C_0= 5.21·10^{-13} m = 3.0	63	170-214·R	170	≤63
K [MPa√m] da/dN [m/cycle]	C_0=1.65·10^{-11} m = 3.0	2.0	5.4-6.8·R	5.4	≤2.0

During stage II growth in the linear crack growth region (Figure2.13), the Paris law can be used to determine the number of cycles to failure by rearranging and integrating Equation 2.5:

$$n_f = \int_{a_{in}}^{a_f} \frac{da}{C(\Delta K)^m} \tag{2.6}$$

Apart from the Paris equation, there are more crack growth formulas such as Bilinear law (a two-stage power law of Paris type employed as an extension of Paris original equation), Forman's equation which includes the R_K (K ratio: K_{min}/K_{max}) dependency and is suitable to describe fatigue crack growth rates beyond the threshold region, and others, which will not be presented here since the specific investigation is taking into consideration only the simple Paris formula.

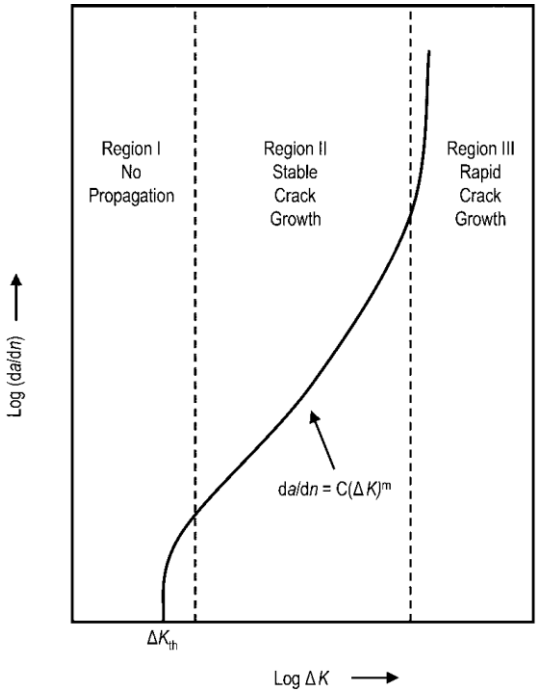

Figure 2.13. Crack propagation curve for fatigue loading (ASM International, 2008)

Finally, in region III, the crack growth rate accelerates, since the fracture toughness of the material is approached, and there is a local tensile overload failure (ASM International, 2008).

2.5 Butt Welds

The welding is an assembly process. The connection between the two parts is obtained by material fusion (Figure 2.14). The continuity of mechanical, thermal, chemical, electrical, waterproofing, durability characteristics is obtained.

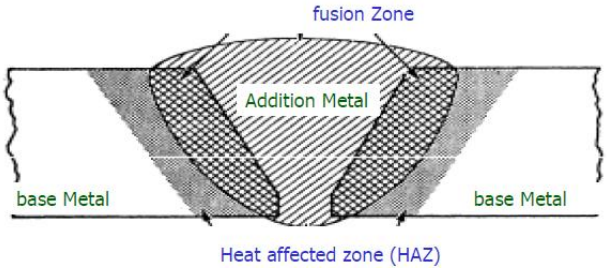

Figure 2.14. Welding principle

Figure 2.15 shows transverse butt welds. Two plates are joined via a transverse welding perpendicular to the load axis (Blondeau R., 2008).

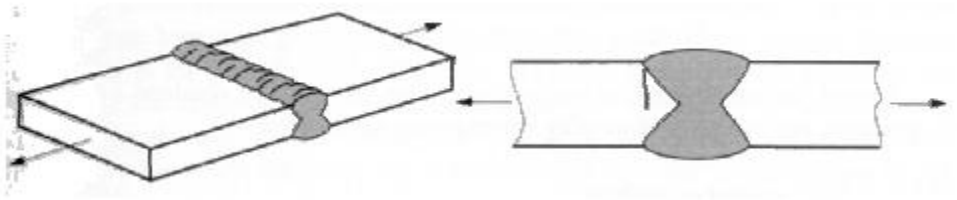

Figure 2.15. Fatigue cracking of a transverse butt weld (Blondeau R., 2008)

For this type of joint, the fatigue crack starts at the weld toe (Figure 2.16) and propagates through the thickness of the sheet, perpendicular to the load direction. The crack is thus not the result of a defect including welding or bad properties of the deposit metal, but the consequence of stress concentrations at the weld toe. In this type of butt welded joint, the influence of the shape of the weld bead is important for determining the endurance characteristics of the joint. This depends greatly on the welding conditions (Al-Mukhtar A., 2010).

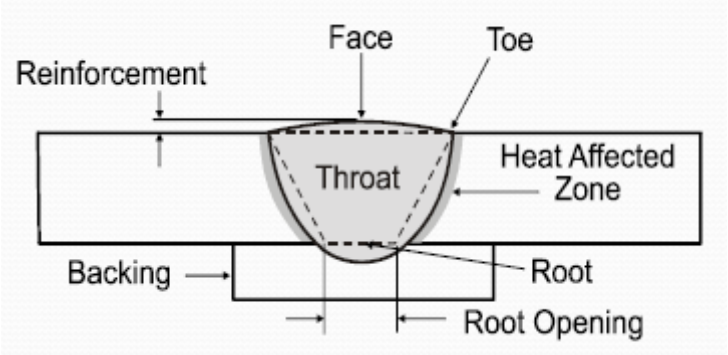

Figure 2.16. Butt weld terminology

3 EVALUATION OF FATIGUE TESTS OF BUTT WELDS

3.1 Introduction

As mentioned before, fatigue has become one of the most important design aspects due to combination of high tensile strength steels and big plate thicknesses, together with high cyclic loads induced by the sea waves and the presence of welded joints.

For these reasons, Germanischer Lloyd in co-operation with a well known steel mill and several shipyards, carried out extensive fatigue tests of butt welded specimens made of a new material class with nominal yield strength of 460 N/mm^2, called YP47 steel. This material represents exactly the trend towards high tensile strength steels in shipbuilding industry and an enhanced fatigue assessment is necessary for a safe application of it. The specimens are of various plate thicknesses in order to be able to extract useful information regarding the plate thickness effect. This project, named as Joined Development Programme II - JDP II - is the second to be done by these companies, following the initial (JDP I) which was performed recently (Doerk O., Fricke W., H. von Selle, Kahl A., 2012) and its main purpose is to support the investigation by providing an increased data base of results.

There are two main objectives of this project. The first one is to investgate the influence of the plate thickness on the fatigue capacity of welded butt joints made of YP47 steel while the second is to investigate the fatigue performance of this high tensile steel.

This first part of the present study deals with the evaluation of these tests. The undertaken task was to design the S – N curves for each series of the tests and to analyze the obtained results in order to extract conclusions regarding the influence of the material and the plate thickness in the fatigue performance. The results are restricted to confidentiality so it was decided to present them in charts without showing the units in the axis. Additionally, the names of the companies involved will also not be mentioned.

In the following subsections initially it will be presented the technical background of the tests (information regarding the thickness effect, the yield strength influence and the design of S-N curves). Then, there will be a description of the tests followed by the presentation of the results. The overall conclusions from this first part will be summed up in the last sub-section.

3.2 Technical Background

3.2.1 Thickness Effect

Thickness effect is the commonly known phenomenon in which the fatigue strength of a component or welded joint decreases with the increasing of plate thickness. The most important reasons for that is the relative notch sharpness. The absolute weld toe radius can be assumed to be the same for a thin and a thick plate weld, which means that the relative radius related to the plate thickness is smaller for thicker plates. As the relative radius is crucial for the notch effect and gradient of the notch stress distribution in plate thickness direction the fatigue strength decreases with an increasing plate thickness (Doerk O., Fricke W., H. von Selle, Kahl A., 2012).

In the relevant rules and guidelines (e.g. Germanischer Lloyd 2003) the thickness effect is governed by the correction factor f_t defined by the following formula (Eq.3.1):

$$f_t = \left(\frac{t_{ref}}{t_{eff}}\right)^n \tag{3.1}$$

Where:

t_{ref} reference plate thickness

t_{eff} effective plate thickness

n exponent of the thickness influence law

Usually, the reference plate thickness equals to t_{ref} = 25mm and is dependent on the structural detail to be investigated. The thickness influence exponent n depends on the particular welded detail and according to Hobbacher (2008) equal to n = 0.2 (Table 3.1) for transverse butt welds in as – welded condition, while GL suggests a less conservative value of 0.17. The background for this is, that according to GL the relative misalignment for thick plate structures is smaller than for thin plate structures. It is important the fact that for different rules and standards the above values of parameters t_{eff} and n might slightly differ.

Table 3.1 Thickness correction exponent (Hobbacher A., 2008)

Joint category	Condition	**n**
Cruciform joints, transverse T-joints, plates with transverse attachments, ends of longitudinal stiffeners	as-welded	0.3
Cruciform joints, transverse T-joints, plates with transverse attachments, Ends of longitudinal stiffeners	toe ground	0.2
Transverse butt welds	as-welded	0.2
Butt welds ground flush, base material, longi-tudinal welds or attachements to plate edges	any	0.1

3.2.2 Yield Strength Influence

Regarding the base material, one can observe a yield strength influence which means that the fatigue strength increases with increasing yield strength, while for the welded joints the fatigue strength is assumed to be independent of the material yield strength. Responsible for this behavior of welded joints is generally the notch sharpness rather than the metallurgy. Figure 3.1 illustrates the relation between the notch sharpness, the material's yield strength and the fatigue strength (Doerk O., Fricke W., H. von Selle, Kahl A., 2012):

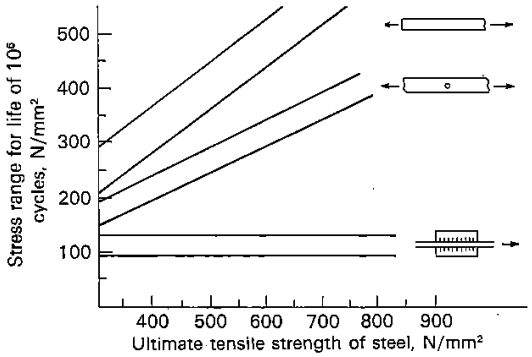

Figure 3.1. Yield strength influence of the fatigue strength for different notch sharpness

3.2.3 Design of S – N Curves and Evaluation Procedure

The results of fatigue tests were evaluated based on the statistical procedure recommended by International Institute of Welding (Hobbacher A., 2008), in order for the characteristic values of the S – N curves to be determined. The following nomenclature was used for the description and evaluation of the fatigue test results:

$\Delta\sigma_N$	nominal stress range
N	number of load cycles
m	slope of the SN curve
p_s	probability of survival
T_N 10:90	scatter between 10 and 90 % probability of survival in terms of N
FAT class	$\Delta\sigma$ at $N = 2 \cdot 10^6$ and $p_s = 97.7\%$

The most common approach for analyzing fatigue data is to fit S-N or crack propagation curves by regression analysis, taking log(N) as the dependent variable. Then, characteristic values are established by adopting curves lying k standard deviations of the dependent variable from the mean. In the case of S-N data, this would be below the mean.

Thus, more precisely, test results should be analyzed to produce characteristic values (subscript k). These are values that represent 95% survival probability (i.e. 5% failure probability) calculated from the mean on the basis of two-sided tolerance limits at the 75% level.

For the evaluation of test data originating from a test series, the characteristic values are calculated by the following procedure (Hobbacher A., 2008):

a) Calculate $\log_{10}$ of all data: Stress range $\Delta\sigma$ and number of cycles N

b) Calculate exponent m and constant logC of the formula:

$$logN = logC - m \cdot log\Delta\sigma \tag{3.2}$$

by linear regression taking stress range as the independent variable, i.e. logN=f(log $\Delta\sigma$).

If the number of pairs of test data n<10, or if the data are not sufficiently evenly distributed to determine m accurately, a fixed value of m should be taken, as derived from other tests under comparable conditions, e.g. m=3 for steel and aluminium welded joints.

Values x_i equal to logC are calculated from the (N, $\Delta\sigma$) test results using the above equations.

c) Calculate mean x_m and the standard deviation Stdv of logC using m obtained in b).

$$x_m = \frac{\sum x_i}{n}, \qquad Stdv = \sqrt{\frac{\sum (x_m - x_i)^2}{n-1}} \tag{3.3}$$

d) Calculate the characteristic values x_k by the formula

$$x_k = x_m - k \cdot Stdv \tag{3.4}$$

The values of k are given in Table 3.2.

Table 3.2 Values of k for the calculation of characteristic values (Hobbacher A., 2008)

n	10	15	20	25	30	40	50	100
k	2.7	2,4	2.3	2.2	2.15	2.05	2.0	1.9

In order to investigate the influence of different parameters on the resulting S - N curves the fatigue test results were evaluated in various ways e.g. with a fixed slope (m = 3.00 for all welded joints, according to the recommendations) and with the slope directly obtained by the tests. In the fatigue tests of relatively smooth notched welded details e.g. butt welds often increased slope exponents m can be observed. So it can be expected that there will be a significant influence whether a fixed slope m = 3.0 or the slope obtained directly by the tests will be employed for the butt weld fatigue test evaluation. As shown in Table 3.2, the number of 10 or more specimens is given as a guiding value for the application of the slope directly obtained by the tests. If less than 10 are tested it is recommended to use a fixed slope of m = 3.0 for welded joints (Doerk O., Fricke W., H. von Selle, Kahl A., 2012).

3.3 Description of the Test

The fatigue tests of transverse loaded butt weld joints were carried out by GL in co-operation with shipyards. For the fatigue test specimens the material used was the YP47 (R_{eHmin} = 460 N/mm^2) and the welding process was the flux-cored arc welding (FCAW) with the consumable being the same material with the base. Four different thicknesses of plates were used: 25, 50, 60 and 80mm and specimens edges got rounded in the weld area (approx. 100mm length) with a radius of R = 1mm (t = 25mm) and R = 3 mm (t = 50, 60 and 80mm) (see Figure 3.4) to avoid corner cracks. The tests were performed under axial load of constant amplitude with a stress ratio of R ≈ 0.1 (most realistic for coaming top area). Sketches of the specimens are shown in following figures:

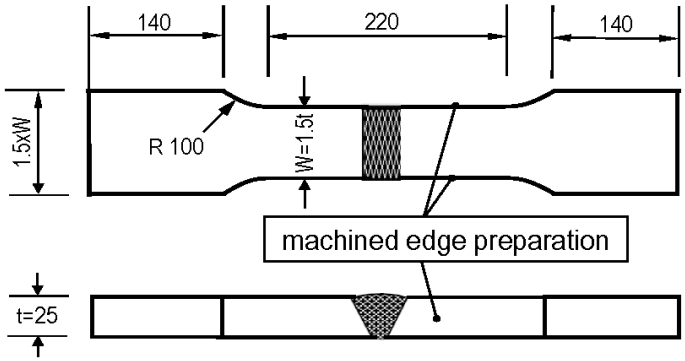

Figure 3.2. Butt weld specimens (t = 25mm)

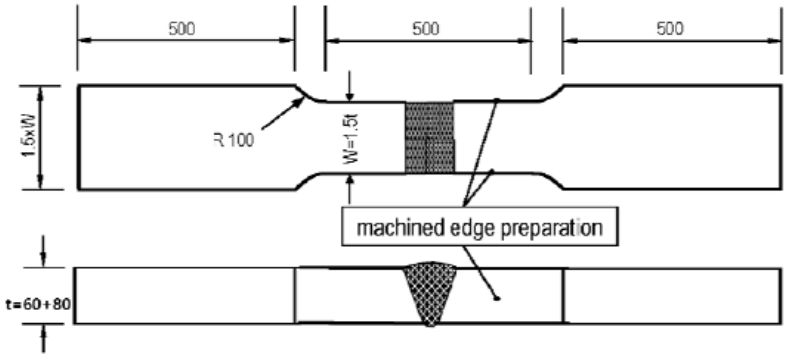

Figure 3.3. Butt weld specimens (thickness range 60 and 80mm)

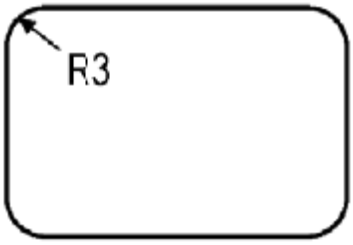

Figure 3.4. Crosse section of butt weld specimens in welded area

There are four different plate thicknesses, which represent lower and upper bounds as well as intermediate values in order to enable a meaningful derivation of the thickness influence exponent. Each shipyard (A, B, C, D, E and P) delivered specific number of specimens of each thickness, so to be able to cover common variations due to different fabrication processes (see Table 3.3). The tests took place in four different testing facilities (TF1, TF2, TF3 and TF4 – Table 3.4), with resonance and servo – hydraulic testing machines and a frequency of 15 to 30 Hz at different load levels (rope of pearls).

Table 3.3. General test matrix

Series	t [mm]	Material	Welding Process	Condition	Final No. of Specimens
B-25: 25_A, 25_B, 25_C, 25_D, 25_E, 25_P	25	YP47	FCAW	as welded	48 (6x8)
B-50: 50_C, 50_P	50	YP47	FCAW	as welded	16 (2x8)
B-60: 60_A, 60_B, 60_C, 60_D, 60_E, 60_P	60	YP47	FCAW	as welded	48 (6x8)
B-80: 80_A, 80_B, 80_C, 80_D, 80_E, 80_P	80	YP47	FCAW	as welded	36 (5,8,8,4,4,7)

Table 3.4. Testing facilities

Name of Series	Testing Company	No of Specimens	Type of Specimens	Material	Thickness [mm]
B-25	TF1	48	Butt Weld	YP47	25
B-50	TF2	16	Butt Weld	YP47	50
B-60	TF3	48	Butt Weld	YP47	60
B-80a	TF4	24	Butt Weld	YP47	80
B-80b	TF2	4	Butt Weld	YP47	80
B-80c	TF3	8	Butt Weld	YP47	80

Figure 3.5 Example of testing facility

3.4 Misalignments

The welding process usually introduces axial and angular misalignments which lead to an increase of stress in the welded joint due to the occurrence of secondary plate bending stresses. Often these additional bending stresses appear at the relevant crack initiation section where they are superimposed with the loading stresses. Since misalignments at welded joints are an unavoidable phenomenon, they have to be taken into consideration while calculating the fatigue strength. In this case, the axial as well as the angular misalignments were measured in the testing facilities and compared to the permissible values of welding qualification according to ISO5817 – Quality levels for imperfections (quality levels B: $e/t \leq 0{,}1$ and C: $e/t \leq 0{,}15$).

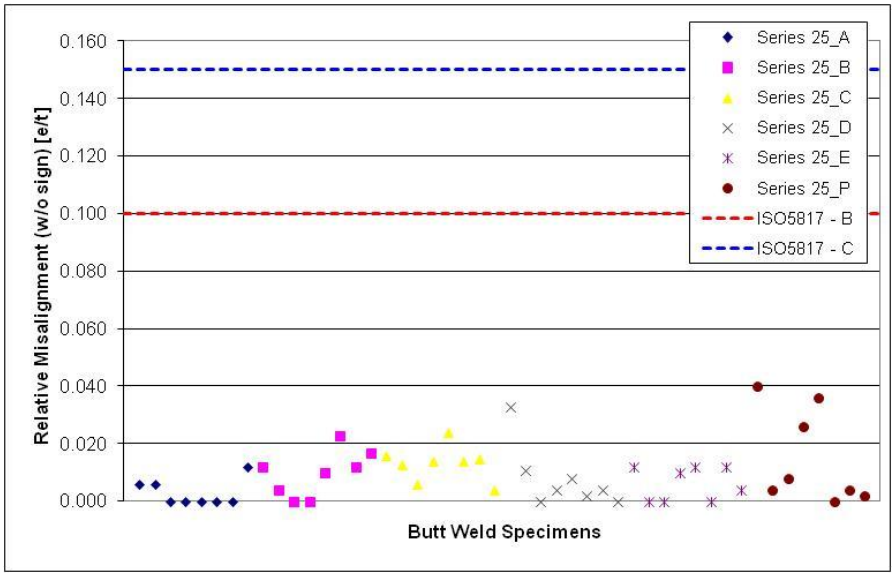

Figure 3.6. Relative axial misalignment (t=25mm)

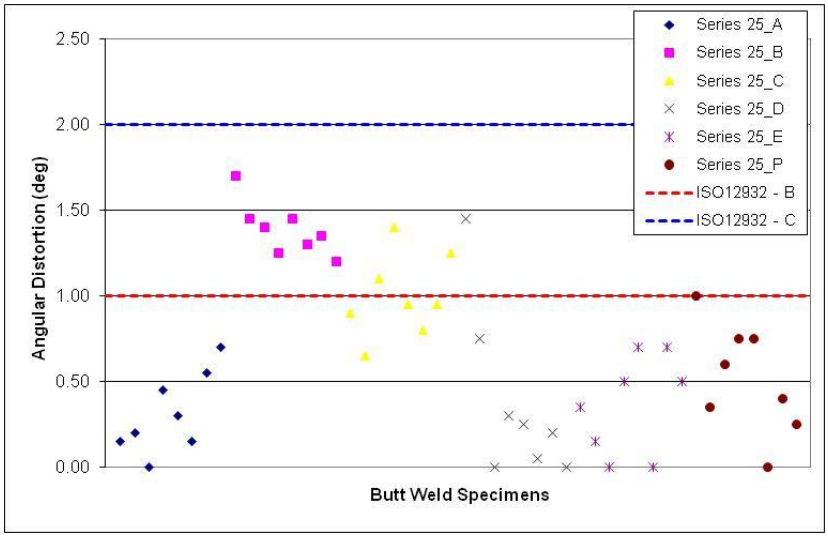

Figure 3.7. Angular misalignment (t=25mm)

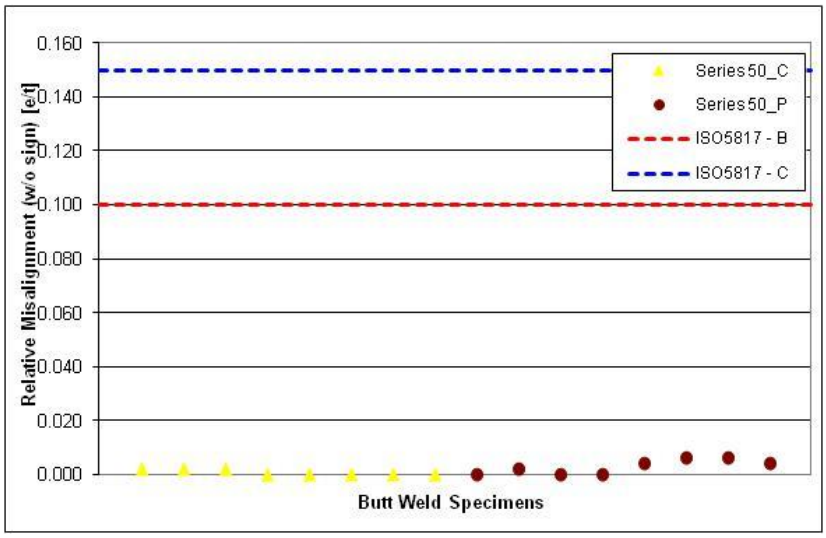

Figure 3.8. Relative axial misalignment (t=50mm)

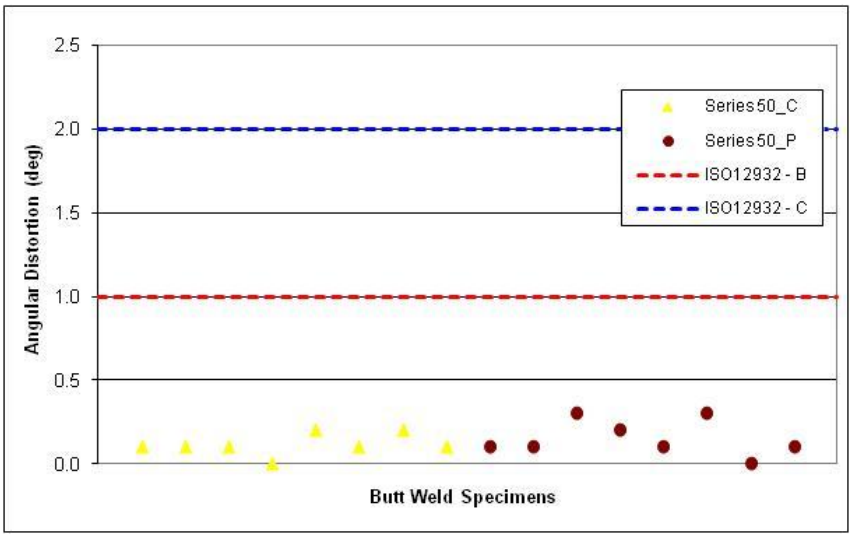

Figure 3.9. Angular misalignment (t=50mm)

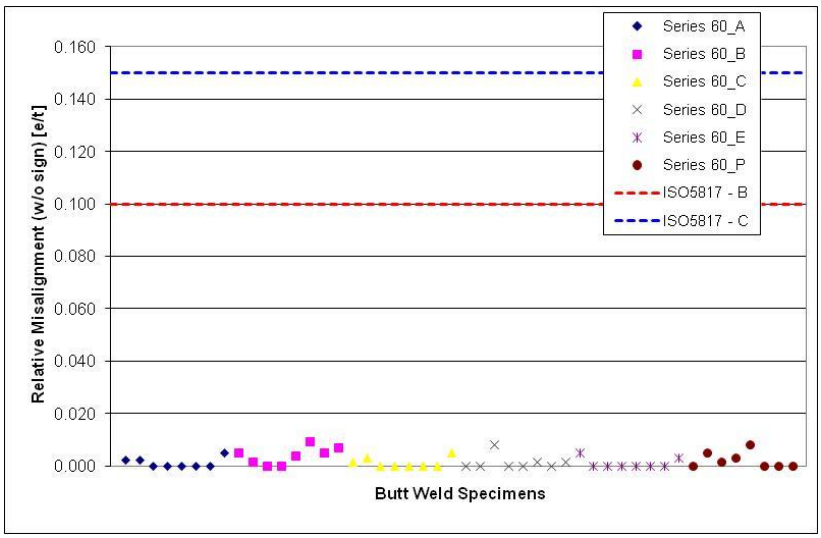

Figure 3.10. Relative axial misalignment (t=60mm)

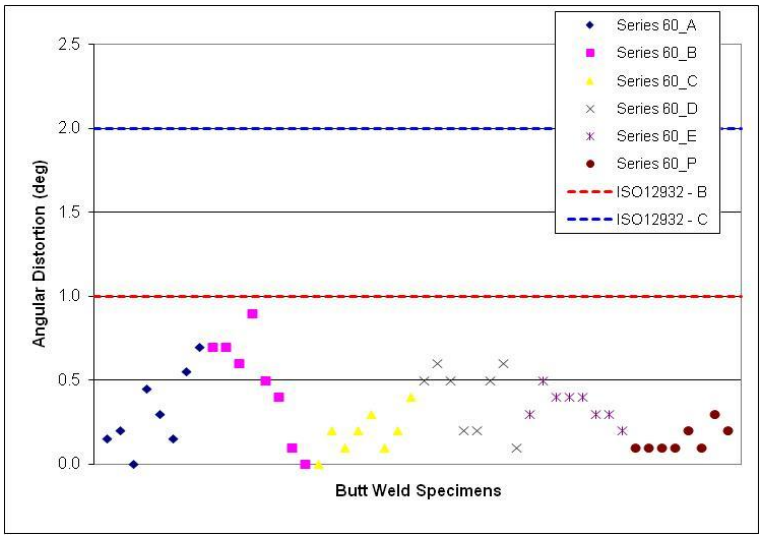

Figure 3.11. Angular misalignment (t=60mm)

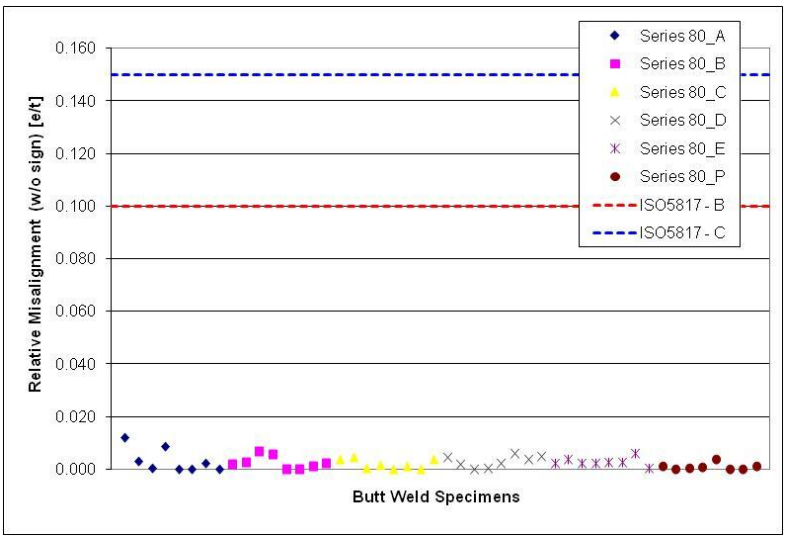

Figure 3.12. Relative axial misalignment (t=80mm)

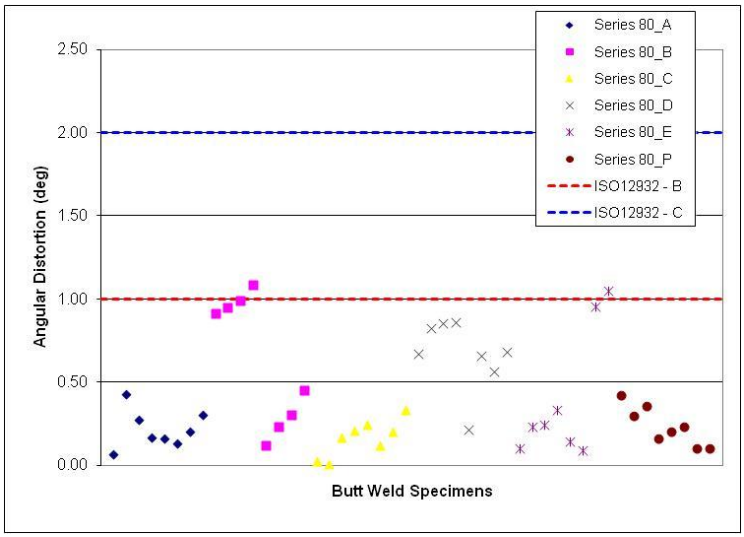

Figure 3.13. Angular misalignment (t=80mm)

Generally, it can be observed that misalignments decrease with increasing plate thickness (as expected), with an exception of the specimens of t=50mm (unexpectedly low values of angular misalignments), which show a very good quality of manufacturing by the relevant shipyards.

The stress magnification factor k_m was calculated according to the recommendations (Hobbacher A., 2008):

$$K_{m,axial} = 1 + 3\frac{e}{t} \tag{3.5}$$

$$K_{m,angular} = 1 + \frac{3}{2} \cdot \frac{a \cdot l}{t} \cdot \frac{tanh(\beta/2)}{\beta/2} \quad \text{with} \quad \beta = \frac{2\lambda}{t}\sqrt{\frac{3\sigma_m}{E}} \tag{3.6}$$

$$\text{combined: } K_m = 1 + \left(K_{m,axial} - 1\right) + \left(K_{m,angular} - 1\right) \tag{3.7}$$

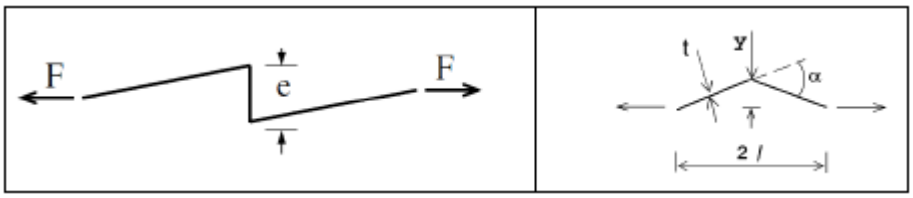

Figure 3.14. Axial misalignment and angular distortion

For the specimen with the larger axial misalignment (e/t=0.04) and with an angular distortion of a=1^o the stress magnification factors were calculated as $K_{m,axial}$ = 1.12 and $K_{m,angular}$ = 1.28, leading to an overall value of K_m = 1.4.

Respectively, for the specimen with the larger angular distortion (a=1.7^o) and with an axial misalignment of e/t=0.012 the stress magnification factors were calculated as $K_{m,axial}$ = 1.04 and $K_{m,angular}$ = 1.36, leading again to an overall value of K_m = 1.4 .

The above values are within the acceptable limits, so overall the misalignment influence can be assumed negligible and already included in the tables of classified structural details.

3.5 Fatigue Test Results

The failure criterion employed is the final fracture of the specimen, since the break of a small scale specimen corresponds quite well to a surface crack with a crack depth equal to the plate thickness in a real (big scale) structure (Doerk O., Fricke W., H. von Selle, Kahl A., 2012). At all fatigue tests the crack initiated at the weld toe of the upper reinforcement of the weld while at some cases run-outs were observed (no visible crack initiation after the tests were stopped at $2 \cdot 10^6$ cycles – marked with arrows in the following figures). Some of the run-out tests were repeated on an increased stress range level and these results were the ones taken into account.

3.5.1 Overall Results

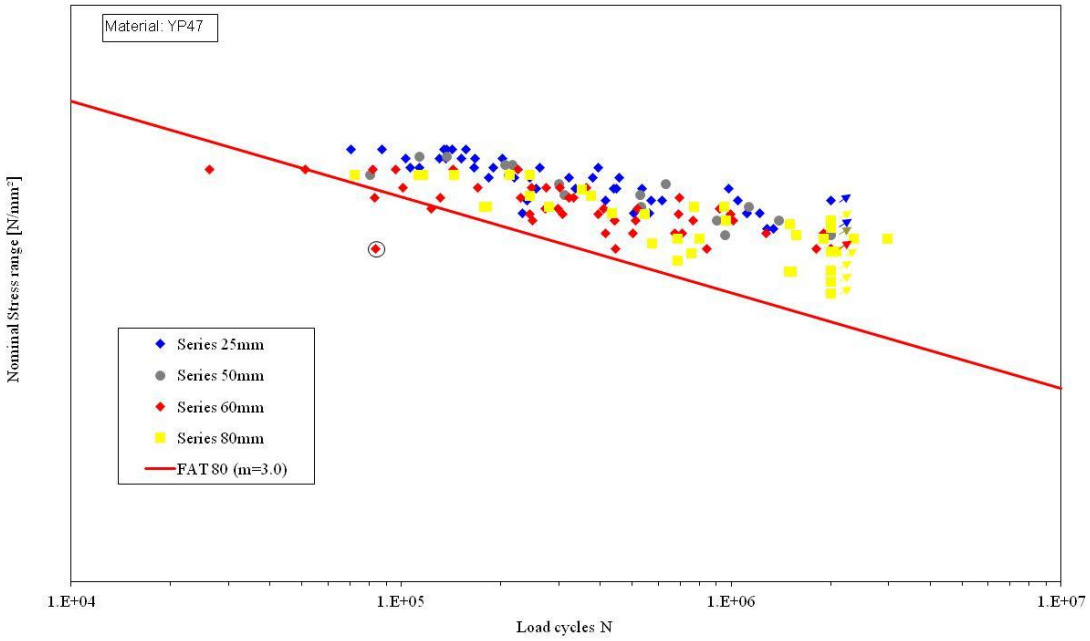

Figure 3.15 Overall results of JDP II

Figure 3.15 shows all the test results of this project (JDP II), together with the design S – N curve from the rules which is relevant to the specific occasion of butt welds. It can be observed that generally there is a good performance of the YP47 specimens, since most of the results lie above the design S – N curve. On the other hand, there is no clear picture of thickness effect. More specifically, it can be commented that the 25mm series indeed show the best performance, while the 50mm series show unexpectedly good behavior which probably can be explained by the very good quality of the manufacture, as shown by the measurement of the misalignments before. The 60mm series shows a bad behavior with some specimens not even reaching the appropriate FAT class and one of them being excluded from

further calculations, as it will be explained later. Finally, the 80mm series have a rather normal performance.

Moreover, (see Figure 3.16) when the results are compared to the ones from JDP I (Doerk O., Fricke W., H. von Selle, Kahl A., 2012), it can be verified that generally there is a similar behavior between the two series of experiments. A knuckle in the order of the results at around $2 \cdot 10^6$ cycles can be also observed.

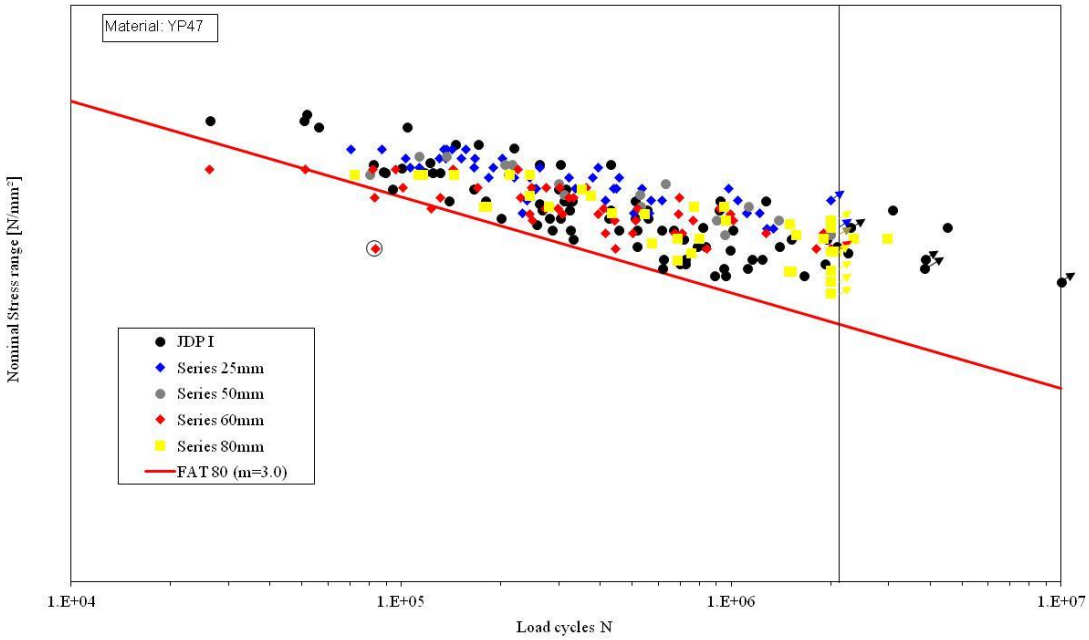

Figure 3.16 Overall results of JDP I & JDP II

3.5.2 Results by Shipyard

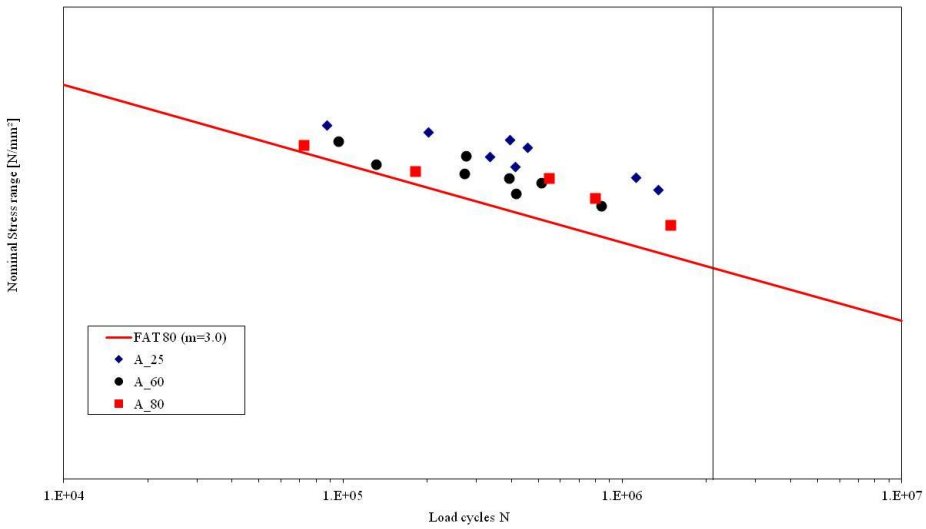

Figure 3.17 Results of A Series

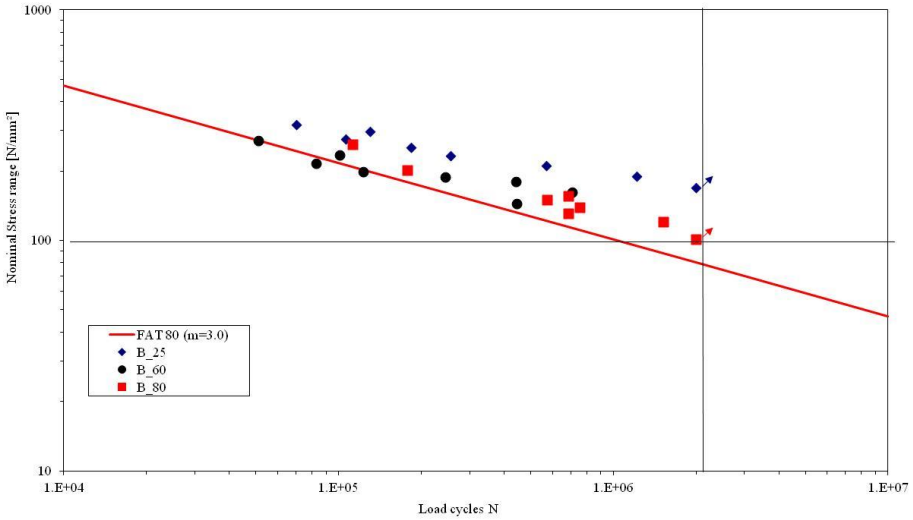

Figure 3.18 Results of B Series

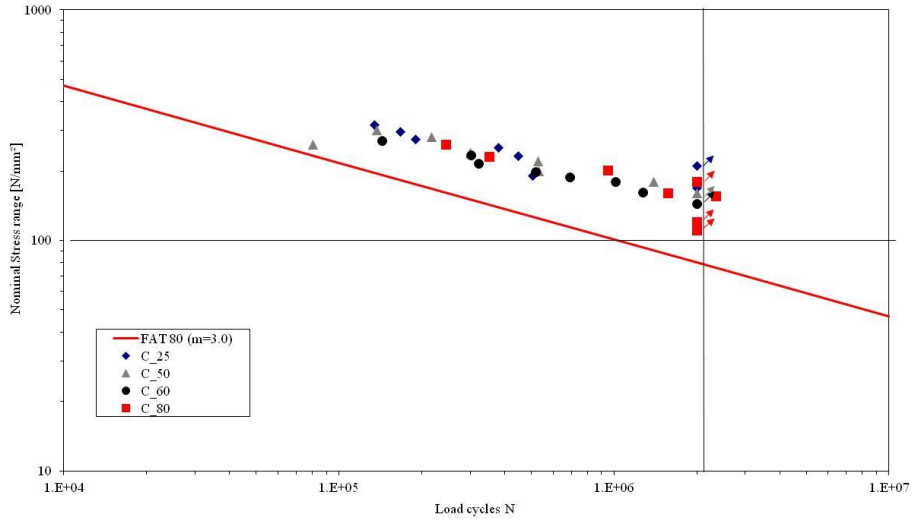

Figure 3.19 Results of C Series

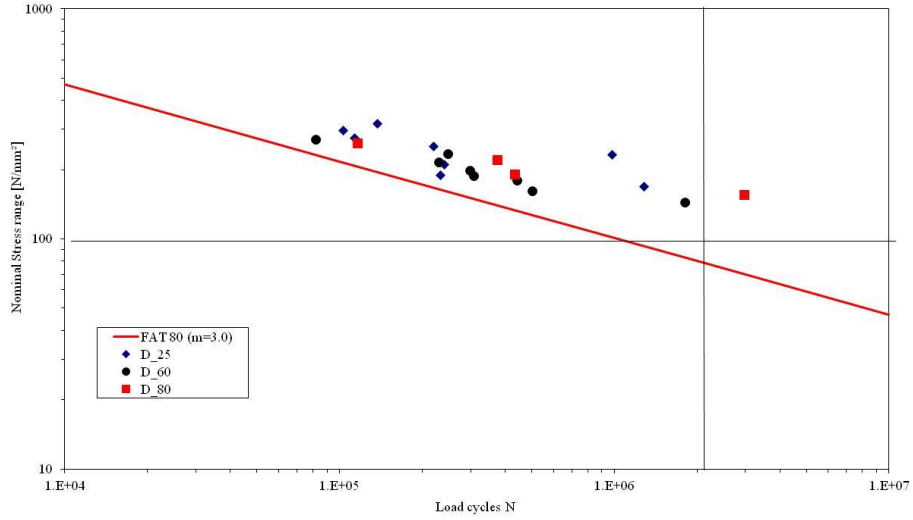

Figure 3.20 Results of D Series

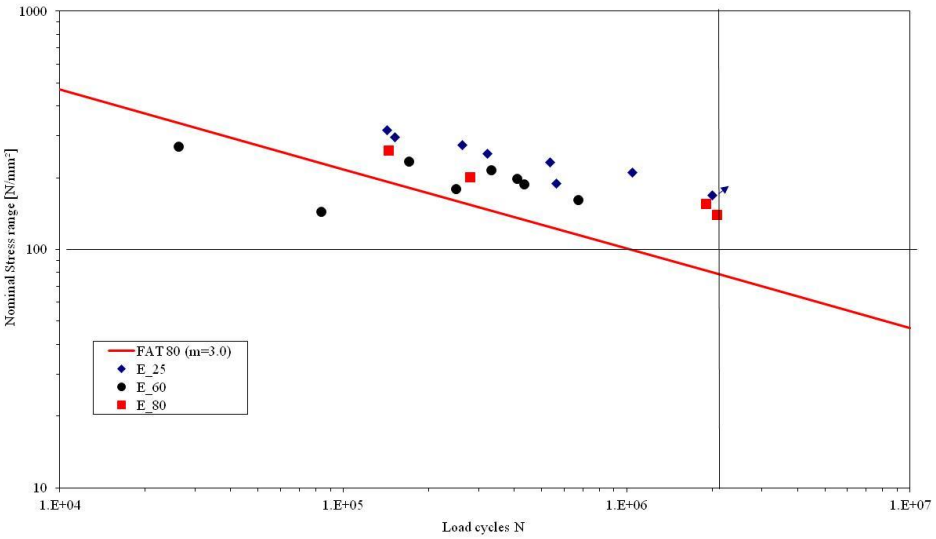

Figure 3.21 Results of E Series

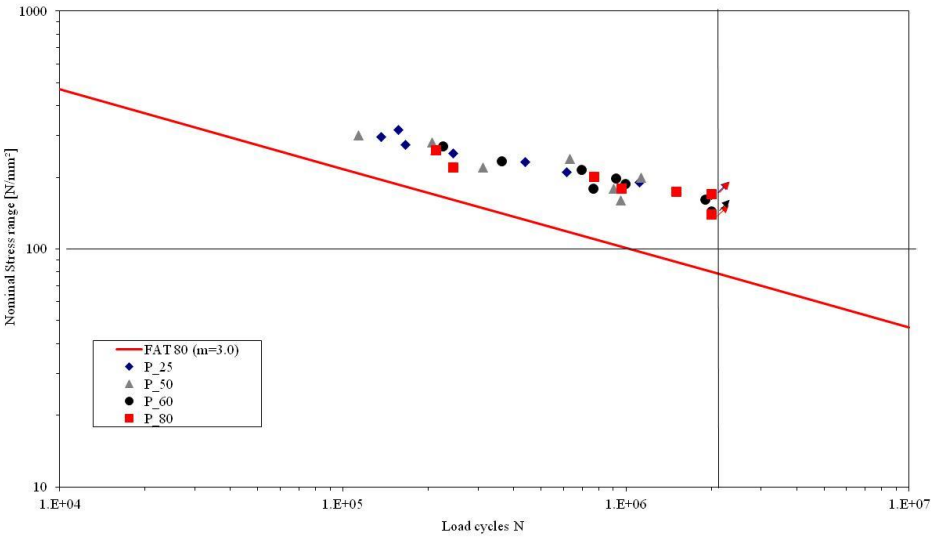

Figure 3.22 Results of P Series

Examining the results yard by yard, it can be observed that only the A series shows the expected performance, regarding the thickness effect, with the 25mm specimens achieving longer lives comparing to the thicker specimens of 60 and 80mm. The results from yards C and P do not show any thickness effect, due to the overall very good quality of manufacturing of the specimens, indicated be the measurement of misalignments (Figures 3.6 – 3.13). Finally, the B, D and E Series do not show any clear effect mainly because of the poor performance of the 60mm sub-series.

3.5.3 Evaluation of subseries by thickness and shipyard

The evaluations and the design of S – N curves initially were done for each thickness – shipyard subseries, for fixed slope (m=3) and for slope obtained from the results (m=free). An example of these evaluations which demonstrates the difference in the results between m=3 and m=free is presented below:

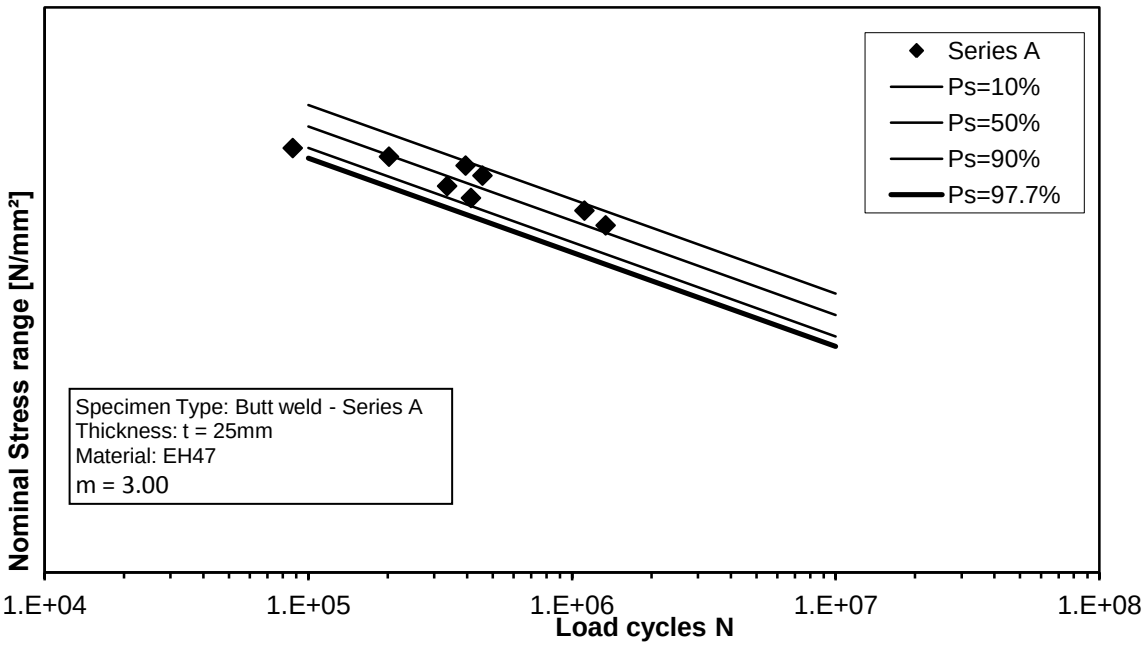

Figure 3.23. S – N curve of subseries 25_A with fixed slope m = 3.00

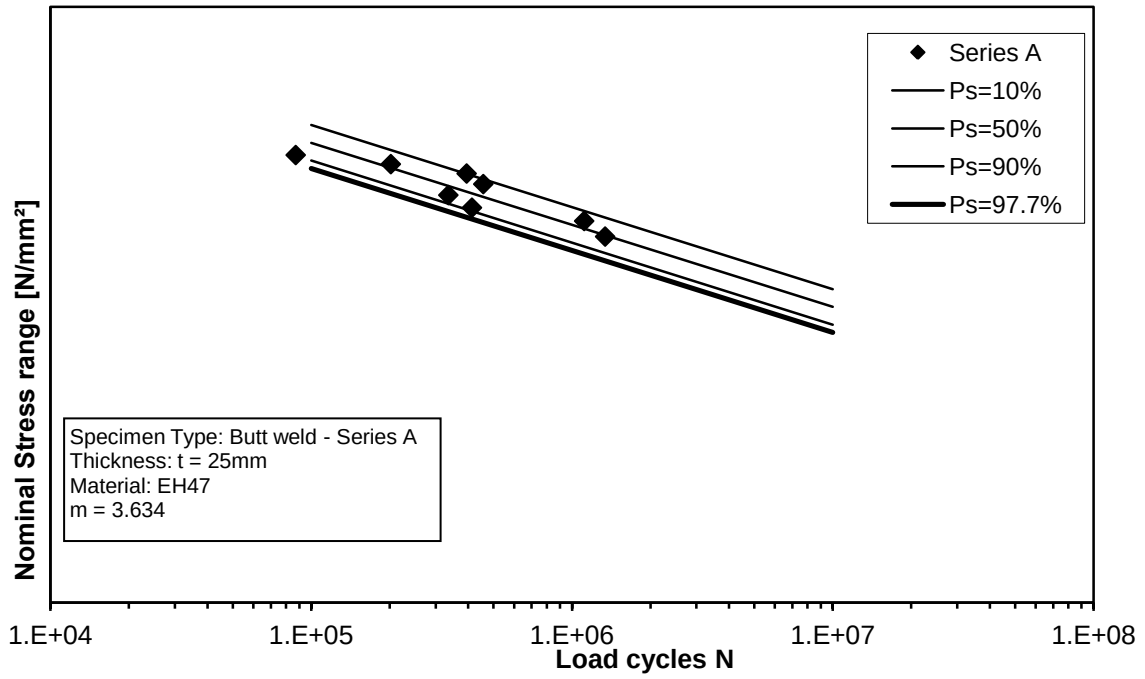

Figure 3.24. S – N curve of subseries 25_A with free slope m = 3.634

The difference in the obtained values of $\Delta\sigma_R$, which is the value of $\Delta\sigma$ for a probability of 97.7% for $2 \cdot 10^6$ cycles, between the above two graphs is 14% while the difference in the scatter is 5%. Such difference is not negligible (especially for the obtained FAT class of the subseries) and shows the importance of the influence of parameter m in the calculations.

In some cases, specific specimens showed unexpected behavior which had great impact to the obtained S – N curve. Such behavior was observed in the subseries 60_E (circled value) and the results are presented below (for m = free):

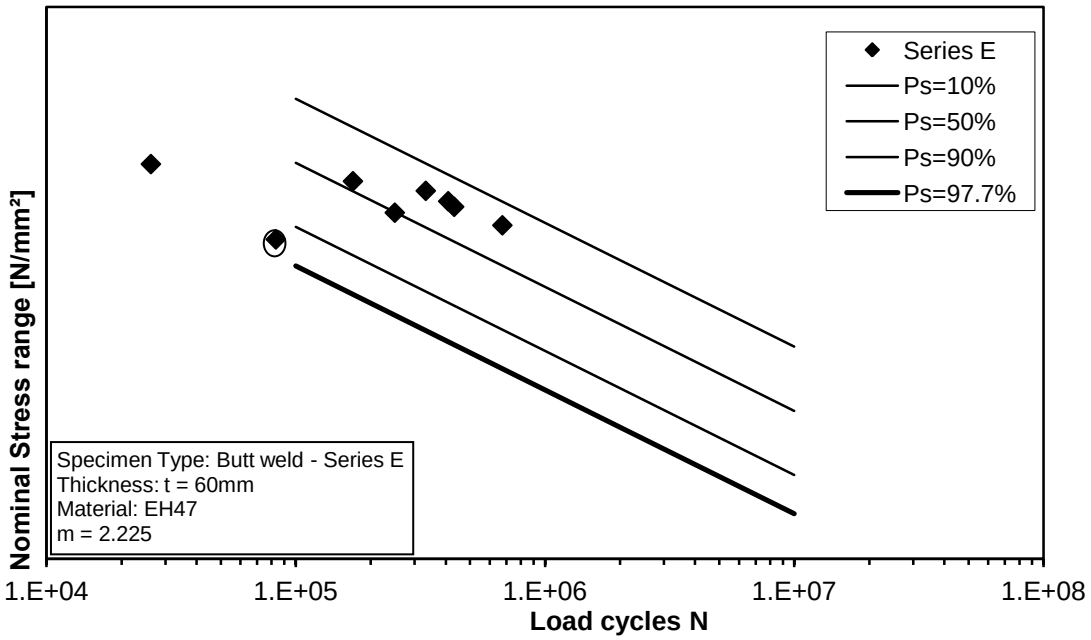

Figure 3.25. S – N curve of subseries 60_E including all specimens

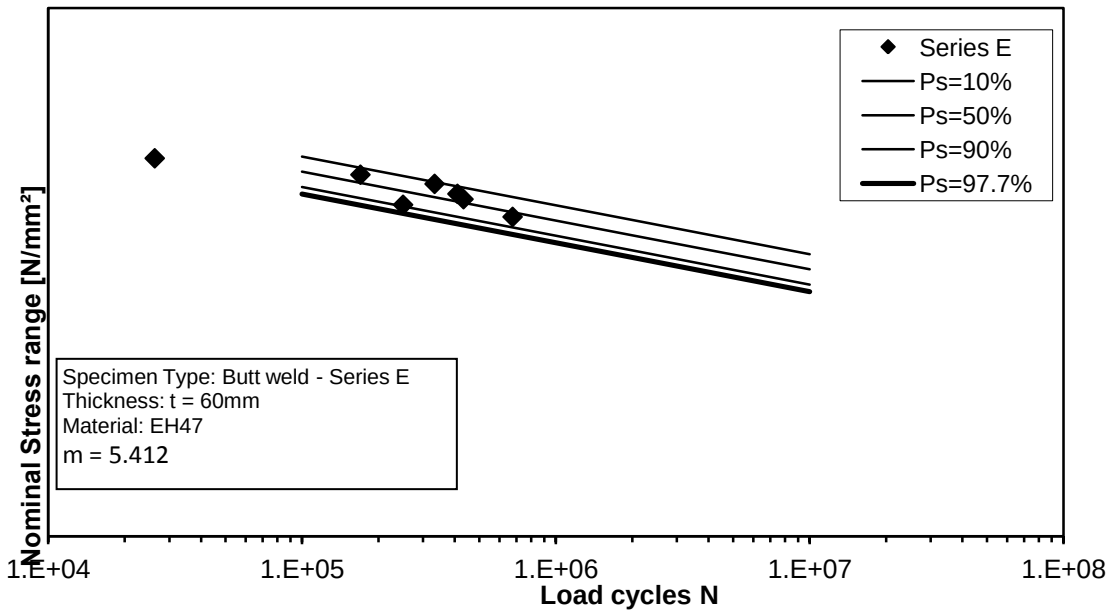

Figure 3.26. S – N curve of subseries 60_E excluding specific specimen

The difference in the results between the whole series ($\Delta\sigma_R$) and the series without the fault specimen ($\Delta\sigma_R'$) is great ($\Delta\sigma_R - \Delta\sigma_R' = 84$ MPa). In such cases the specimen considered to be wrongly manufactured (problem with the material or/and welding procedure) and was excluded from the calculations.

After performing the above described evaluation for each subseries of each thickness and shipyard for fixed and free slope, the FAT class of each of it was calculated and compared with the FAT class from the rules modified accordingly by the reduction factor f_t, as calculated by Equation 3.1 (right axis, see Figure 3.27), for two different values of parameter n (one from IIW equal to 0.2 and one from GL equal to 0.17):

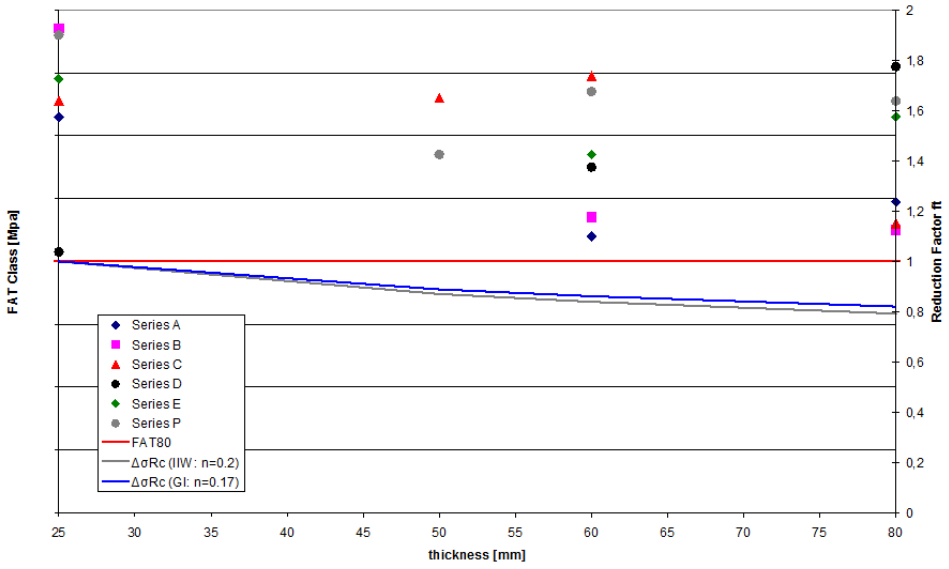

Figure 3.27. Plate thickness effect for slope m directly obtained by the tests

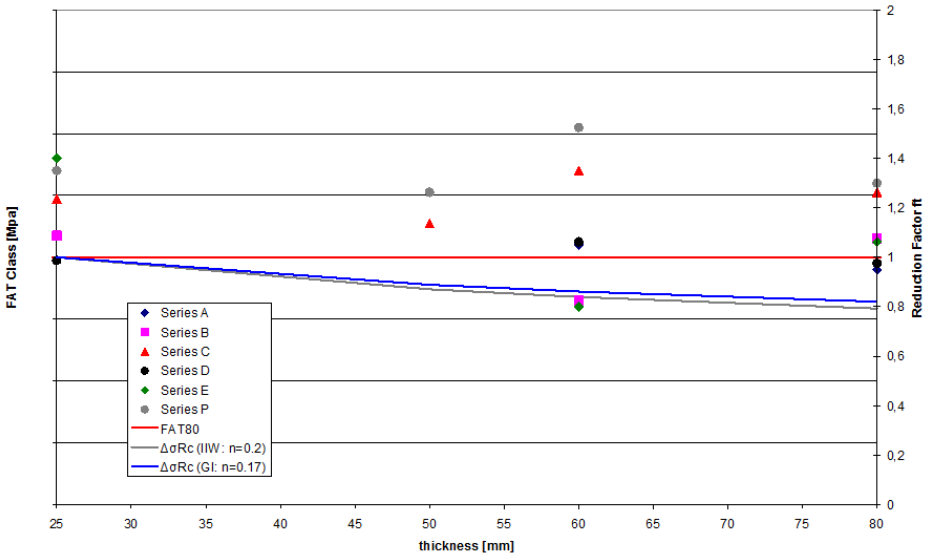

Figure 3.28. Plate thickness effect for slope m = 3.00

Once again, it can be observed the non-clear plate thickness effect, especially for specific series. Interesting is the fact that for the evaluations done for the value of the slope m directly obtained by the results, all the series show adequate fatigue performance and they are above the relevant FAT class without including the reduction from the parameter f_t. On the other hand, for the results obtained for m = 3.00, the performance is worse and for specific series of 60mm is even worse than the adjusted relevant FAT class.

3.5.4 Evaluation of series by thickness

Finally, an evaluation of overall series by thickness (all specimens of same thickness regardless the shipyard) took place and the results are shown in the Figure 3.29. For the values obtained for free slope, the expected thickness influence is not fully visible due to the unexpectedly good performance of 50mm series for both mean and FAT values. On the other hand, for the results obtained for fixed slope m=3.00, the results for the 60mm series gain very low values, affecting much more the form of the curve.

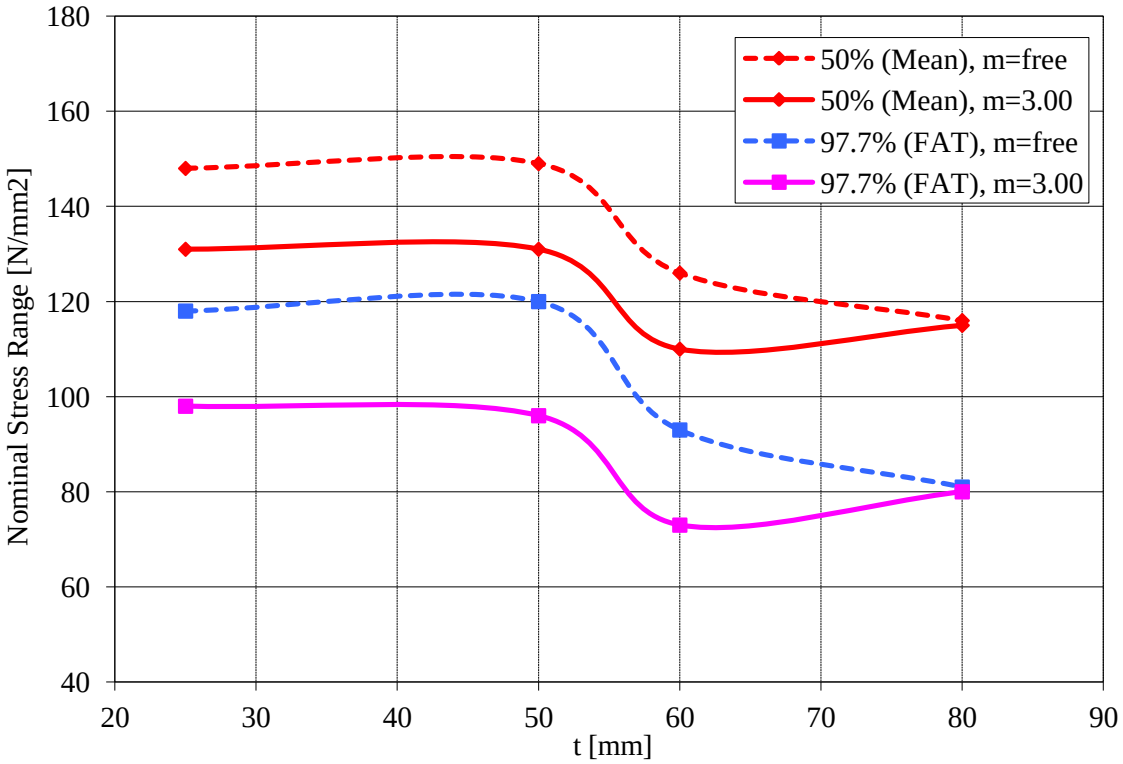

Figure 3.29. Influence of thickness, evaluation by thickness

3.6 Conclusions

The overall conclusions could be summed up in two statements. First, the fatigue performance of the material YP47 is proven to be generally good. Very few specimens failed below the relevant design S – N curve (Figure 3.16) and the obtained results for the subseries are also satisfying (Figures 3.17 – 3.22). On the other hand, there was no clear thickness effect in the results. The last statement can be partially explained by the large number of manufacturers and testing facilities, which led to large scatter on the results. There will be a further investigation regarding this matter in following chapter.

4 INVESTIGATION OF PARAMETERS C & m OF PARIS EQUATION

4.1 Introduction

The second part of this thesis is describing an assessment based on fracture mechanics concept in which the parameters C and m of the Paris crack growth equation are investigated. The analysis is based on experimental results of fatigue tests carried out by Germanischer Lloyd in co-operation with Korean shipyard (von Selle, Doerk, Kang, Kim, 2011). Specifically, the specimens used were butt welded 80 mm plates made of higher tensile steel and they were tested under a special two-level load history which resulted in creation of beachmarks on the fatigue crack surfaces. These beachmarks gave valuable information regarding the crack initiation location and the crack propagation phase that was used for the numerical assessment. The numerical calculations were performed by the software Fraunhofer IWM VERB 8.0 (see sub-section 4.3.1).

The objective is to directly calculate the parameters C and m of Paris equation which fit to the actual experimental results. The obtained values are to be compared with the ones recommended from literature, e.g. International Institute of Welding.

At first, a brief description of the fatigue tests will take place, followed by a presentation of the VERB software and the model used. Next, the obtained results will be presented and finally the chapter will end with a summary of the conclusions.

4.2 Description of the Test

Germanischer Lloyd in co-operation with Korean shipyard carried out butt weld fatigue tests. The tests were performed under constant amplitude axial load on a 12MN resonance testing machine with a frequency of approximately 33Hz and a stress ratio of approximately R=0.1. The butt welded specimens were of 80 mm thickness and made of higher tensile strength steel E40, while the welding technique was electro gas welding (EGW). These characteristics ensured that the test conditions corresponded to the actual loading conditions of the coaming and coaming top plate of large container vessels (Figure 4.1) and so for the test to be as close to the shipbuilding practice as possible.

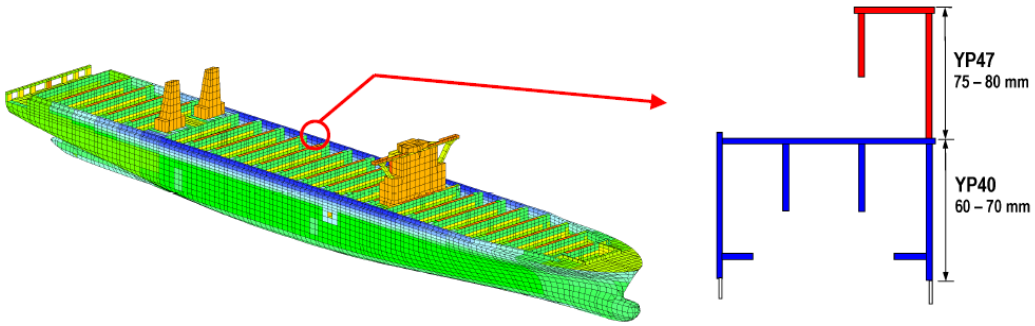

Figure 4.1. Coaming and top plate of large container vessel – 13000TEU (Doerk, O., Roerup, J, 2009)

The butt welds of the test were of two categories: as welded condition and post welded treated condition of ultrasonic impact peening (UP).

The ultrasonic hammer peening method UP for welded joints is well known, but it is not so frequently used as grinding. Up to now it is not included in the Rules and Recommendations since it is not common practice in shipbuilding industry.

The effect of the UP method is based on two different mechanisms, the smoothening of the weld toe radius and the degradation of tensile residual stresses. Generally, the requirement for achieving a fatigue strength improvement by post weld treatment techniques is an effective application of the particular treatment method within the manufacturing process (von Selle, Doerk, Kang, Kim, 2011).

Figure 4.2 shows a sketch of the butt weld specimens. The data for the base material is given in Table 4.1. Table 4.2 shows the parameters of the welding process, consumables and condition.

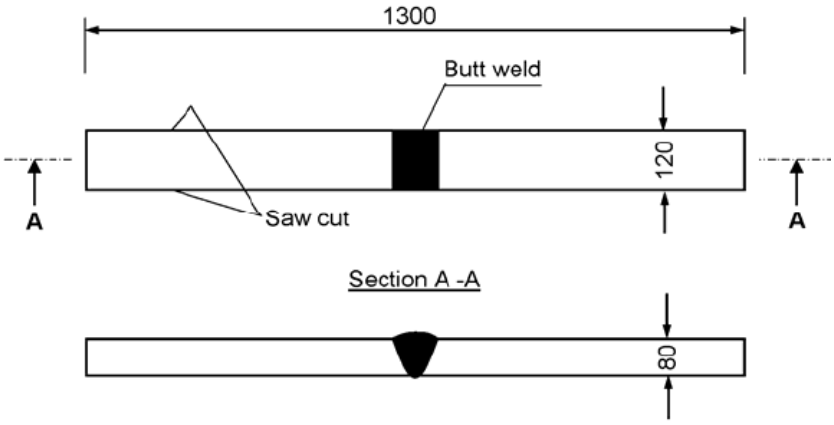

Figure 4.2. Geometry of the butt weld specimens (von Selle, Doerk, Kang, Kim, 2011)

Table 4.1. Actual material data for the base material of the butt weld specimens (von Selle, Doerk, Kang, Kim, 2011)

Name	Tensile Test			Impact Test	Chemical Composition [%]														
	Y.P.	T.S.	E.L.	-40° C [J]	C	Si	Mn	P	S	Cu	Ni	Cr	Mo	V	Nb	S-AL	N	Tl	Ceq
GL E40	408 MPa	512 MPa	28 %	383 (AVE)	0.08	0.14	1.55	0.08	0.02	0.01	0.02	0.03	0.0	0.0	0.018	0.045	-	0.012	0.35

Table 4.2. Welding process, consumables and condition (von Selle, Doerk, Kang, Kim, 2011)

Process	Brand name	Position	Diameter	Manufacturer	Current (A)	Voltage (V)	Speed (cm/min)	Heat input (KJ/cm)
EGW Tandem	DSW-50GTF	Face side	1.6 mm	KOBELCO	375	39	3.1	608
	DSW-50GTR	Root side	1.6 mm		400	42		

The edges of all specimens were milled, in order to be clear of notches near the weld bead made from thermal cutting. This measure reduced the specimen breadth to approx. 100mm. Additionally, the edges around the weld were rounded in order to shift the crack initiation location towards the centre of the specimens. Finally, the measured misalignments were comparatively low, as expected for the plate thickness of 80mm.

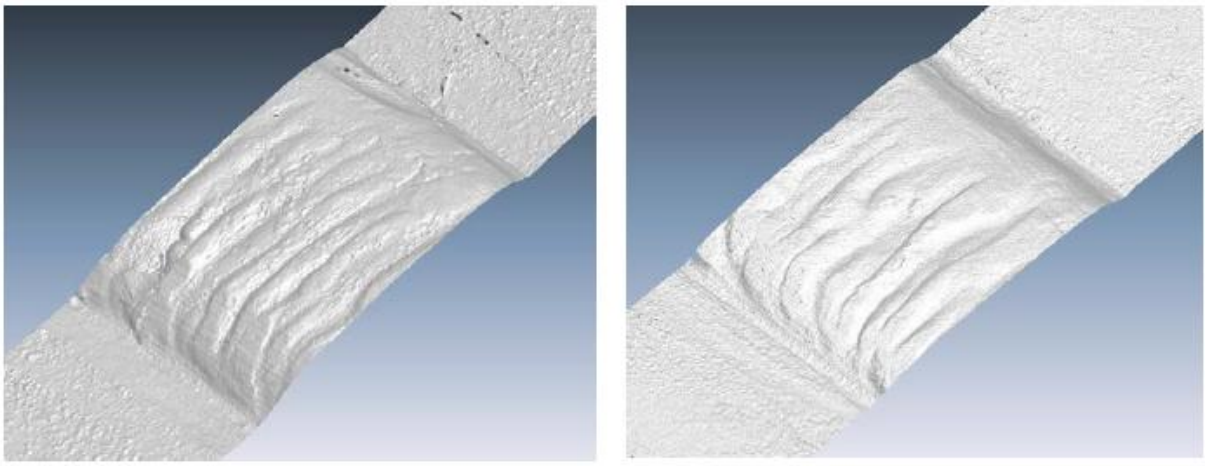

Figure 4.3. Laser scan of typical weld surfaces in as welded (left) and UP treated condition (right), (von Selle, Doerk, Kang, Kim, 2011)

For all fatigue tests of the butt welds specimens the final rupture of the specimen was employed as the failure criterion. In this way the comparability between the tests' results in as welded conditions and in UP treated conditions was ensured. Furthermore for fatigue tests of small scale specimens this failure criterion is commonly used in the corresponding rules and guidelines.

The most important characteristic of the specific test is the fact that the fatigue tests were carried out with a special two-level load history. After a certain amount of load cycles, depending on the load level, the applied stress range was reduced to approximately 50% of the initial value for a small number of load cycles. This was realized by increasing the lower stress level while the upper stress was kept simultaneously constant. These reduced load cycles do not contribute notable to the damage sum of the specimen but results in clearly visible beachmarks on the fatigue crack surface (von Selle, Doerk, Kang, Kim, 2011). These beachmarks give valuable information regarding the crack initiation location and the crack propagation phase, which were used in the numerical calculations and investigation of C and m Paris equation parameters.

4.3 VERB Software and Crack Propagation Calculations

4.3.1 General

IWM VERB is a PC program for fracture assessment of components containing crack-like defects. The computational basis of the program consists of methods and solutions of elastic and elastic-plastic fracture mechanics while the assessment methodology follows internationally recognized guidelines and documents. The name VERB is an acronym of „Versagensbewertung von rissbehafteten Bauteilen" standing for "Failure Assessment of Cracked Components". Since 1988, the program has continuously being developed at Fraunhofer Institute for Mechanics of Materials IWM, Freiburg.

The program VERB can be used to assess the influence of crack-like defects on component's strength or its remaining lifetime.

Calculations at cyclic loading include:

- Determination of the number of cycles required for the crack to propagate from an initial to a final size;
- Determination of the final crack size for given an initial crack size and a number of load cycles;
- Fatigue proof for a cracked component.

Crack propagation under cyclic loading is calculated by integrating a material specific crack growth equation, which in this case will be the Paris equation (Equation 2.5).

4.3.2 Computational Model and Procedure

In order to simulate the previously described tests, it was necessary to define the computational model. In VERB, the input of an analysis model includes the selection of the structural model, the loading type and the crack type.

As a structural (component) model it was chosen the ‘plate’ option, with geometry (wall thickness, t, and plate width, W) equal to that of the actual specimens. The loading type is cycling loading with a constant stress range equal to the one from the actual tests and defined by a cyclic upper and a cyclic lower membrane stress. The secondary stress was decided to remain zero, since its impact in the specific investigation is negligible.

Figure 4.4. Fatigue crack surface of specimen U7

Regarding the crack, after observing the fatigue crack surface (Figure 4.4), it was chosen the ‘quarter – elliptical corner crack’ as a type (Figure 4.5). The geometry of the crack (crack depth, a, and crack length, c) is measured from the fatigue crack surface.

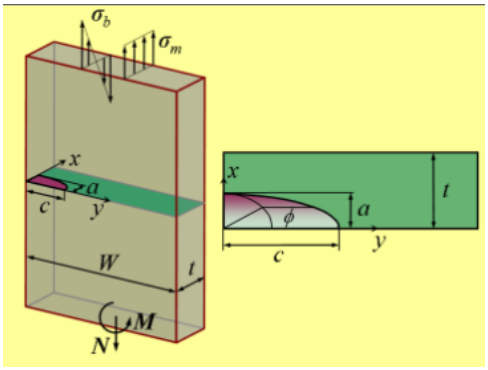

Figure 4.5. Model of VERB: plate with quarter elliptical corner crack

The procedure for the calculations is the following: For each specimen, it is known from the tests the stress range (Δσ in MPA) as well as the number of cycles between each beachmark (which is created when the stress range is lowered based on the two-level load history concept). Additionally, the dimensions of the beachmarks, which can be assumed as the dimensions of the crack while it propagates, can be measured from the final fracture surface (Figure 4.4). Therefore, it is able to insert this information (initial and final geometry of the

crack) to VERB and then by keeping constant the parameter m of Paris equation (Eq. 2.5), find the parameter C (by best-fit procedure) which will lead to a crack propagation with the same number of cycles as the ones from the actual tests. The procedure is carried out for three different values of the parameter m, equal to 2.5, 3 and 3.5, close to the value suggested by literature (m=3.00, Table 2.1) It is repeated for each beachmark by beachmark step, as well as the overall initial – to – last beachmark.

The solution method used by VERB can be found in the relevant Appendix.

4.4 Results

4.4.1 General

The total number of specimens modeled was eleven, seven in as welded condition (u1, u2, u3, u4, u5, u7 and u8) and four in post welded treated condition (up1, up2, up3 and up5). For each of them, the simulation of crack propagation performed step by step between each beachmark, as well as an overall one from the initial to the last beachmark. The value for the slope m kept constant and equal to 2.5, 3 and 3.5 (three sets of investigations) while the parameter C took such value that would lead to a crack propagation with the same number of cycles as the one from the test. The rest of the parameters took values according to the recommendations (IIW, Table 2.1): ΔK_{th}=5.5MPa·m$^{1/2}$, K_c=900MPa·m$^{1/2}$. The objective was to find a combination of parameters that would remain the same for each step, as well as through the overall propagation, since C and m are material parameters.

The investigation made for specimen u7 will be presented in detail, followed by the overall results. The detailed results for each specimen can be found in the relevant Appendix.

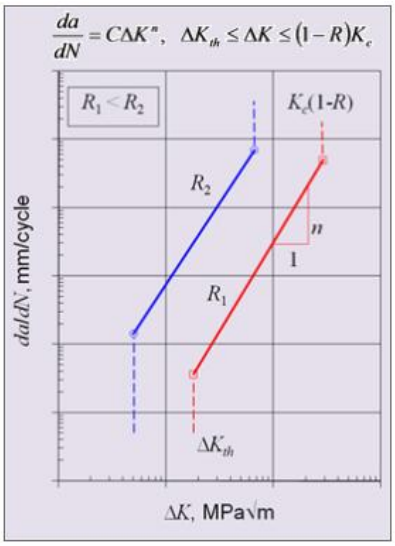

Figure 4.6. Paris equation and graph (snapshot from VERB software)

4.4.2 Specimen u7

Specimen u7 was tested under axial constant tensile loading of stress range equal to $\Delta\sigma$=170MPa ($\Delta\sigma_{up}$=190MPa, $\Delta\sigma_{low}$=20MPa, R≈0.1). The geometry of the specimen was measured; the total length was found equal to W=107mm while the thickness was found equal to t=80mm.

As it can be seen from the Figure 4.4, in the crack surface of the area there are several beachmarks, resulted from the two-load level history applied during the fatigue test, which match the crack while it propagates. The geometry of the crack together with the relevant number of cycles for each beachmark can be found in the following table:

Table 4.3. Geometry of the crack and number of cycles during the propagation for specimen u7

beachmark	**crack depth a [mm]**	**crack length c [mm]**	**Ntot**	**N**
initial	15	24	0	-
1	24	31	38700	38700
2	32	37	58200	19500
3	38	45	68200	10000
4	70	68	85300	17100

Every two beachmarks define a step of the propagation. For each step, the relevant parameter C that leads to a crack propagation of same number of cycles as the test was found by trials. Unfortunately, the C values were not the same for each step, though the parameters suppose to characterize the material. The reason for that might be the lack of accurate and detailed modelling of the actual geometry of the specimens. From these step – by – step values of C, together with the number of cycles N for each step which was used as a weight factor, a total mean value C_{mean_weight} was calculated. Additionally, an overall best fit value $Call_{best\_fit}$ was calculated by the software for the whole propagation from the first directly to the last beachmark. These two overall values (C_{mean_weight} and $Call_{best\_fit}$) were compared.

The results of this procedure for three different values of slope m are shown in the following graphs:

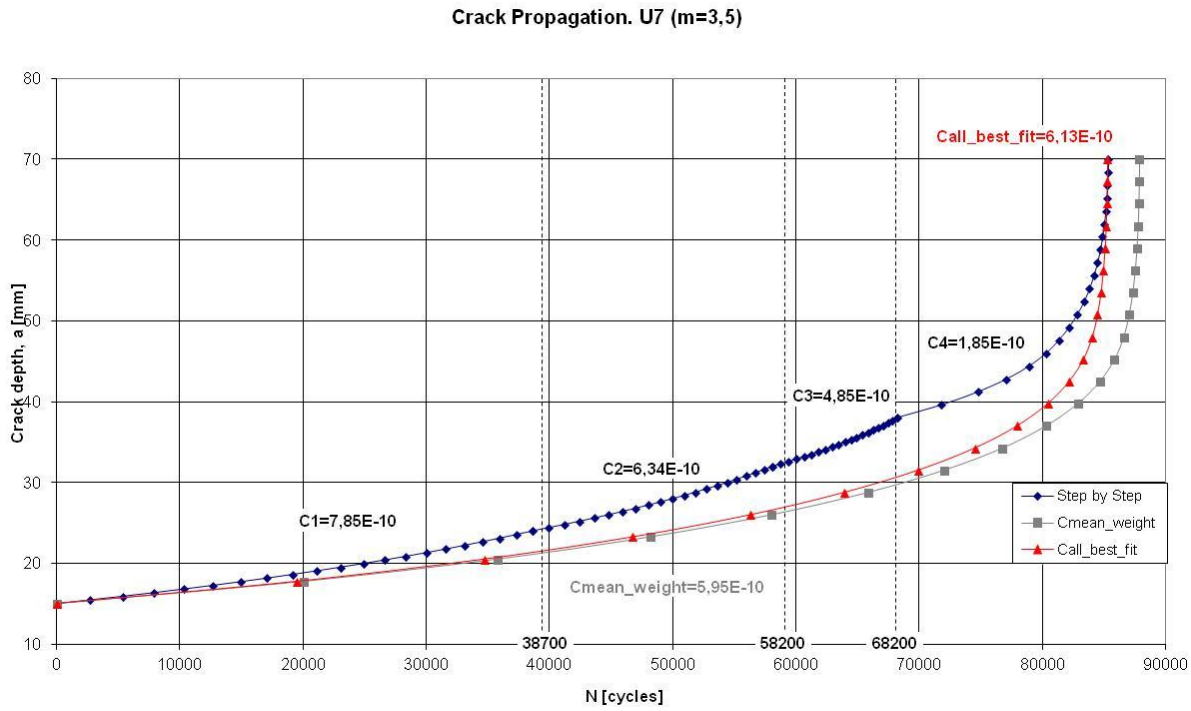

Figure 4.7. Crack propagation for specimen u7 (m=3.5)

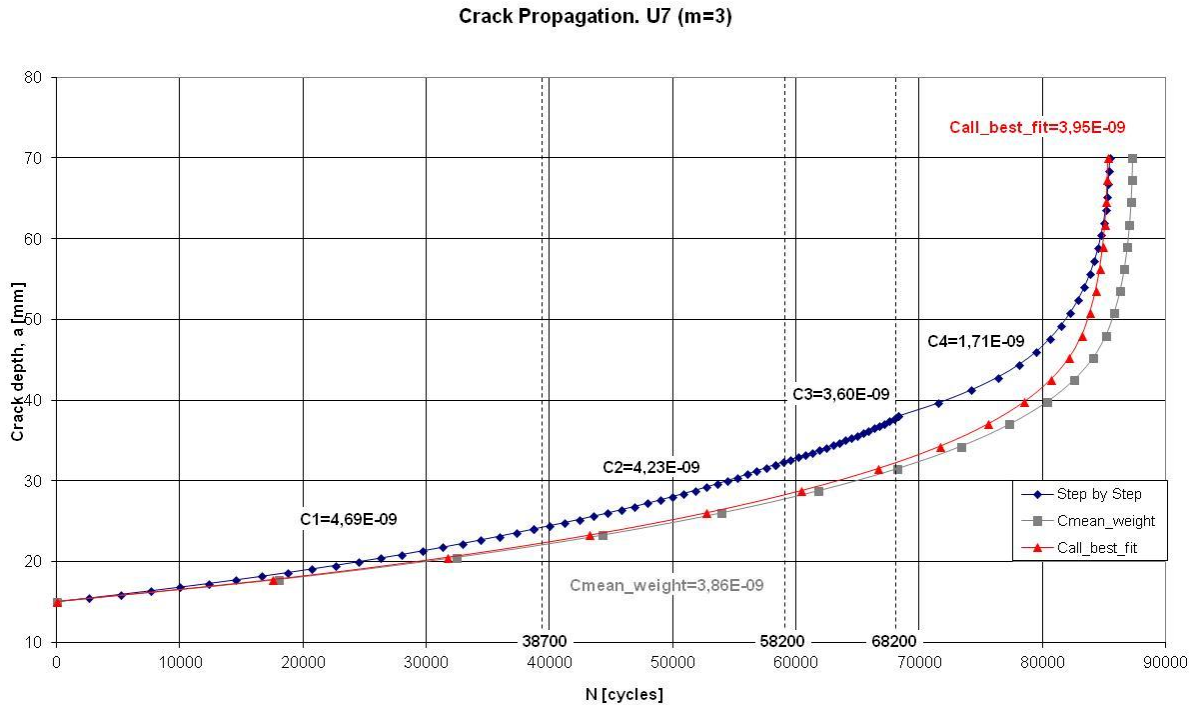

Figure 4.8. Crack propagation for specimen u7 (m=3.00)

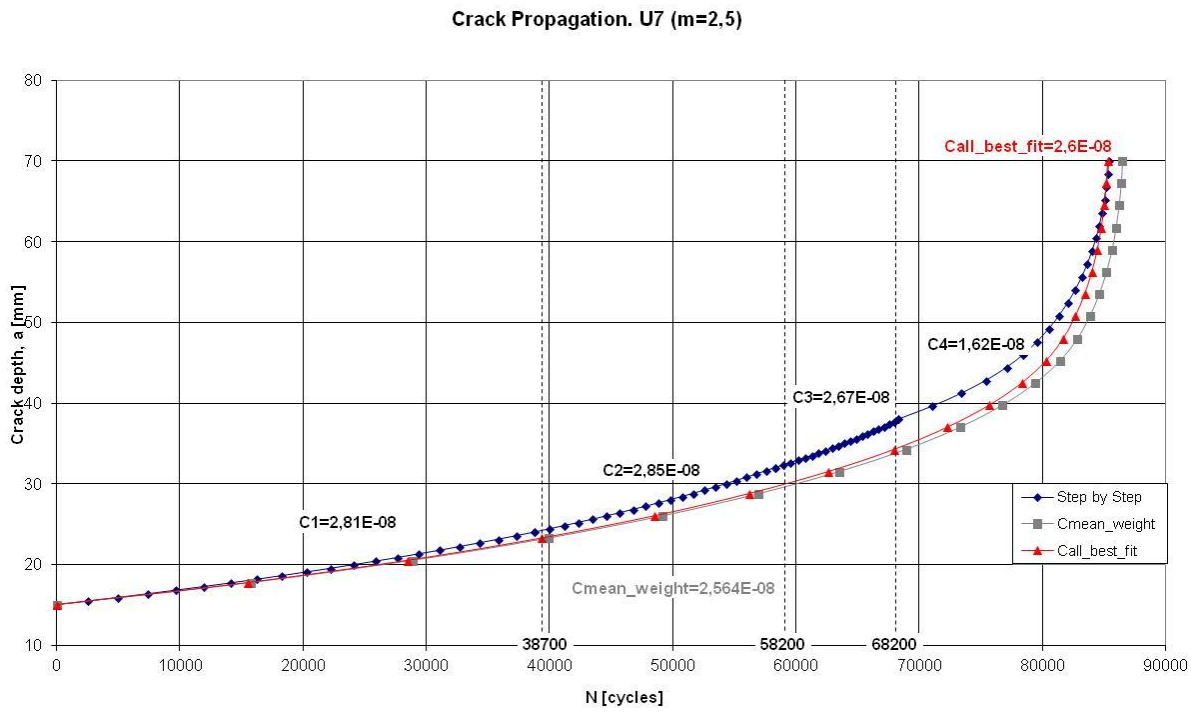

Figure 4.9. Crack propagation for specimen u7 (m=2.5)

For each step, the relevant value for parameter C has been found: C1 for 0 to 38700 cycles, C2 for 38700 to 58200 cycles, C3 from 58200 to 68200 cycles and C4 from 68200 to the end (85300 cycles). As mentioned before, these values are not the same and their difference varies from very small values (C1 to C2 for m=2.5: 1.42% difference) to relatively big (C3 to C4 for m=3.5: 61.86% difference). Generally, smaller differences between the obtained values are observed for m=3.00 and 2.5, while for m=3.5 the differences are bigger. Additionally, the calculated overall values C_{mean_weight} and $Call_{best\_fit}$ match to each other, as well as to the step – by – step propagation, better for m=2.5 and 3.00 rather than for m=3.5. Specifically:

for m=2.5: C_{mean_weight}=2.56E-08, $Call_{best\_fit}$=2.6E-08

for m=3.00 C_{mean_weight}=3.86E-09, $Call_{best\_fit}$=3.95E-09

for m=3.5 C_{mean_weight}=5.95E-10, $Call_{best\_fit}$=6.13E-10

This behaviour (mismatch of obtained values for m=3.5) is observed in all the specimens, so for this reason it was decided the investigation for m=3.5 not to be taken into account.

4.4.3 Overall Results

The above described investigation was repeated for all the specimens. The overall results are presented in the table below:

Table 4.4. Overall results of parameter C of crack propagation

	[Mpa]			[mm]				
specimen	**stress range**	**up stress**	**low stress**	**initial crack depth**	**final crack depth**	**C_all$_{best_fit}$ (for m=2,5)**	**C_all$_{best_fit}$ (for m=3)**	**total cycles N**
u1	250	280	30	12	48	2.12E-08	2.83E-09	50000
u2	230	255	25	5	37	3.66E-08	5.65E-09	54500
u3	190	210	20	8	40	3.39E-08	5.26E-09	59700
u4	180	200	20	24.5	42.5	2.185E-08	2.785E-09	23200
u5	240	265	25	10	46	2.591E-08	3.560E-09	45900
u7	170	190	20	15	70	2.60E-08	3.95E-09	85300
u8	210	235	25	14	39	2.537E-08	3.665E-09	50500
up1	210	235	25	34	47.5	2.050E-08	2.100E-09	6900
up2	250	280	30	11	40	3.44E-08	4.77E-09	32500
up3	180	200	20	31	50	3.20E-08	3.82E-09	12000
up5	190	210	20	2.5	27	1.30E-08		352800

In the specimen up5 the crack did not initiate from the weld root, which is the general crack initiation location, but the failure started at internal weld defects, so the model used was different (embedded crack) and it was decided to be excluded from the general evaluation.

As it can be seen from the table, the obtained values for all the specimens are of the same order of magnitude for each value of m: E-08 for m=2.5 and E-09 for m=3.00. It cannot be observed a difference between the as-welded specimens and the post-welded treated specimens.

The average value, as well as the upper limit (for more conservative results), of the obtained values is shown in the following table:

Table 4.5. Average value and upper limit of the overall results for m=2.5 and m=3.00

	C_all$_{best_fit}$ (for m=2,5)	**C_all$_{best_fit}$ (for m=3)**
A.V:	2.78E-08	3.84E-09
upper limit:	3.66E-08	5.65E-09

Compared to the recommended from the literature (IIW, Table 2.1) value of C=1.65E-08 (for da/dn in [mm/cycle] and ΔK in [MPa·m$^{1/2}$]) for m=3.00, the obtained value of C is smaller (difference of one order of magnitude) which leads to slower crack propagation thus longer lifetime. Therefore, the obtained result is less conservative than the one suggested from literature.

4.5 Conclusions

This part focused on the investigation of the parameters C and m of the Paris crack growth equation. The computations were based on experimental results obtained from fatigue tests of butt welds made of plates of the higher tensile steel YP40 of thickness t=80mm. The motivation was mainly the fact that the recommended values from the literature are about normal steel and there is no specification regarding higher tensile material.

The obtained value of the C parameter is varying for each step of the propagation for all the specimens, which is not expected since the parameter is characterizing the material, therefore theoretically there must have been a constant value through the overall crack propagation. A possible explanation, as already mentioned, is the inability of the software to define the geometry in high accuracy which leads to non-accurate values of the Stress intensity factor.

Moreover, there is a higher miss-match between the step – by – step C values and the mean C_{mean_weight} value when the parameter m is equal to 3.5; therefore it was decided to be excluded from further evaluations.

Finally, the overall obtained value for the C parameter from the evaluation of all the specimens (C=5.65E-09) is smaller than the one recommended from the literature (1.65E-08). This leads to less conservative results. Therefore it is suggested to be used with extra caution later on. Nevertheless, it can be explained since the recommended value is about mild steel so it may indicates an impact of the yield strength to the crack propagation phase of the fatigue life of the plate.

5 NOTCH STRESS & FRACTURE MECHANICS INVESTIGATIONS OF BUTT WELDS

5.1 Introduction

The last part of this thesis deals with the more detailed investigation of the thickness effect. Two different approaches are examined: the notch stress approach and the fracture mechanics one. For the first, notch stress calculations according to the recommendations (Fricke, 2008) were performed for the butt weld specimens from the tests described on the first part. The specimens were of various thicknesses (25mm, 50mm and 80mm) and different weld shape profiles. The thickness of the plate, the geometry of the weld as well as the concept of fictitious notch rounding and undercut on the notch are examined. The maximum value of the notch stress, as well as the stress distribution is calculated and the thickness effect is investigated.

In addition to the notch stress calculations, fracture mechanics calculations were performed using the software FRANC2D (a 2dimensional crack propagation simulation) and VERB, by initiating cracks of various lengths to the weld toe. The Paris law was employed with material parameters according to the recommendations, as well as according to the findings of the previous part. To investigate the weld notch and shape influence, the calculations were performed for a constant stress distribution and for a stress distribution obtained by the notch stress calculations, both using the same nominal stresses. The calculated Stress Intensity Factors are compared to the results obtained by empirical solution. Finally, the predicted life time of the specimens is calculated and the thickness effect is investigated.

5.2 Notch Stress Approach

5.2.1 Background of the Approach

The notch stress approach considers the increase in local stress at the notch formed by the weld toe or the weld root, based on theory of elasticity, i.e. without consideration of elastic-plastic material behavior. The micro-structural support effect of the material, which considers the effect on fatigue behavior of the inhomogeneous material structure under a stress gradient, can be taken into account by different hypotheses in the (elastic) notch stress approach (Fricke, 2008).

Very important is the notch rounding approach, which is based on the idea that the stress reduction in a notch due to averaging the stress over a certain depth can alternatively be

achieved by a fictitious enlargement of the notch radius. The sharp notches in the cross-sectional model have to be fictitiously rounded in order to obtain the fatigue-effective maximum notch stress resulting in the prospective fatigue notch factor of the welded joint by reference to the nominal stress. The fictitious radio ρ_f is calculated by the following formula (Neuber, 1968):

$$\rho_f = \rho + s \cdot \rho^* \tag{5.1}$$

where ρ = actual notch radius

s = factor for stress multi – axiality and strength criterion

ρ^* = substitute micro – structural length

In the present investigation, the conservative approach proposed by Radaj (1990) in which an actual radius of zero is assumed so that the fictitious radius, now considered as the reference radius, is r_{ref} = 1mm.

5.2.2 Models

In order to perform the notch stress calculations, butt weld specimens from the tests described in the first part were modelled. The specimens were of various thicknesses (25mm, 50mm and 80mm) in order for the thickness effect to be investigated. Moreover, the impact of the weld shape was examined. For this cause, different geometries of the weld reinforcement were modelled (Table 5.1). Specifically, the first group (a) of models had weld shapes directly and randomly taken from the actual specimens of the fatigue tests performed by Germanischer Lloyd. In the second group (b) the notch of the weld raises proportionally to the thickness so for thicker specimens the notch is sharper. In the third group (c) the weld geometry is exactly the same for all specimens and in the last group (d) the geometries of the welds are similar to the ones of the first group but now undercut of a radius of 1mm is introduced so for the Notch effect to be clearly demonstrated, according to the recommendations (D. Radaj, M. Vormwald, 2013). In all cases, the weld profiles were modelled as idealized - rounded, characterized by the weld toe radius r and the weld flank angle θ (Figure 5.1).

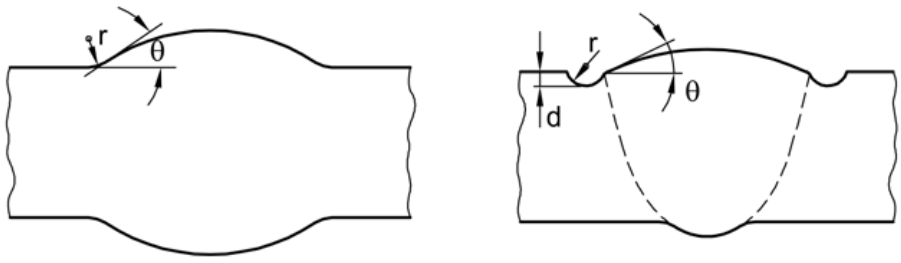

Figure 5.1. Rounding of weld toes of a butt weld and a butt weld with undercut (Fricke, 2008)

Table 5.1. Geometries of the specimens

	overall		upper reinforcement			lower reinforcement		
specimen	length (mm)	width (mm)	height (mm)	width (mm)	angle (deg)	height (mm)	width (mm)	angle (deg)
25	110	37.5	3.1	15	28	3	8	41.7
50a	250	75	3.6	21.9	19.7	2.5	6	28.3
80a	250	120	3.5	32	15.4	2.5	6.5	40.9
50b	250	75	6	20	29.7	3	12	23.9
80b	250	120	10	30	36.5	3	14	23.8
50c	250	75	3.1	15	28	3	8	41.7
80c	250	120	3.1	15	28	3	8	41.7

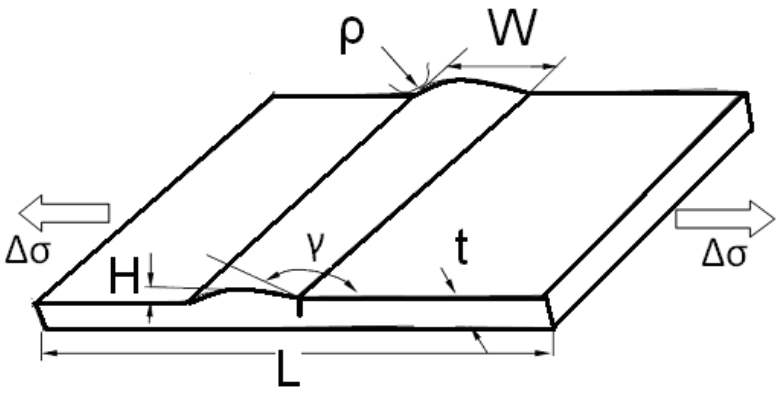

Figure 5.2. Weld geometrical parameters of butt welds (Al–Mukhart A., 2010)

The software which was used to define the geometry of the specimens was ANSYS Workbench (Figures 5.3 – 5.4.). It was applied half symmetry of the model.

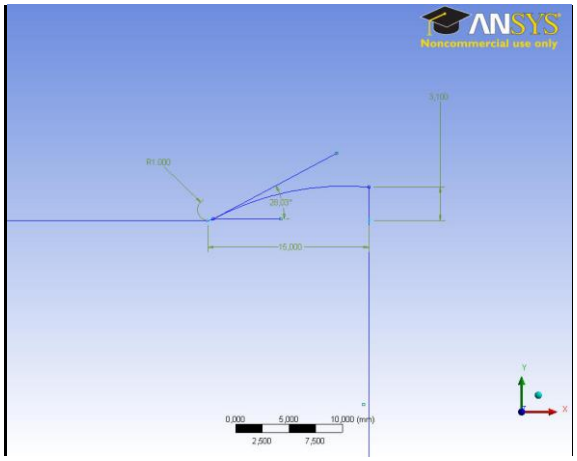

Figure 5.3. Geometry of the specimen 25, defined in ANSYS Workbench

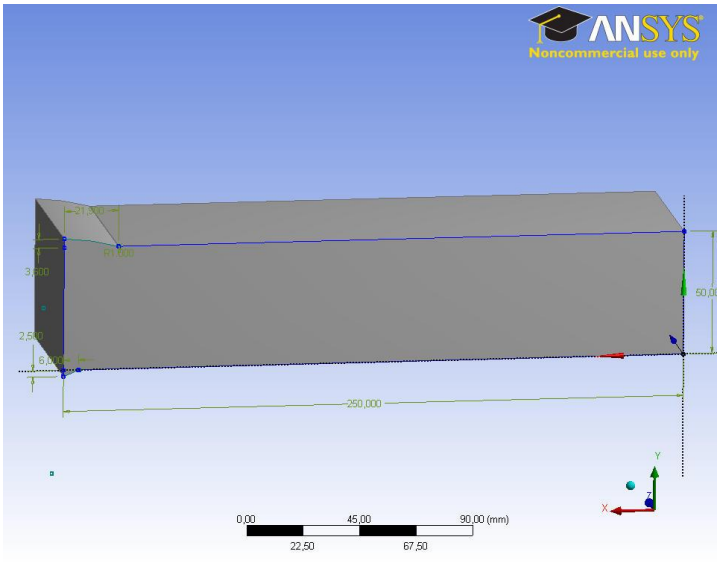

Figure 5.4. Geometry of the specimen 50a, defined in ANSYS Workbench

The same software was used to mesh the models according to the recommendations (Fricke, 2008). Thus, the discretization of the structure was performed such that a relatively coarse overall mesh was established, which was locally refined in the neighborhood of the notches under consideration. The mesh was gradually refined towards the notched area avoiding large steps in element size and excessive element distortion. The objective was to produce a mesh at the notch which was fine enough to model the steep stress increase normal and tangential to the notch surface and so yield the notch stress with sufficient accuracy.

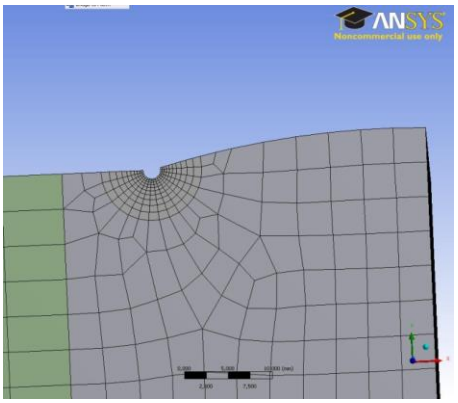

Figure 5.5. Detail of the meshing near the notch of the specimen 80d (undercut)

Regarding the material, high tensile steel properties were applied with Young modulus equal to E = 206000 N/mm^2 and Poisson's ratio ν = 0.3.

The nominal stress range was equal to 254 N/mm^2. For the specimens including undercuts (group 'd'), the applied stress was reduced in order to have a stress equal to the nominal at the section of the undercut (Table 5.2).

Table 5.2. Applied stress for specimens with undercuts

specimen	thickness [mm]	width [mm]	original area [mm^2]	area of undercut [mm^2]	area at the section of undercut [mm^2]	applied stress [MPa]
25d	25	37.5	937.5	37.5	900	243.84
50d	50	75	3750	75	3675	248.92
80d	80	120	9600	120	9480	250.825

Constrains were applied in order for the rigid body motion to be avoided: u_x in the symmetry plane, u_y in both lower corners and u_z in one of them (Figure 5.6).

The calculations were performed by the software ANSYS Classic. The results are presented in the following section.

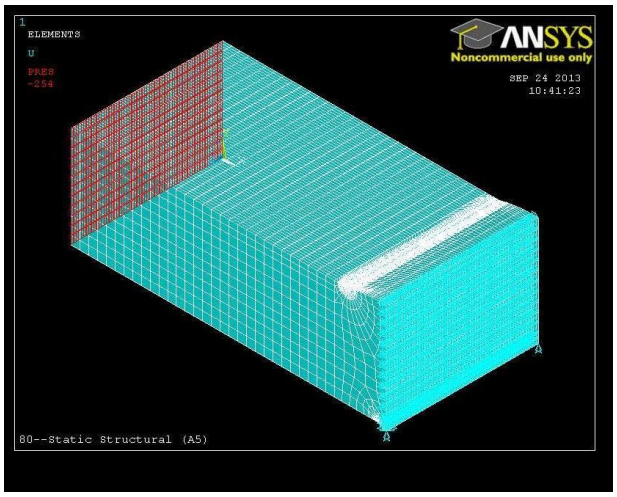

Figure 5.6. Model of the specimen 80a in ANSYS Classic

5.2.3 Results

For every specimen it was calculated the stress distribution (see sample in Figure 5.7). The peak value at the upper notch was observed as well as the principal stress distribution through the thickness at the relevant cross section at the weld toe.

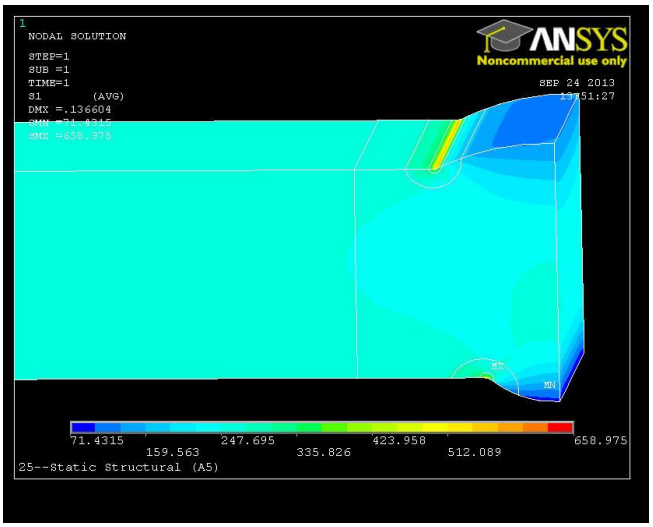

Figure 5.7. Sample of principal stress distribution (t=25mm)

Comprehensive results of the notch stress calculations are presented in the following figures for the various groups of specimens. The principal stress distribution over the plate thickness is plotted at the relevant section at the upper weld toe. The coordinate z starts at the bottom side of the specimen and runs in thickness direction towards the topside.

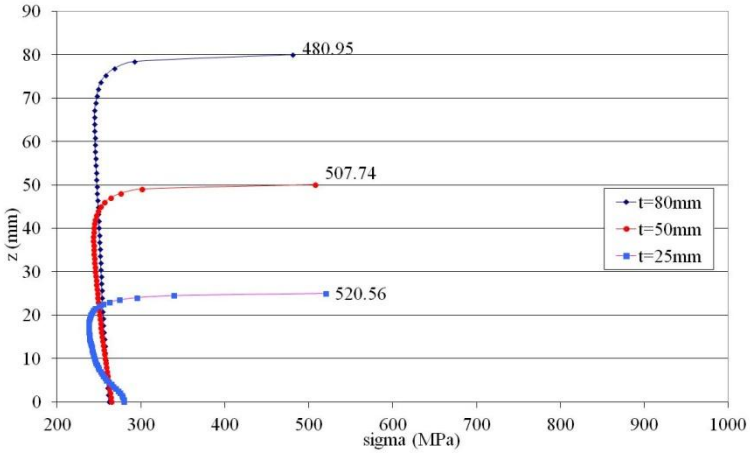

Figure 5.8. Max. Principal stress distribution at the relevant cross section at the weld toe, ‘a’ group

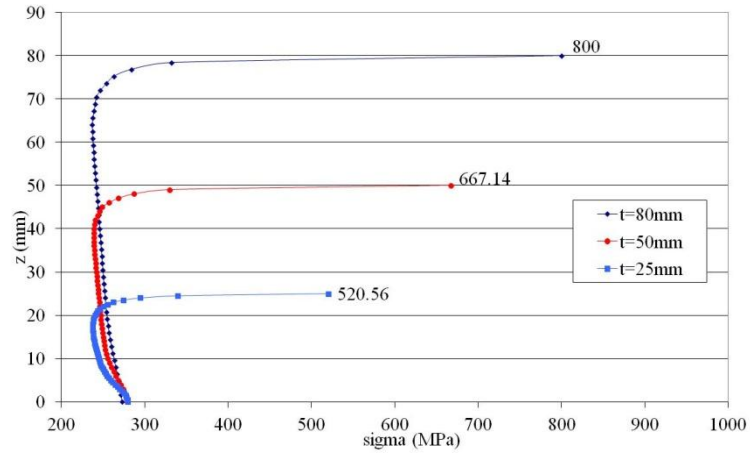

Figure 5.9. Max. Principal stress distribution at the relevant cross section at the weld toe, ‘b’ group

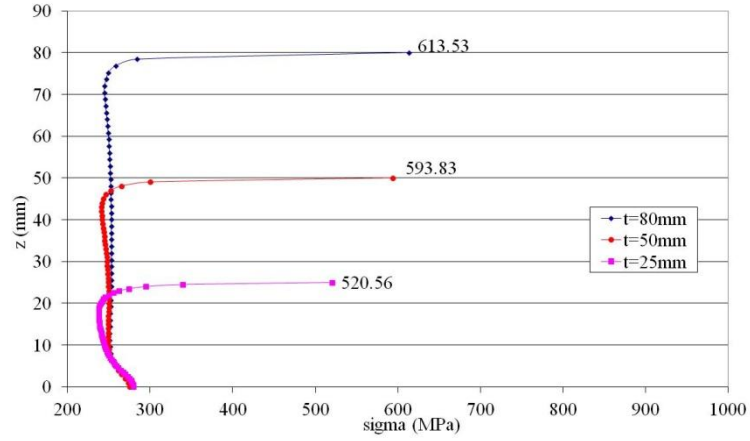

Figure 5.10. Max. Principal stress distribution at the relevant cross section at the weld toe, ‘c’ group

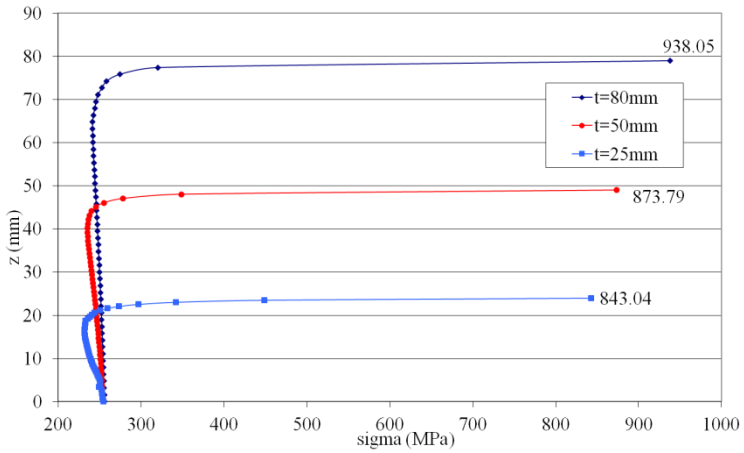

Figure 5.11. Max. Principal stress distribution at the relevant cross section at the weld toe,'d' group

The above figures illustrate the great impact of the weld shape on the stress distribution. The results for the first group show a dependency on the thickness opposite to the expected one since the maximum value of the notch stresses decreases with an increasing plate thickness. This can be explained by the fact that the weld geometries of the specimens were randomly chosen by the actual specimens of the tests. Specifically, examining the detailed geometries of the specimens (Table 5.1) it can be observed that the angle of the upper toe (where the notch stress is calculated) is increasing for thinner specimens. This results in the higher stresses for the thinner specimens. As described in the first part the number of manufacturers is quite high (six different shipyards), and as a result the geometries vary in such extent so to affect the notch stress values. This can be a possible explanation for the not expected results regarding the plate thickness of the first part.

On the other hand, for the three other groups of specimens the stress distribution depends on the plate thickness in the expected way since the maximum value of the notch stresses increases with an increasing plate thickness reflecting the thickness influence. The obtained values vary with the geometry of the reinforcement, with the maximum ones to be observed for the specimens with undercuts, as expected.

The elastic notch stress concentration factor K_t is defined as the ratio of the maximum notch stress σ_k to the nominal stress σ_n, determined under the assumption of linear – elastic material behavior (Radaj D., Sonsino C.M., Fricke W., 2006):

$$K_t = \frac{\sigma_k}{\sigma_n} \tag{5.2}$$

There are various formulas in the relevant literature which predict the value of the factor K_t. In the present study, and in order to evaluate the obtained results, the following is used (Anthes R.J., Köttgen B., Seeger T., 1993):

$$K_t = 1 + \alpha(sin\theta)^{\lambda_1}\left(\frac{t}{\rho}\right)^{\lambda_2} \tag{5.3}$$

where in the case of butt welds under tension α is a coefficient equal to 0.728, λ_1 is an exponent equal to 0.932, λ_2 is an exponent equal to 0.382, ρ is the radius of the notch (in this case equal to 1mm) and θ the weld toe angle.

The results regarding notch stress values and the relevant elastic notch stress concentration factors K_t are presented in the following table (the 'd' specimens are not included in this table since butt welds with undercuts cannot be evaluated with the previous formula):

Table 5.3. Notch stress values and K_t factor (Nominal stress range 254MPa)

Specimen	Stress at upper notch [N/mm^2]	K_t (Eq.5.2)	K_t (Eq.5.3)
25	520	2.05	2.23
50	508	2.00	2.18
80	481	1.89	2.13
50b	667	2.63	2.69
80b	800	3.15	3.39
50c	594	2.34	2.60
80c	618	2.43	2.92

The values of K_t obtained by the FEM analysis match quite well with the ones predicted by the literature, especially for the 'a' and (even more) 'b' group of specimens, while for the 'c' group of butt welds there is a bigger difference in the values. In any case, the general tendency of the result indicated by the equation 5.3 is the same with the one obtained from the analysis.

Further calculations regarding the plate thickness effect were performed, based on the recommendations (Hobbacher A., 2008). The thickness reduction factor f_t is calculated as the ratio of notch stress values for the 25mm specimen over the 50mm and 80mm specimen. The exponent n is calculated from the following equation:

$$f_t = \left(\frac{25}{t}\right)^n \tag{5.4}$$

The value of exponent n given in the recommendations varies between 0.17 and 0.2 (depending on the consideration of misalignments).

The calculation of the expected life time of the specimens is based on the following equation:

$$N = N_D \left(\frac{\sigma_a}{\sigma_D}\right)^{-k} \tag{5.5}$$

where N is the expected life time of the specimen in cycles

σ_D is the fatigue class (FAT) for the specific detail, equal to 225N/mm^2

$N_D = 2 \cdot 10^6$ cycles, where the fatigue class is determined

σ_a is the obtained notch stress value

k = 3

The detailed results are presented in the following table and chart:

Table 5.4. Detailed calculations regarding notch stress approach

Specimen	Stress at upper notch [MPa]	f_t	exponent n	expected life time [cycles]	N_t/N_{25}
25	520	1.00		162020	1.00
50	508	1.02	-0.03	173775	1.07
80	481	1.08	-0.07	204712	1.26
50b	667	0.78	0.36	76772	0.47
80b	800	0.65	0.37	44495	0.27
50c	594	0.88	0.19	108697	0.67
80c	618	0.84	0.15	96519	0.60
25d	843	1.00		38027	1.00
50d	873	0.97	0.05	34240	0.90
80d	940	0.90	0.09	27428	0.72

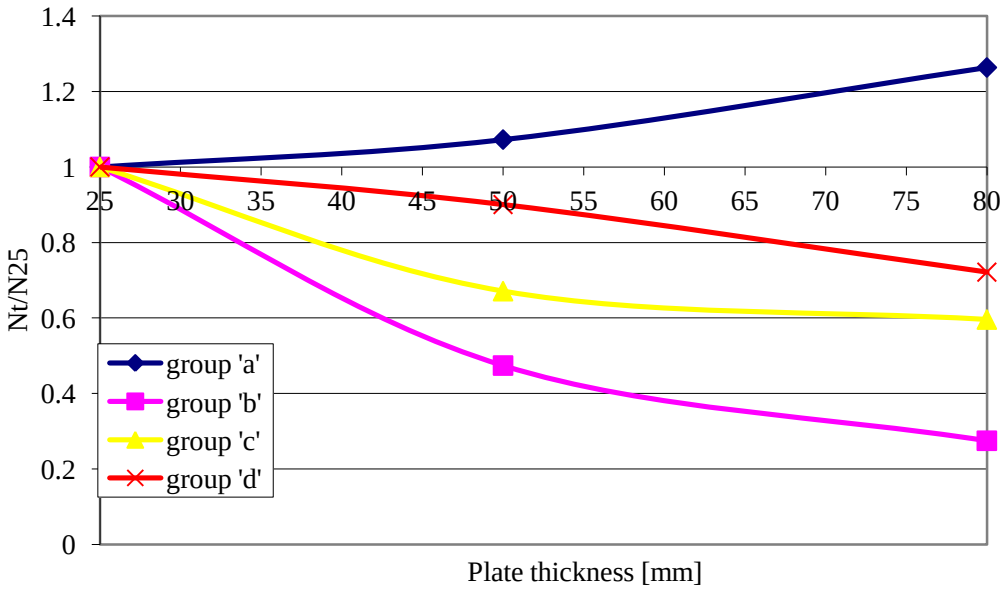

Figure 5.12. Thickness effect calculated by the notch stress approach

The above diagram confirms that the first group of specimens does not follow the expected tendency. According to the relevant literature (e.g. Nguyen N.T., Wahab M.A., 1995), the fatigue life of the welded joints is decreased by increasing the values of the angle of the toe, and this statement verifies the above behavior. On the contrary, the other groups have the expected tendency. More specifically, the obtained values for the exponent n match very well with the ones from recommendations for the group ‘c’, while for the group ‘b’ is higher and for group ‘d’ is lower. Moreover, the relatively high obtained notch stress values for the ‘b’ and ‘d’ specimens lead to shorter life times compared to the ‘c’ specimens.

5.3 Fracture Mechanics Approach

5.3.1 Introduction

In this part, fracture mechanics method is applied in order for the fatigue life of the butt welds to be assessed. Cracks are initiated in the weld toe of the specimens, where stress concentrations occur. In order to calculate the fatigue life of welds and to analyze the propagation progress of the cracks using fracture mechanics approach, an accurate calculation of the Stress Intensity Factor (SIF) is required, which makes the specific factor a parameter of great importance. SIF describes the fatigue action at the tip of the crack in terms of crack propagation, since weld geometry conditions may differ in various weld joints, traditional empirical relations become invalid in some cases and new models may have to be created for the new local stress distribution and to find the accurate SIF calculations.

In this work SIF has been calculated using the FRANC2D, a 2-dimensional crack propagation simulation FEM program. FRANC2D has been proved to be of high accuracy and it predicts the direction of crack propagation by using the maximum normal stress criterion (Al–Mukhart A., 2010).

Initially, the modeling procedure is described using FRANC2D. An investigation regarding the impact of various parameters in the crack propagation calculation is followed. The calculated SIF are used in order for the fatigue life to be evaluated using the Paris equation. Additionally, further calculations are performed using VERB software in order to compare the results and also to utilize the stress profiles obtained from Chapter 3.

Finally, the predicted life times are evaluated and conclusions regarding the thickness effect are derived.

5.3.2 Modelling of the butt welds with FRANC2D

The modelling and the analysis were carried out by the 2-dimensional FE program FRANC2D, developed by Cornell Fracture Group from Cornell University, USA. The specific software is FE – based simulator for curvilinear crack propagation in planar structures. The models were again 25, 50 and 80mm butt weld specimens, similar to the group 'a' – random geometries of reinforcements directly picked from the actual specimens of the tests – and 'b' – sharper notches for thicker specimens - of the previous investigation but with no detailed geometries in the notches (fictitious fillet) because of the inability of the software to model in high detail. The analysis was undertaken with the assumption of isotropic elastic material, same for the base and the weld.

The material used is the high tensile steel YP47, with nominal yield strength of 460 N/mm^2, modulus of elasticity E = 206000 N/mm^2 and Poisson's ratio $\nu = 0.3$.

The applied tensile axial stress was equal to 254 N/mm^2.

The determination of the Stress Intensity Factors (SIF) for the 2-dimensional butt welded joints has been carried out using Linear Elastic Fracture Mechanics (LEFM) analysis, a method well encoded in automatic crack propagation of FRANC2D software. For every crack length, the values of the SIF were calculated during crack propagation steps by FRANC2D program with suitable boundary conditions, loading, crack growth criteria, and crack direction criteria (Al–Mukhart A., 2010).

For the definition of geometry and the generation of the mesh, software CASCA was used which is a pre-processor of FRANC2D. In the present study the FE mesh consists of 8-nodded quadrilateral elements.

The half symmetry of the model was applied (the validation of this assumption will be examined later). The symmetry plane was supported in the x – direction and a uniform stress distribution was applied at the other side along the y – direction. In the supported side, one node was locked in the y – direction in order to prevent the model from performing rigid body motions and rotation (Figure 5.13).

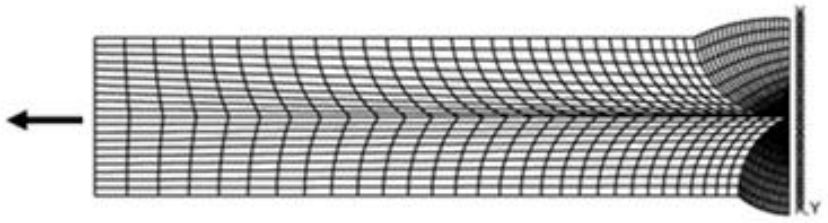

Figure 5.13. Mesh configurations, boundary conditions and applied stress for half butt model

As mentioned before, in order to define the geometry and generate the mesh the program CASCA was used which is distributed together with FRANC2D. It is possible for the mesh to be generated by other software, as long as a translator is available to convert the mesh description to a format compatible to FRANC2D (Wawrzynek P., Ingraffea A., 1993). The procedure of creating the geometry and the mesh of the model is simple and straightforward (Figure 5.14). Initially, the outline is created and then it is divided in sub-regions (a). Next, the boundaries of the sub-regions are divided in the desirable number of segments (b). Finally, the assigning of the type of elements and the meshing of the geometry is carried out (c).

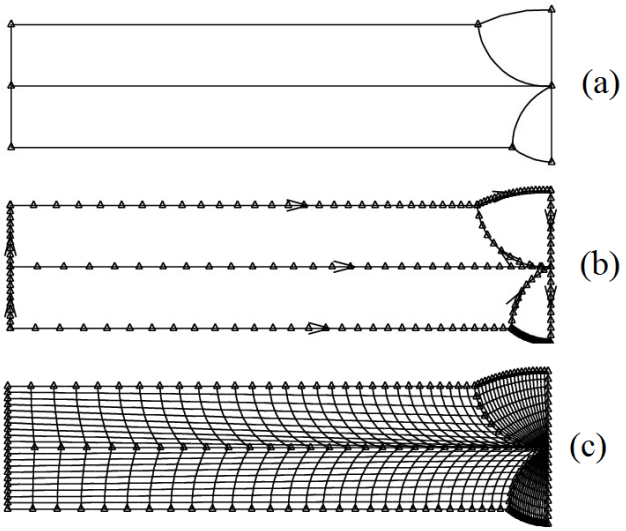

Figure 5.14. Generation of geometry and mesh of the 25mm butt weld model (CASCA program)

Regarding the crack propagation, in the butt welds a crack can initiate from either the weld toe or the root, since these are the locations where the maximum stress concentrations are observed. On the present work, the calculations were made for cracks initiating from the toe, based on the fact that, according to relevant literature (Smith I.F.C., Smith R.A.,1983), this occasion is dominant, and also because this is the case on the specimens of the test described in Chapter Three (see subsection 3.5).

The software starts the simulation of crack growth by placing a non-cohesive edge crack of specific initial length a_{in} at the weld toe of the butt weld, in the interface between weld and base material, i.e. the location where critical tensile stresses is predicted to occur. The existence of such crack-like imperfections results in the elimination of the first stage of fatigue life, the crack initiation stage so the fatigue assessment is focused on the stage of crack growth. After determining the location and the initial length, the user needs to define the magnitude of the crack increment Δa and the number of the crack propagation steps (see sub-section 5.3.4). The crack propagation mode was chosen to be automatic, meaning that the crack path was not defined but the direction was being modified according to the program's prediction, based on the direction of maximum hoop stress around the crack tip (Wawrzynek P., Ingraffea A., 1993). There is also the possibility of manual propagation, in which the user needs to define the new location step by step. While the crack is propagating, the mesh around the tip is re-configured automatically. The above described procedure is presented in the following figure:

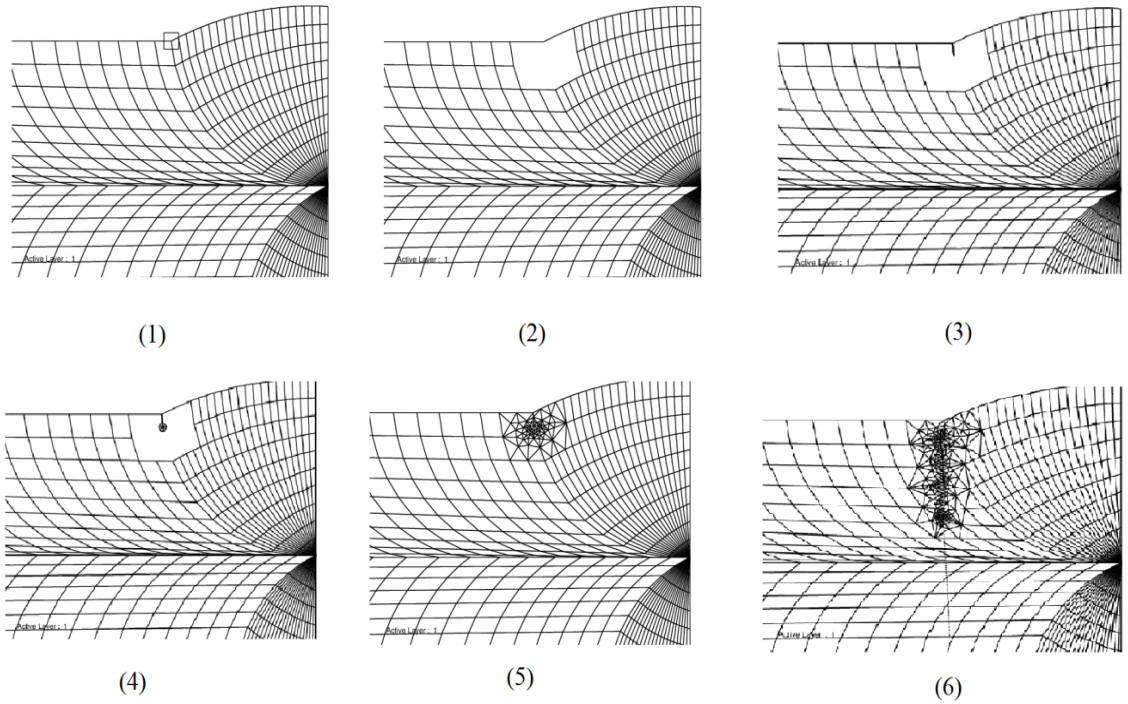

Figure 5.15. Crack growth performed by FRANC2D: 1)selection of the location of the crack initiation, 2)delete of the nearby mesh, 3)selection of the length and angle of the crack, 4)meshing near the tip of the angle, 5)meshing of the nearby area, 6)automatic propagation

5.3.3 Calculations of Stress Intensity Factors (SIF) and Crack Propagation Life

The main expression for the calculation of SIF was given in section 2.4 (Eq. 2.4). In this formula, Y is a correction function that depends on the specific specimen geometry. It is a function of the crack length to thickness ratio *f* (*a*/*t*). The secant type of analytical expression for *f* (*a*/*t*) is given by the following equation (Shukla A., 2008):

$$Y = f(a/t) = \left(sec\frac{\pi\alpha}{2t}\right)^{1/2} \tag{5.6}$$

In the present study, FRANC2D was used to calculate the opening mode SIF using fracture mechanics approach where the stress ranges were fully effective (i.e., the crack remains open during the propagation period where the initiation time is discarded). The influence of K on fatigue crack growth was based on the maximum tangential stress criterion (Erdogan F., Sih G.C., 1963). This criterion assumes that the predicted propagation path of the fatigue crack is perpendicular to the maximum principal stress and the crack grows under opening mode and stress ranges were fully effective (Nykänen T., X. Li, Björk T. Marquis G., 2005 and Al–Mukhart A., 2010).

For the validation of the prediction results, the range of SIF for the welded specimens was calculated using the following empirical equation (Broek D., 1968):

$$\Delta K = \Delta\sigma\sqrt{\pi a}(1.12 - 0.23(a/t) + 10.55(a/t)^2 - 21.72(a/t)^3 + 30.39(a/t)^4) \tag{5.7}$$

where $\Delta\sigma$ is the stress range, *a* is the crack length and *t* is the thickness of the plate. The results from the above equation were used in order to validate the ones obtained by FRANC2D.

Regarding the crack propagation life calculations, in order for FRANC2D to determine the number of cycles N until failure, the Paris equation (Eq. 2.6) is used. Specifically, integration of the equation is performed between the initial crack length a_{in} up to the final length a_f:

$$dN = \frac{da}{C(\Delta K)^m} \rightarrow \int_0^N dN = \int_{a_{in}}^{a_f} \frac{da}{C(\Delta K)^m} = \frac{1}{C}\int_{a_{in}}^{a_f} \frac{da}{[Y\Delta\sigma(\pi a)^{1/2}]^m} \tag{5.8}$$

In the above equation, the expression of ΔK was used (Eq. 2.4).

Finally, the number of cycles for one increment is (Al–Mukhart A., 2010):

$$N = \frac{1}{CY^m(\Delta\sigma)^m\pi^{m/2}} \frac{\left[a_{in+1}^{\left(1-\frac{m}{2}\right)} - a_{in}^{\left(1-\frac{m}{2}\right)}\right]}{1-\frac{m}{2}} \tag{5.9}$$

In the previous equation the geometry factor Y is not included as a function of crack length over thickness (a/t), but as a constant. Otherwise it would lead to a form which is not able to be solved analytically. Nevertheless, Y constantly changes while crack propagates, thus the integration in any case cannot be performed analytically. Hence, the SIF is estimated numerically by using the FEM and then, accordingly to the calculated SIF, the fatigue life is evaluated.

5.3.4 Influence of Various Parameters

In this sub-section the influence of various parameters in the crack growth calculations performed by FRANC2D will be examined.

- Initial, a_{in} and final, a_f length of crack:

Fracture mechanics approach assumes an already existing deflection of specific initial length a_{in}. This crack can be used to predict fatigue life and strength of the growth of the crack to its final size a_f. For welds in structural metals, crack initiation occupies only a small fraction of the life and it can be assumed negligible (Alam M.S., 2005). These deflections are not physical cracks, generated during the welding procedure, but they must be regarded as fictitious ones, initiated in specific locations of high stress concentration in order for the LEFM to be able to describe the fatigue mechanisms. It is therefore difficult to relate the derived model to actual detected flaws in the weld. Furthermore, the initial cracks are often so small that LEFM is not applicable. Initial cracks used in fatigue analyses are often in the range of 0.05-0.2 mm, while initial crack, a_{in} is usually measured or approximated to 0.1-0.2 mm for welds (Al–Mukhart A., 2010). For the present study, the value of a_{in}=0.2mm was applied, inspired by similar studies (Nykänen T., X. Li, Björk T., Marquis G.,2005) and recommendations (BSI, 2005), while further investigation was performed for larger values (a_{in}=1 and 1.5mm) in order to demonstrate the impact of the specific parameter in the obtained life time of the specimen.

Regarding the final length of the crack, for the present study it was applied the concept which assumes the life of the component to be finished when the length of the crack is equal to the one-half of the sheet thickness (Lindqvist J., 2002. Al–Mukhart A., 2010). In any case, the final length of the crack does not have a significant impact on fatigue life.

- Size of meshing:

The specific parameter is very important in all the FE calculations, since it has a great impact on the computational time. Though in the present study and because of the small size of the models there was no such problem. There is no specific guideline regarding the appropriate size, ratio or density of the mesh but just recommendations such as need for finer mesh in the notches and the locations of high stress concentrations. Nevertheless, a small investigation regarding the impact of the mesh took place, in which fatigue crack growth calculations for the 25mm butt weld were performed, with a_{in}=0.2mm and Δa=0.5mm. It was observed no actual difference in SIF's calculations with the improvement of the mesh (Figure 5.16) and as a result it was decided the application of coarse mesh for the remaining calculations.

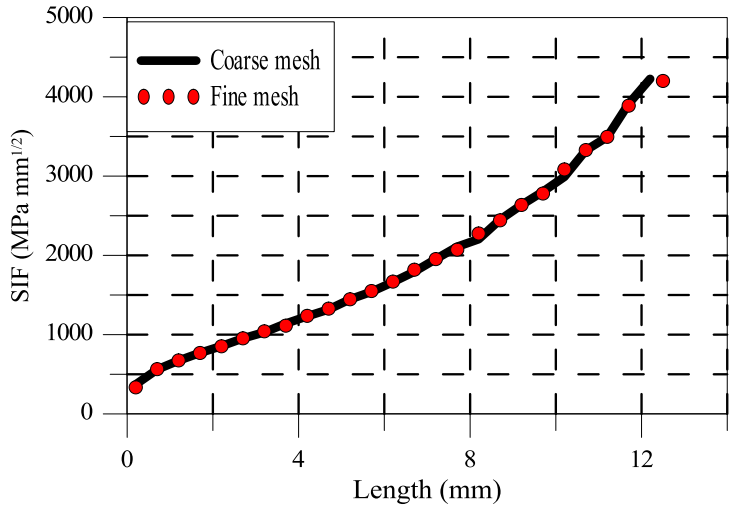

Figure 5.16. Effect of mesh density in the convergence of the results for crack growth calculations

- Crack increment Δa:

The crack increment Δa defines the size of the step for crack propagation and can affect the results, since for very big increments there will be loss of accuracy, while for very small step the computational time over – increases. Investigation of this parameter took place, by calculating the SIF for a crack propagation in the 25mm butt weld with a_{in}=0.2mm and two different crack increments of 0.2 and 0.5mm.

As it can be observed from Figure 5.17, there is no influence on the results and so it was decided the application of the bigger crack increment in the rest of the calculations.

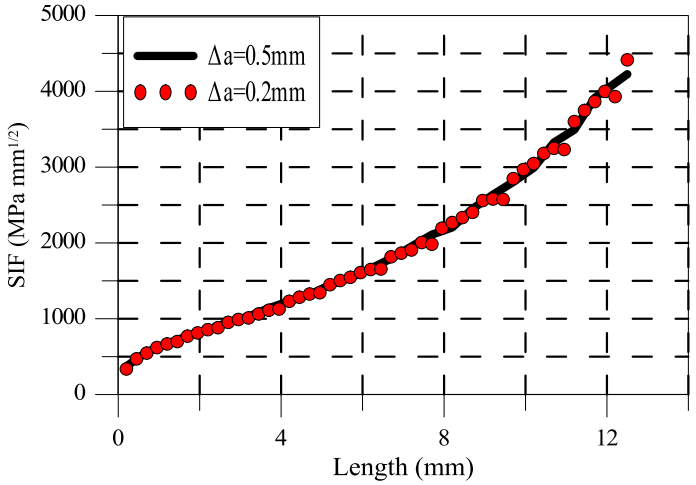

Figure 5.17. Effect of crack increment in the convergence of the results for crack growth calculations

- Effect of symmetry:

Butt weld specimen is symmetrical about the y – axis and this is considered as an advantage since it can reduce the size of the models. The comparison between the calculations performed in whole and in half butt weld model (Figure 5.18) (for a_{in}=0.2mm and Δa=0.5mm) proved that there is no significant difference in the obtained SIF's results. Therefore, the half symmetry of the model is considered as a reasonable approximation and it was decided to be applied for the next calculations.

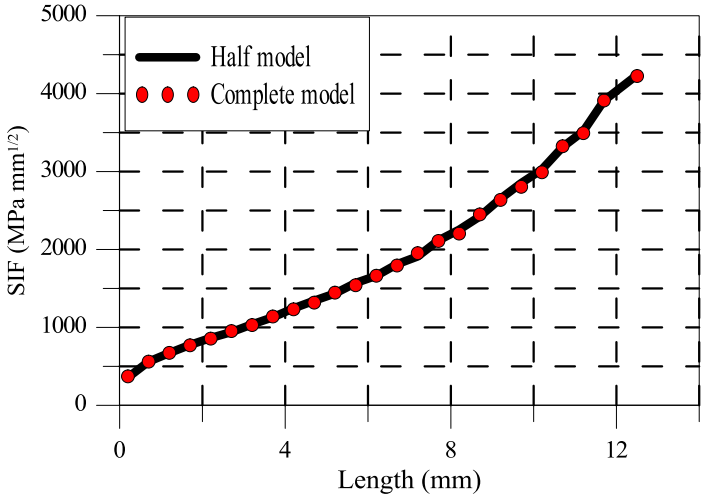

Figure 5.18. Effect of symmetry in the convergence of the results for crack growth calculations

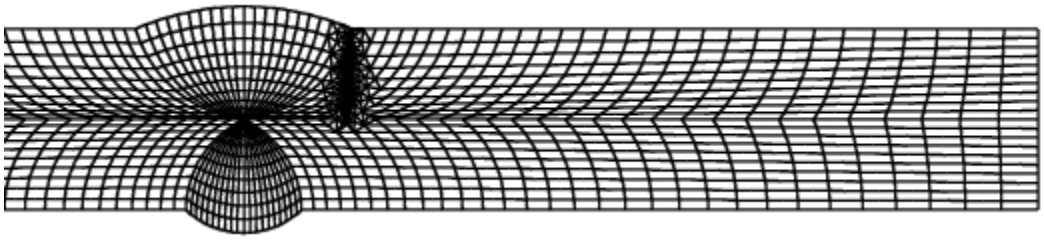

Figure 5.19. Final crack in the complete 25mm butt weld model

- Location of the crack initiation:

In every butt weld there is the upper and the lower reinforcement, which both considered as notches where stress concentration is observed, and therefore a potential location for a crack to initiate. The differences between the initiation of the crack in upper and lower notch were examined.

At first, the stress concentration in the two notches was calculated, for the 25mm butt weld model under 254MPa of tensile stress (Figure 5.20).

The stress distributions through thickness in the relevant sections of the two notches from the FRANC2D calculations were plotted and compared with the ones obtained from the ANSYS for the same model (Figures 5.21-5.22). Additionally, the SIF results for the two propagations (from upper and lower notch for a_{in}=0.2mm, Δa=0.5mm) were also plotted (Figure 5.23).

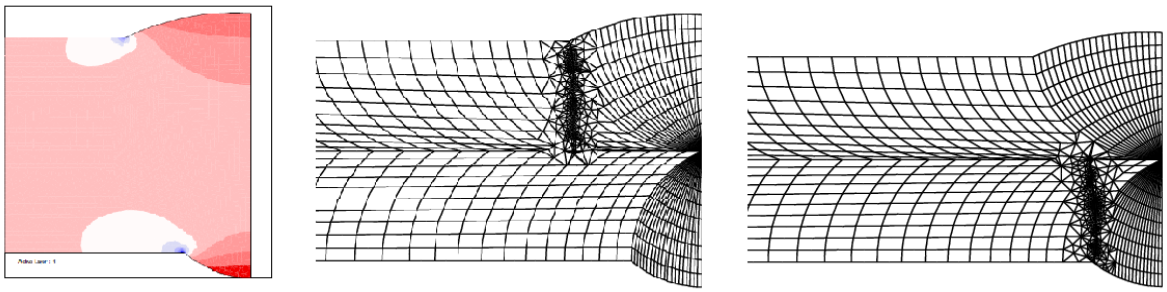

Figure 5.20. Stress distribution calculated by FRANC2D and crack propagation

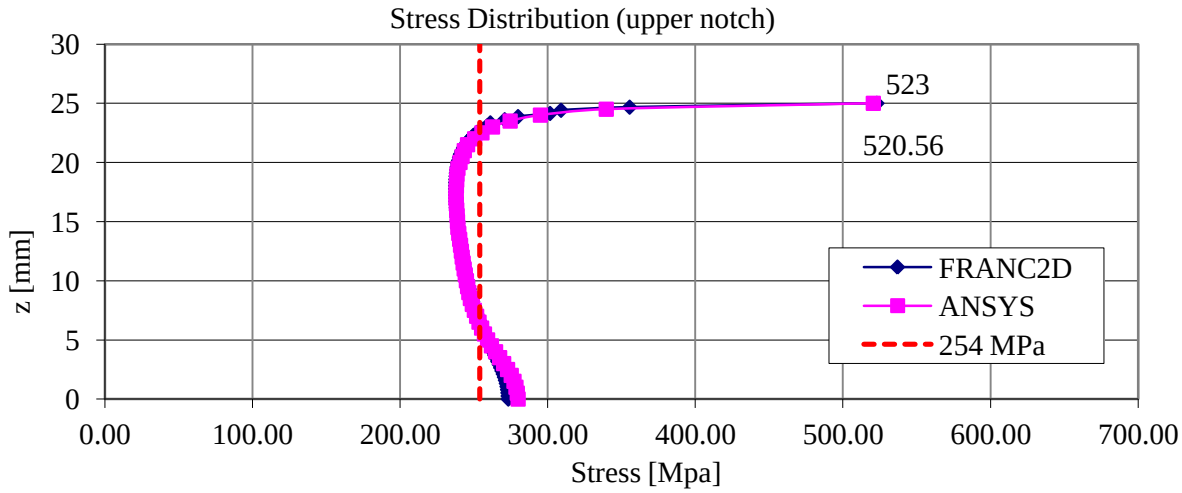

Figure 5.21. Stress distribution in the relevant section of the upper notch

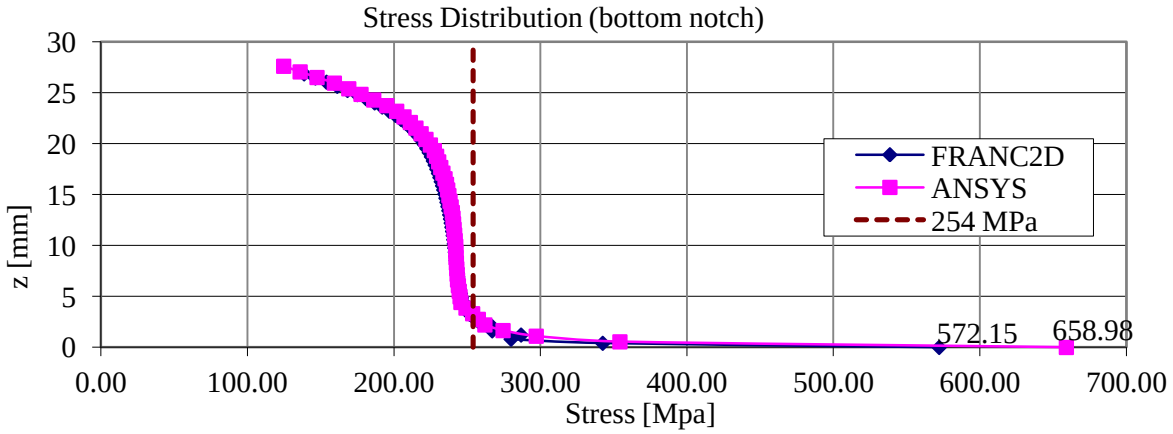

Figure 5.22. Stress distribution in the relevant section of the bottom notch

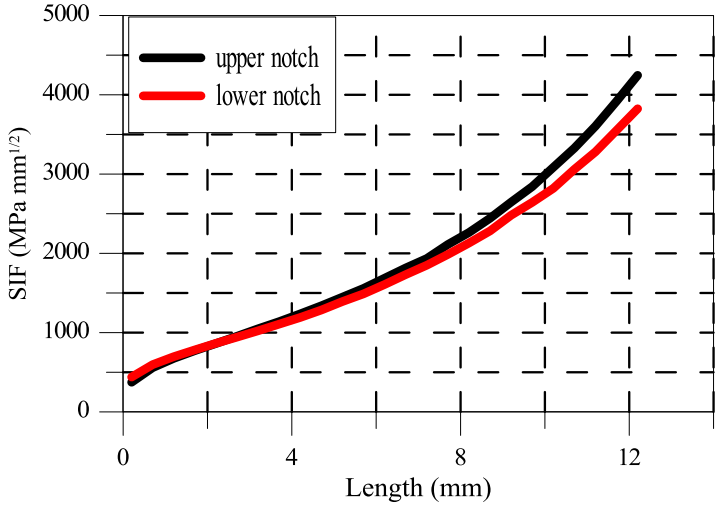

Figure 5.23. SIF values for crack propagations initiating from the upper and lower notch

From the above figures it can be observed that in the lower notch the stress concentration is higher than the upper one, due to the fact that the geometry in the bottom reinforcement (Table 5.1 for the 25mm specimen) creates a sharper notch than in the upper part (bigger angle θ). Moreover, regarding the results from the two programs (ANSYS – FRANC2D), though they almost match for the upper notch, in the case of the lower notch it can be observed a significant difference in the notch stress value. This happens because of the difference in the modeling of the geometry of the reinforcement, since, as mentioned before, the model in FRANC2D does not contain high details (fictitious rounding etc).

Finally, from Figure 5.23 it can be seen that in the last parts of the propagation the obtained SIF values are higher in the case of upper notch. This can be explained by the fact that when crack initiated from the bottom, while it propagates it reaches the upper reinforcement (Figure 5.20), so the remaining section is bigger than when it initiates from the upper and since SIF is highly dependent on the local geometry, the obtained results are different.

For the remaining calculations, it was decided that the crack initiates from the upper notch since (and due to the higher obtained SIF values) it was considered as the less safe situation.

5.3.5 Verification of the FRANC2D results

In order to verify the results for the SIF of the 25mm but weld obtained from FRANC2D, a comparison with the ones obtained by the empirical solution (Eq.5.7) takes place (Figure 5.24). As it can be seen, the results match well.

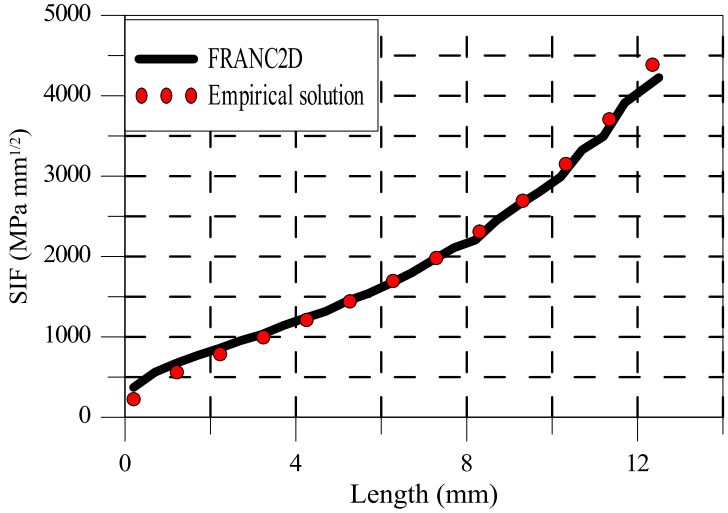

Figure 5.24. Comparison between results obtained from FRANC2D and empirical solution (Eq. 5.7) for butt weld of t=25mm, a_{in}=0.2mm, Δa=0.5mm and Δσ=254MPa

5.3.6 Results for group 'a' of the specimens

The results from the crack growth calculations for the 'a' group (see Table 5.1) of butt welds of 25, 50 and 80mm performed by FRANC2D are presented below.

At first, the distribution of stresses was calculated. For the 25mm butt weld, the stress on the upper notch before the initiation of the crack was found equal to 523 N/mm^2 (Figure 5.25).

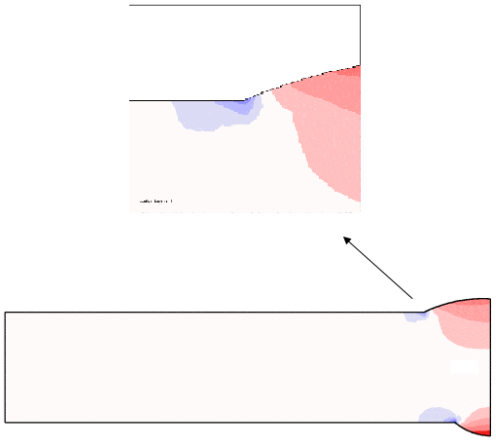

Figure 5.25. Stress distribution at the 25mm butt weld and stress concentration location without crack

At this moment, the crack of a_{in}=0.2mm is initiated at the upper notch (Fig.5.26, from left to right: a) selection of the location of the crack, b) delete of the nearby mesh, c) selection of the tip of the crack (length, angle), d) re-mesh of the nearby area).

The local stress will be affected by the presence of the crack; in the tip of the crack the stress will reach the value of 1599 N/mm^2 (Figure 5.27).

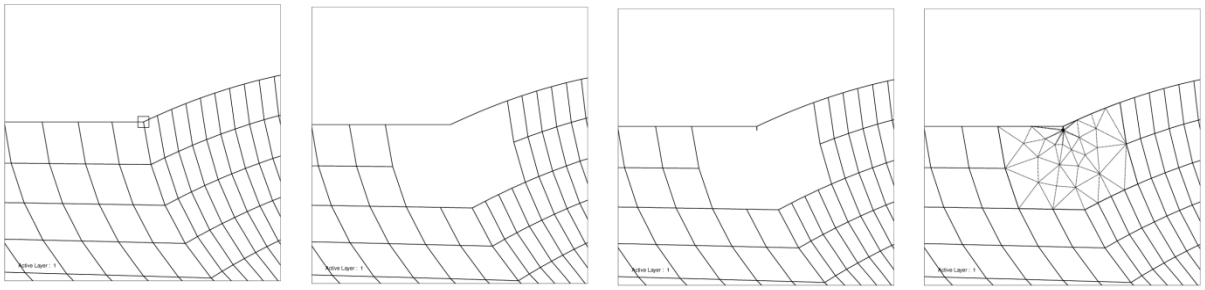

Figure 5.26. Initiation of an edge crack of a_{in}=0.2mm at the upper notch,

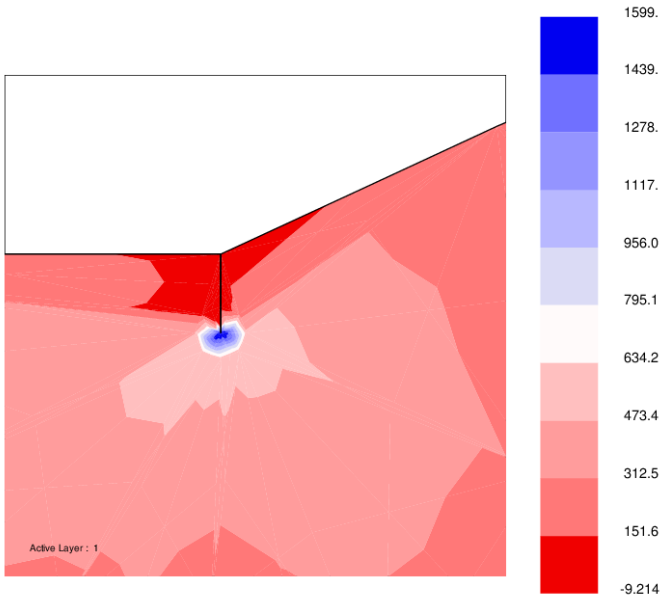

Figure 5.27. Stress distribution after the initiation of a crack of 0.2mm length

The crack will propagate in the automatic mode as described before – the direction of the path is calculated for every step by the program – until the final length of the crack a_f reaches the half of the thickness of the specimen (Figure 5.28).

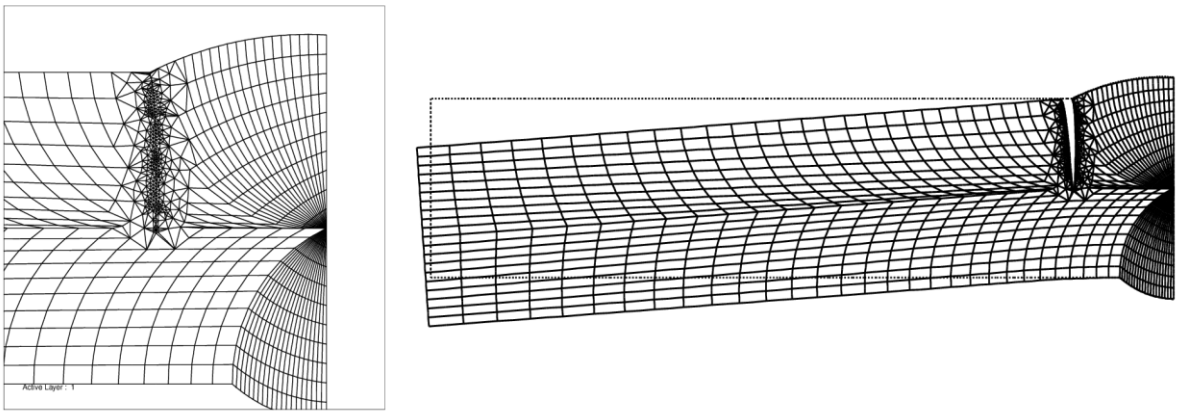

Figure 5.28. Final crack and deformation of the 25mm butt weld

For the specific crack propagation, FRANC2D calculates the values of SIF (Figure 5.29):

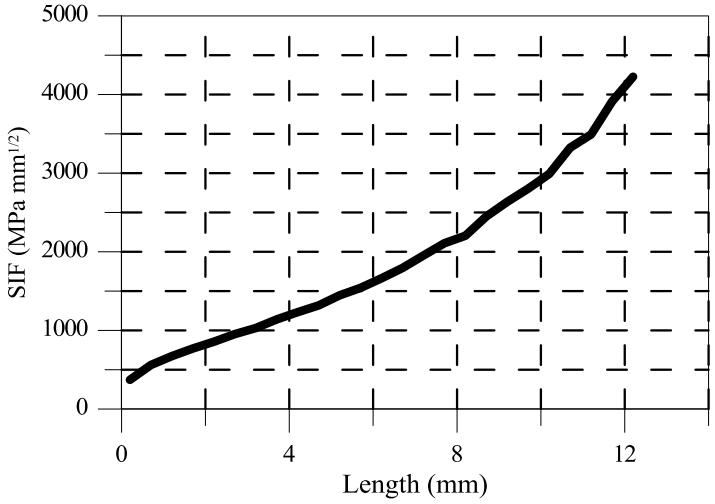

Figure 5.29. SIF values for the crack propagation in the 25mm butt weld

After the calculation of the SIF, FRANC2D uses Paris equation (Eq.5.8) in order to calculate the fatigue life of the specimens. As explained in the user's guide of the software (Wawrzynek P., Ingraffea A., 1993), the specific equation is very simple and may not be appropriate for some materials, nonzero load ratios, and very high or very low SIF ranges. Moreover, the simple application of Paris equation does not take into account the effects of residual stresses and crack closure, where the latter effects are being included within the stress ratio *R*. Thus, in many cases, it is more appropriate to calculate the extract SIF vs. crack length history within FRANC2D, and use this information with a more sophisticated growth model. Nevertheless, in the context of the present study the accuracy of the results is considered satisfactory.

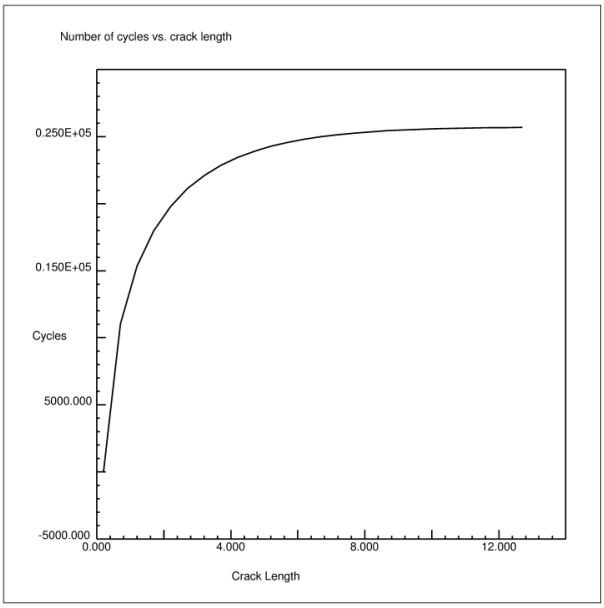

Figure 5.30. Life time of 25mm butt weld

Initially, the values for the parameters C and m of the Paris equation are the ones suggested by the International Institute of Welding (Table 2.1). The fatigue life of the 25mm is plotted in the diagram of Figure 5.30.

Similar procedure is performed for the 50 and 80mm butt welds. The obtained stress distributions through thickness in the relevant cross section of the upper notch are presented in the below figure:

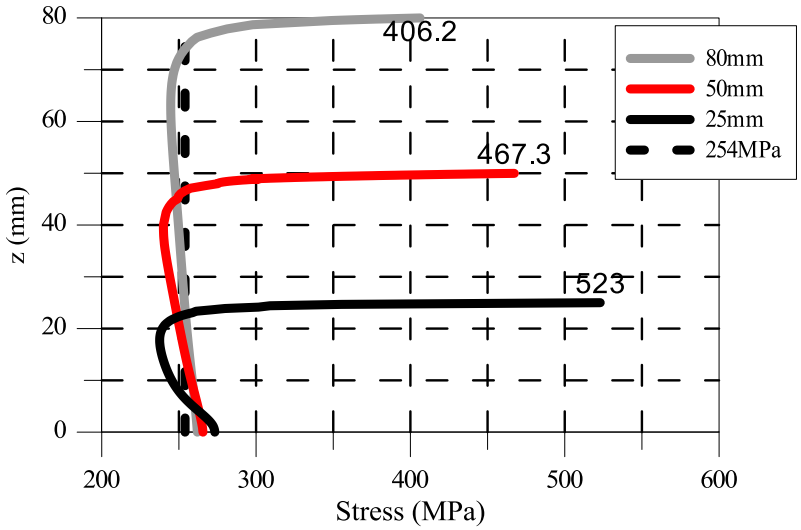

Figure 5.31.Max. Principal stress distribution at the relevant cross section at the upper weld toe

From the above, it can be observed that the notch stresses follow a tendency opposite to the expected which is the one based on thickness effect. This behavior is similar to the one observed in Figure 5.8 of the previous section, where same calculations were performed from

the ANSYS software. Generally, and as explained before, the results from ANSYS give higher and more accurate results, since the models contain more detailed geometry of the notches. The similarity in behavior is expected, since the geometry of the notches is the same (group ‘a’ specimens).

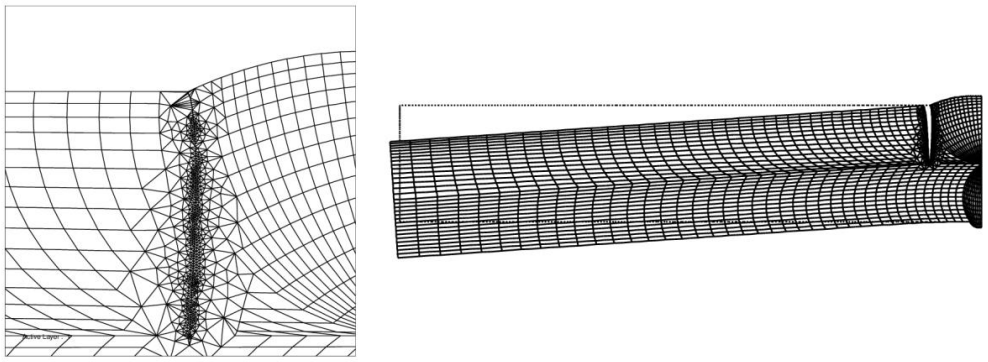

Figure 5.32. Final crack and deformation of the 50mm butt weld

Cracks of a_{in}=0.2mm are initiated in upper notches of the 50 and 80mm specimens and crack propagation occurs until the length becomes equal to the half of the thickness (Figure 5.32).

The obtained SIF values for the crack propagation in the 50 and 80mm butt welds are plotted in the following figure. The SIF values of the initial crack at the notch are marked on the graph.

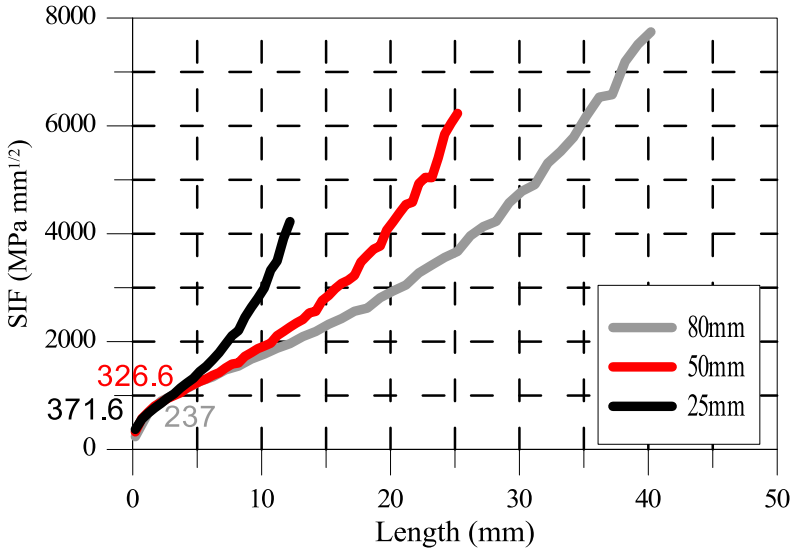

Figure 5.33. SIF values for the crack propagation in the 25, 50 and 80mm ‘a’ butt welds

The SIF for the initial crack in the regime of the notch is higher for the 25mm, followed by the one for 50mm and the smallest is for the 80mm. It can be explained by the fact that the geometry of the reinforcement for the thinner specimen creates sharper notch, and additionally the 25mm model is the one which shows the higher stress value in the notch. Both these parameters (geometry – stress) affect the SIF value (Eq.2.4). For longer cracks, the

SIF increases as expected since the stresses in the tip of the crack also increase. Important is the fact that for same length of crack (e.g.12.5mm) the SIF for the 25mm is much higher. This can be explained by the fact that SIF is strongly linked with the geometry of the specimen and especially with the thickness (Eq.5.7).

Using again the Paris equation and the recommended values for C and m, FRANC2D calculates the lifetimes for the 50 and 80mm butt welds which are found equal to 27000 and 32000 cycles respectively, longer than the one for the 25mm (25000 cycles, Fig.5.30). The specific results are in accordance with the notch stress approach results (Fig.5.12-a) which show reverse tendency to the one expected because of the thickness effect. The explanation is the same: the geometry of the reinforcements of the specimens is proved to be of great impact – sharper notch in the 25mm butt weld ('a' group of specimens) leading to higher SIF values which results in smaller fatigue life.

Similar calculations of fatigue life time have been performed with FRANC2D for longer initial cracks a_{in}=1.0 and 1.5mm. Additionally, the fatigue life of the butt welds with cracks of a_{in}=0.2mm was calculated but this time the C parameter of the Paris equation was not the one recommended by IIW ($5.21 \cdot 10^{-13}$), but the one calculated in the previous chapter for m=3: $C=1.79 \cdot 10^{-13}$ (SIF in [$N \cdot mm^{-2/3}$], da/dn in [mm/cycle]). Though the specific values are corresponding to the material E40 with nominal yield strength of 408 N/mm^2 and not the one used in the present model (YP47, nominal yield strength of 460 N/mm^2), the idea is that still it might match better than the values given from IIW, which are for mild steel. In any case, it should be noted that these results should be considered as less conservative than the ones calculated with IIW recommendations.

The results are summarized in the following table and diagram:

Table 5.5. Fatigue life (cycles) of butt welds of different thicknesses for various parameters

thickness of specimen	C=5.21E-13, m=3 (IIW)			C=1.79E-13, m=3
	a_{in}=0.2mm	a_{in}=1mm	a_{in}=1.5mm	a_{in}=0.2mm
25	25000	11600	8400	72000
50	27000	13600	11000	84000
80	32000	15000	13000	96000

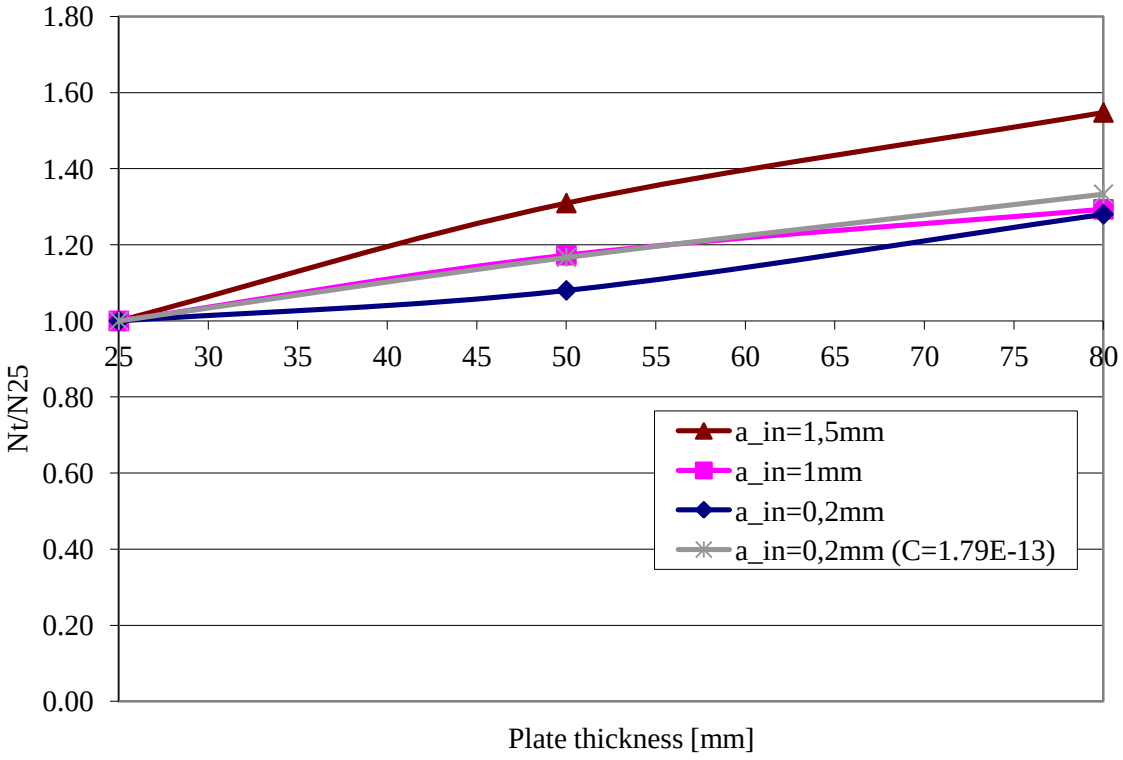

Figure 5.34. Thickness effect of group 'a' specimens – Fracture mechanics approach

The obtained values of fatigue life for longer initial cracks follow, as expected, the same tendency as the one for a_{in}=0.2mm: longer lifetime for thicker specimens, opposite to the thickness effect. For longer initial cracks the life time decreases rapidly, as expected, since with bigger cracks the crack propagation time which is needed in order for the crack to reach the critical length is decreasing. Finally, when the life time is calculated with the parameter $C=1.79 \cdot 10^{-13}$ (m=3) of the Paris equation, the obtained results are much higher (but still following the same tendency). As commented before, these values are considered less conservative. They should be used more as an indication that the IIW parameters possibly lead to too conservative results, rather than directly applied in real cases.

5.3.7 Results for group 'b' of the specimens

Similar calculations were repeated for the 'b' group of butt welds (Table 5.1). The summary of the results is presented in this sub-section.

As seen before (Fig.5.9), the notch stresses are higher for the thicker specimens in this case. Also, the notches for the thicker specimens are sharper. All these lead to the following obtained values for SIF for a crack propagation with a_{in}=0.2mm:

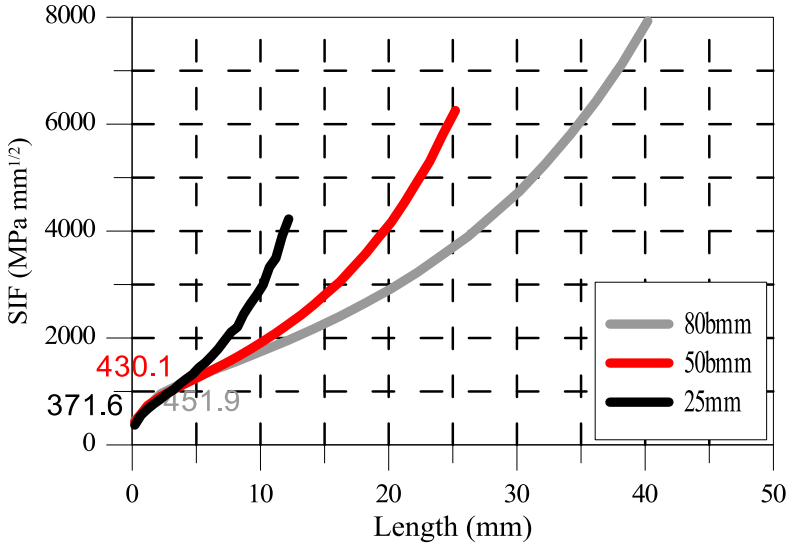

Figure 5.35. SIF values for the crack propagation in the 25, 50 and 80mm 'b' butt welds

Compared to the previous case for the 'a' specimens (fig.5.33), it can be observed a similarity in the obtained results through the crack propagation. The difference is located in the SIF values of the regime of the notch (i.e. for the beginning of the propagation), where now it is higher for thicker specimens. Using as before the Paris equation with the recommended from IIW values for C and m, FRANC2D calculates the fatigue life of the specimens (Figure 5.36). Obtained fatigue life times follow the expected tendency, regarding the thickness effect: shorter life times for thicker specimens.

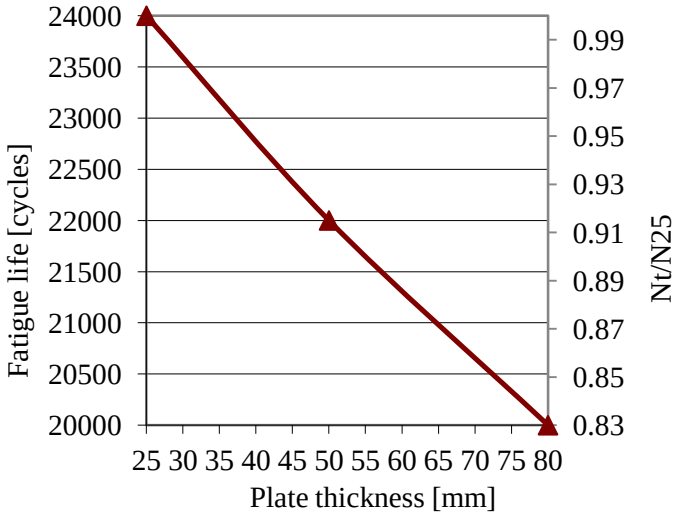

Figure 5.36. Life time and thickness effect for 'b' group butt welds – Fracture mechanics approach

5.3.8 Results from VERB

Further fracture mechanics calculations were performed by software VERB. Details about the specific software can be found in section 4.3. The computational model used in VERB was this of a plate with extended surface crack (Fig.5.37), which simulates a crack similar to the one simulated by FRANC2D. The solution method used by VERB for the specific computational model can be found in the relevant Appendix.

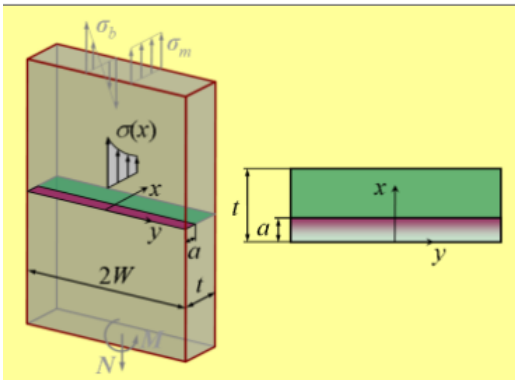

Figure 5.37. Model of VERB: plate with extended surface crack

Initially, in order to check the compatibility of the obtained results between FRANC2D and VERB, a simple case was examined. A basic geometry of t=25mm without any notches was modeled in FRANC2D (Fig.5.39) and calculations were performed in VERB for a constant stress range of $\Delta\sigma$=254 N/mm^2. The obtained SIF results from the two different programs match (Fig.5.38), leading us to the conclusion that the models for the two different programs have been set correctly.

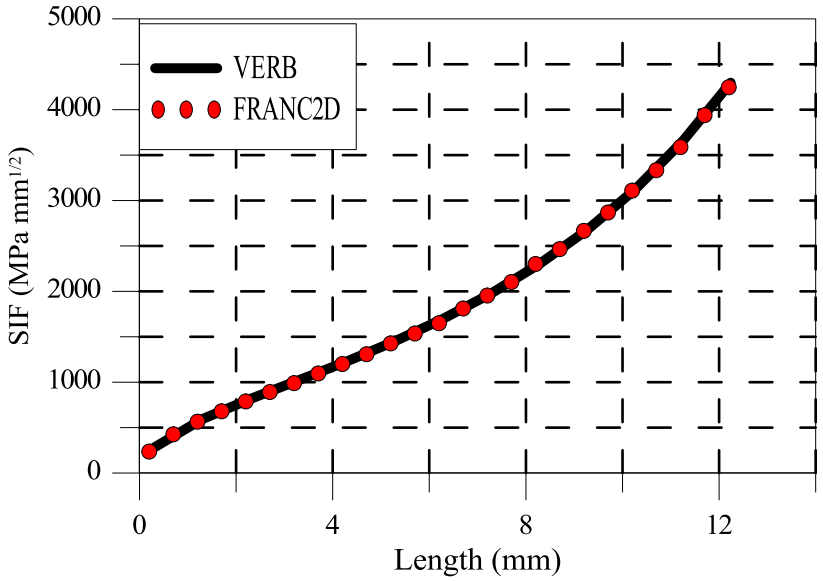

Figure 5.38. Comparison of SIF results between VERB and FRANC2D for 25mm simplified geometry

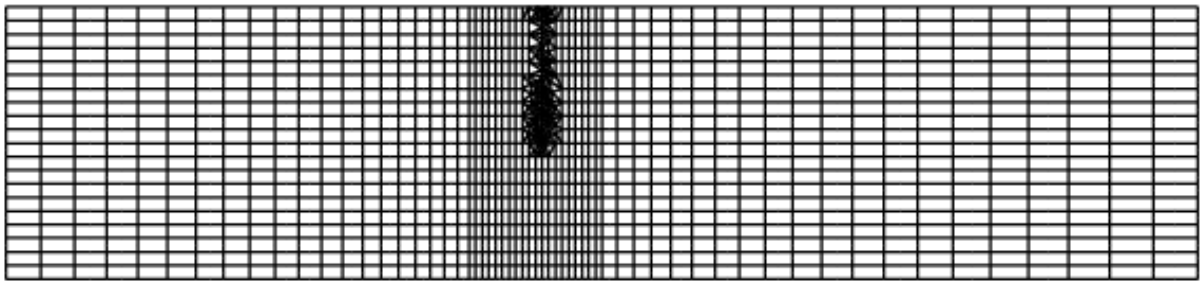

Figure 5.39. Simplified geometry of FRANC2D model

Next, the above results of VERB calculations (constant stress range Δσ=254MPa) are compared with the one previously calculated from FRANC2D for 'a' group of specimens (Table 5.3) for various initial crack lengths and for C and m parameters the ones recommended from IIW. They are presented in the following table:

Table 5.6. Comparison of results for fatigue life (cycles) between FRANC2D ('a' group) and VERB (Constant stress range Δσ=254MPa)

thickness of specimen	FRANC2D			VERB		
	a_{in}=0.2mm	a_{in}=1mm	a_{in}=1.5mm	a_{in}=0.2mm	a_{in}=1mm	a_{in}=1.5mm
25	25000	11600	8400	53000	15000	10000
50	27000	13600	11000	59000	19000	13000
80	32000	15000	13000	63000	21000	16000

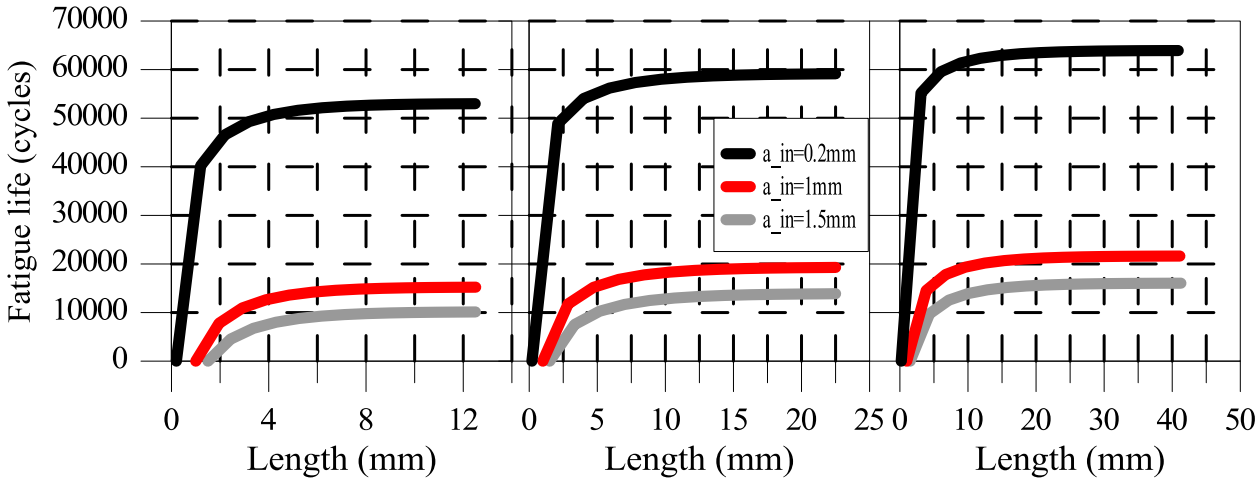

Figure 5.40. Fatigue lives for various initial crack lengths for 25mm (left), 50mm (centre) and 80mm (right) butt welds, calculated by VERB (Δσ=254MPa, constant)

The difference in values between the computer codes is bigger for the short initial cracks (e.g. fatigue life of 25mm with crack of initial length a_{in}=0.2mm is calculated equal to 25000 cycles by FRANC2D and 53000 cycles by VERB – over double value). It can be explained by the fact that the shorter the initial crack, the closer to the notch. This means that the tip of the crack is located closer to the higher stress concentration area. Since in the above calculations VERB did not include a stress profile but a constant stress range, it did not take into account

the notch stress and the result is this difference in the obtained values, which decreases for longer initial cracks because the notch effect weakens. The absence of stress profile is also the reason for not observing the thickness effect in the results from VERB.

A final set of calculations was performed by VERB. This program cannot model specific geometries (like the reinforcement of a butt weld) but, instead, it uses predefined ones such as plates, cylinders etc. In order to include the effect of the notch in the calculations, the stress is now inserted not as a stress of constant range, but as a stress profile – the one obtained by the calculations of ANSYS. Specifically, the profile obtained for the 'c' group of specimens (fig.5.9) is selected, since it was the one which led to the expected fatigue life results, according to notch stress approach.

The results regarding the expected fatigue life for an initial crack of a_{in}=0.2mm for the various thicknesses of specimens are presented in Figure 5.41 (in the left vertical axis as a number of cycles while in the right one as a ratio over the fatigue life of the 25mm specimen, N_{25}). At this case, thickness effect can be observed. The obtained values for the fatigue life are smaller in comparison with the ones calculated from the notch stress approach (table 5.3), which is reasonable since in fracture mechanics only the crack propagation phase is taken under consideration.

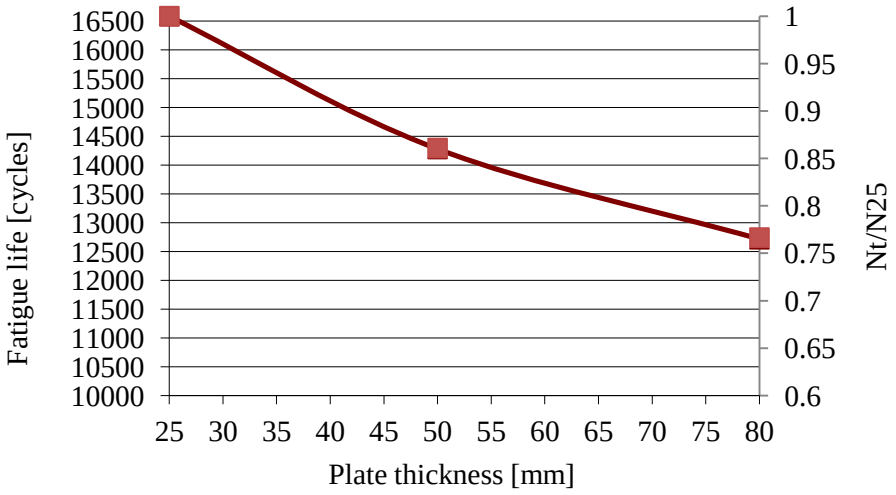

Figure 5.41. Life time and thickness effect for 'c' group butt welds – calculations made by VERB with stress profile obtained by ANSYS

The overall results for cracks with initial length a_{in}=0.2mm are plotted in the following diagram:

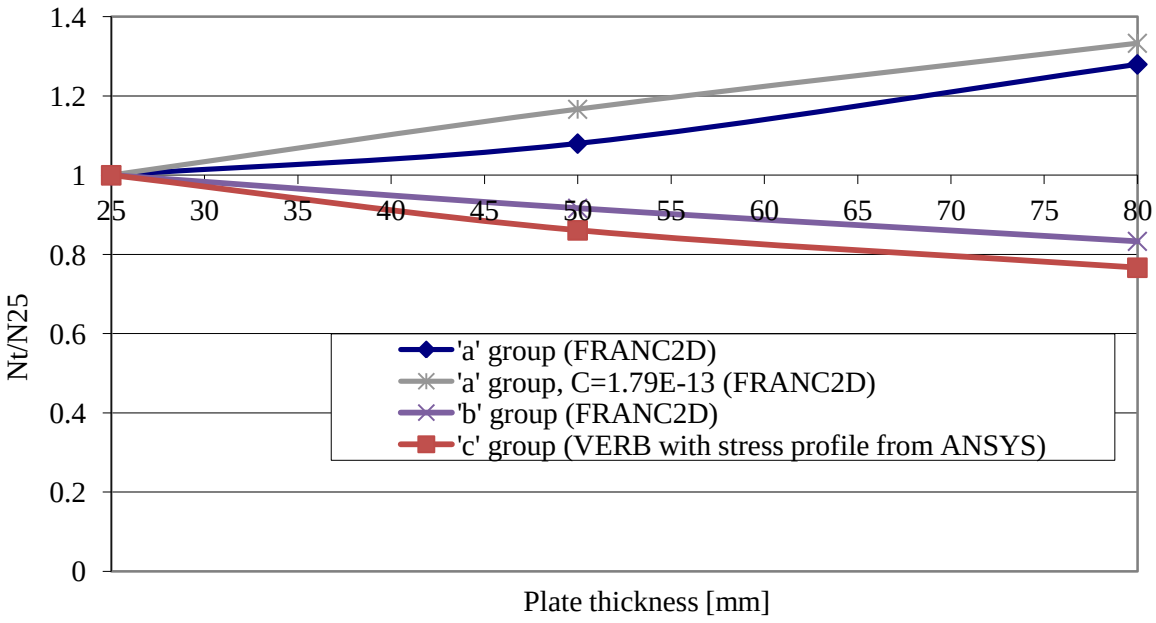

Figure 5.42. Overall results (a_{in}=0.2mm)

5.4 Conclusions

In this part of the study further investigation of the thickness effect on butt weld fatigue strength took place by applying the notch stress approach and fracture mechanics methods. Butt weld specimens of various thicknesses and weld reinforcement geometries were modeled and analyzed by different programs.

The main findings from the notch stress approach investigation were that value of notch stress, as well as the stress distribution, are dependent on the weld geometry and the thickness of the specimen. Specifically, the group ‘a’ of the specimens shows notch stress results opposite to the thickness effect, with the butt weld of 25mm having the higher value compared to the thicker ones (Fig.5.8). The reason for that behavior is that the angle of the toe of the weld is bigger compared to the other ones, creating a sharper notch. Thickness effect could be observed in the other group of specimens (Figs.5.9-5.11).

Moreover, evaluation of the fatigue life of the specimens took place based on recommendation (Fig.5.12), with the result being directly influenced by the notch stress results. The values of exponent n of the Eq.5.4 calculated for group ‘c’ of specimens (Table 5.4.) matched very well with the values from literature, which can be explained by the fact that the specific specimens have an average weld profile same as the one recommended for notch stress calculations.

Regarding the fracture mechanics approach, initially a small investigation regarding the calculation of SIF, parameter of great importance for the fracture mechanics approach, took place. The FRANC2D software was used and the results were compared with the ones obtained by empirical formula (Fig.5.24).

Regarding the results obtained by FRANC2D, for the group ‘a’ of specimens the same tendency as before was observed: stress distribution (Fig.5.31) similar to the one obtained from ANSYS leading to longer propagation life times for thicker specimens, opposite to the thickness effect. For cracks with longer initial length the tendency remain the same but the number of cycles decreases, as expected. If parameters C and m of Paris equation take the values previously calculated (Chapter 4), the results follow the same tendency but this time the number of cycles is much higher, leading to less conservative results (Table 5.5). On the other hand, the results for ‘b’ group of specimens show a reduction of the life time for thicker specimens, following the expected thickness effect (Fig.5.36).

For the calculations performed by VERB, when a constant stress range was applied no thickness effect could be observed (Fig.5.40), while on the contrary, when the stress profile obtained by ANSYS calculations for ‘c’ group was used, the reduction on the life time for thicker specimens was obvious.

Commenting on the overall results obtained from the two approaches (Figures 5.12 and 5.42), it could be stated that there is a matching between them, with the geometry of the reinforcement proven to be of great importance. Group ‘a’ for both approaches fail to show the expected decrease of life time with increasing thickness of the plates, which is not the case for group ‘b’ and ‘c’.

6 OVERALL CONCLUSIONS AND SUGGESTIONS FOR FURTHER INVESTIGATION

This work consists of three main parts: the first part describes the evaluation of fatigue tests of butt welds carried out by Germanischer Lloyd together with a well known steel mill and several shipyards. In the second part it is presented an investigation regarding the parameters C and m of Paris crack growth equation, based on fatigue tests again carried out by Germanischer Lloyd. And finally in the third part a deeper investigation of the thickness effect takes place by means of notch stress and fracture mechanics approach.

The objective was the fatigue performance of butt welds made of the higher tensile steel YP47 to be examined, and especially the thickness effect. The motivation of the specific study derived by the fact that the trend to increase the size of container ships leads to a coincidence of big plate thicknesses, higher tensile strength steels, high cyclic loads and welded joints, hence an enhanced fatigue assessment is essential for a safe and successful application of components characterized by this coincidence.

In the first part the evaluation was based on statistical assessments given in the relevant guidelines. The misalignments were examined and it was found that they lie into the accepted limits; therefore no further consideration was given. The fatigue performance of the material YP47 was proved to be good, since very few of the specimens failed below the relevant design S – N curve. Moreover, when the results are compared to the ones from former project (Doerk O., Fricke W., H. von Selle, Kahl A., 2012), it can be verified that generally there is a similar behavior between the two series of experiments and a knuckle in the order of the results at around $2 \cdot 10^6$ cycles can be also observed.

On the other hand, there is no clear picture of thickness effect. More specifically, it can be commented that the 25mm series indeed show the best performance, while the 50mm series show unexpectedly good behavior which probably can be explained by the quality of the manufacture, as shown by the measurement of the misalignments previously. The 60mm series shows a bad behavior with some specimens not even reaching the appropriate FAT class. Finally, the 80mm series show a rather normal performance.

Regarding the second part, the overall obtained value for the C parameter from the evaluation of all the specimens (C=5.65E-09) is smaller than the one recommended from the literature (1.65E-08). This leads to less conservative results. Nevertheless, it can be possibly explained

by the fact that the recommended value is about mild steel so it may indicates an impact of the yield strength to the crack propagation phase of the fatigue life of the plate.

In the last part the notch stress approach investigation revealed the great dependency of the value of the notch stress, as well as the stress distribution through the thickness, on the geometry of the weld. For this cause, different geometries of the weld reinforcement were modelled (Table 5.1). Specifically, the first group (a) of models had weld shapes directly and randomly taken from the actual specimens of the fatigue tests performed by Germanischer Lloyd. In the second group (b) the notch of the weld raises proportionally to the thickness so for thicker specimens the notch is sharper. In the third group (c) the weld geometry is exactly the same for all specimens and in the last group (d) the geometries of the welds are similar to the ones of the first group but now undercut of a radius of 1mm is introduced so for the Notch effect to be clearly demonstrated, according to the recommendations

Some specimens (group 'a') failed to show the expected thickness effect because of particularities in the geometry of the notch. Specifically, for the specimens that the toe angle was increasing for thinner specimens, the notch stresses showed opposite to the expected tendency. This can be a possible explanation for the non-clear plate thickness effect on the results of the first part, since the specimens of this group were directly modeled from the actual specimens of the tests. On the other hand, the thickness effect could be observed in the other group of specimens. The value of the exponent n was evaluated and compared to the recommendations and for specific group ('c') matched perfectly.

Regarding the fracture mechanics approach, initially a small investigation regarding the calculation of SIF, parameter of great importance for the fracture mechanics approach, took place. The FRANC2D software was used and the results were validated by an empirical formula. Moreover, the stress distribution findings were matching the results obtained by the notch stress approach. For the group 'a' longer propagation life times for thicker specimens, opposite to the thickness effect, were observed. For cracks with longer initial length the tendency remain the same but the number of cycles decreases, as expected. When the parameters C and m of Paris equation use the values found in the second part, the results follow the same tendency but this time the number of cycles is much higher, leading to less conservative results. On the other hand, the results for 'b' group of specimens show a reduction of the life time for thicker specimens, following the expected thickness effect.

Finally, for the calculations performed by VERB, when a constant stress range was applied no thickness effect could be observed since there is no notch effect, while on the contrary, when

the stress profile obtained by ANSYS calculations for ‘c’ group was used, the reduction on the life time for thicker specimens was obvious.

This work’s main objective was the investigation of the fatigue performance of butt welds made of the YP47 steel and it was achieved, since an overall study regarding this topic took place. Evaluation of experimental results, fracture mechanics methods and notch stress investigation; all these different approaches, linked to each other, were covered and useful conclusions were conducted.

Nevertheless, further work is recommended to be carried out. Regarding the evaluation of the experimental results, misalignments can be further considered and so their impact on the results can be fully examined. Moreover, further tests are recommended to be carried out since the main aim of supporting the initial project with increased data base was not achieved due to the absence of thickness effect.

Additionally, the investigation of parameters C and m of Paris equation showed a significant difference between obtained values and the ones given in guidelines. Evaluation of more experimental results could possibly lead to an update of the existing recommended values.

Regarding the fracture mechanics approach, recommendations for future works include the studying of the impact of the residual stresses in the SIFs, the application of more advanced formulas for the prediction of life time than Paris equation such as the Bilinear Law or NASGRO, the studying of the impact of environmental parameters such as temperature or corrosion effects and the studying of different location of crack initiation such as the root of the weld.

Finally, similar investigation can be carried out for components made of different materials (different steel alloys, titanium alloys etc) or even different weld type such as cruciform fillet welded joints.

7 REFERENCES

- Al–Mukhart A.M., The safety analysis concept of welded components under cyclic loads using fracture mechanics, 2010
- Alam M.S., Structural Integrity and Fatigue Crack Propagation Life Assessment of Welded and Weld-Repaired Structures, Ph.D. Dissertation, Louisiana State University, USA, 2005.
- Amrane, A., Fatigue Assessment of Ship Structures, Presentation, University of Liege, 2012
- Anthes R.J., Köttgen B., Seeger T., Stress Concentration Factors for Butt and Cruciform Joints, 1993
- ASM International, Elements of Metallurgy and Engineering Alloys, Chapter 14, ASM International, Materials Park, Ohio, USA, 2008
- Blondeau R., Metallurgy and Mechanics of Welding, ISTE Ltd, 2008.
- British Standards Institution, Guidance on Methods for the Acceptance of Flaws in Structure, PD 6493, BS 7910, Appendix J, 2005.
- Broek D., Some Considerations on Slow Crack Growth, International Journal of Fracture, Vol. 4, No. 1, 1968.
- Doerk, O. and Roerup, J.: Development of Toughness and Quality Requirements for YP47 Steel Welds Based on Fracture Mechanics, Proceedings of the 19th International Offshore and Polar Engineering Conference (ISOPE), Osaka, 2009.
- Doerk O., Fricke W., H. von Selle, Kahl A., Validation of Different Fatigue Assessment Approaches for Thick Plate Structures Made of High Tensile Strength Steel YP47, International Institute of Welding, IIW Doc. XIII-2421-12, 2012.
- Erdogan F. and Sih G.C., ASME J. Basic Eng., Vol. 85, pp. 519–527, 1963
- Fett, T., Munz, D., Stress Intensity Factors and Weight Functions, Computational Mechanics Publications, Southampton UK, Boston USA, 1997
- Fricke, W. (Editor): Guideline for the Fatigue Assessment by Notch Stress Analysis for Welded Structures, International Institute of Welding, IIW Doc. XIII-2240r1-08/XV-1289r1-08, 2008.
- Fricke, W., Petershagen, H. and Paetzold, H., Fatigue Strength of Ship Structures, 1997

- Germanischer Lloyd, Rules and Regulations, I – Ship Technology, Part 1: Seagoing Ships, Chapter 1 – Hull Structures, Hamburg, 2013
- Hobbacher A. (Editor): Recommendations for Fatigue Design of Welded joints and Components, International Institute of Welding, IIW Doc. XIII-2151r4-07/XV-1254r4-07, Paris, France, December 2008.
- Lindqvist J., Fatigue Strengths Thickness Dependence in Welded Construction, M.Sc. Thesis, Borlänge, Sweden, 2002
- Meyers M.A. and Chawla K.K., Mechanical Metallurgy—Principles and Applications, Prentice-Hall Inc., 1984
- Newman, J.C.Jr., Raju, I.S., Stress-intensity factor equations for cracks in three dimensional finite bodies subjected to tension and bending loads, NASA Technical Memorandum 85793, Lengley Research Center, Hampton, VA, 1984
- Niemi, E. 1995, Recommendations concerning Stress Determination for Fatigue Analysis of Welded Components
- Nguyen N.T., Wahab M.A., The Effect of Residual Stresses and Weld Geometry on the Improvement of Fatigue Life, Journal of Materials Processing Technology, Vol. 48, pp. 581–588, 1995.
- Nykänen T., X. Li, Björk T. and Marquis G., A Parametric Fracture Mechanics Study of Welded Joints with Toe Cracks, Engineering Fracture Mechanics, Vol. 72, No. 10, pp. 1580–1609, 2005.
- Radaj, D., Design and Analysis of Fatigue – Resistant Welded Structures. Abington Publishing, Cambridge (UK), 1990
- Radaj D., Sonsino C.M., Fricke W., Fatigue Assessment of Welded Joints by Local Approaches, Woodhead Publishing Ltd, 2006
- Radaj D., Vormwald M., Advanced methods of fatigue assessment, 201310.1007/978-3-642-30740-9, Springer, 2013
- Rigo, P. and Rizzuto, E., Analysis and Design of Ship Structure, Chapter 18 of Ship design and construction, Society of Naval Architects and Marine Engineers, 2003-2004

- von Selle H., Doerk O., Kang J.K. and Kim J.H., Fatigue tests of butt welds and plates edges of 80 mm thick plates, Advances in Marine Structures p:511-519, 978-0-415-67771-4, Taylor & Francis Group, London, 2011
- Shukla A., Practical Fracture Mechanics in Design, 2nd edition, Taylor and Francis, Group, LLC, 2008.
- Smith I.F.C. and Smith R.A., Fatigue Crack Growth in a Fillet Welded Joints, Engineering Fracture Mechanics, Vol. 18, No. 4, pp. 861-869, 1983.
- Wawrzynek P. and Ingraffea A., FRANC2D: A Two-Dimensional Crack Propagation Simulator, Version 3.1 User's Guide, 1993.

APPENDIX A – DETAILED RESULTS OF CRACK PROPAGATION FROM CHAPTER 4

Specimen u1

Table A.1. Geometry of the crack and number of cycles during the propagation for specimen u1

beachmark	crack depth a [mm]	crack length c [mm]	Ntot	N
initial	12	20	0	-
1	24	31	33500	33500
2	36	43	45000	11500
3	48	50	50000	5000

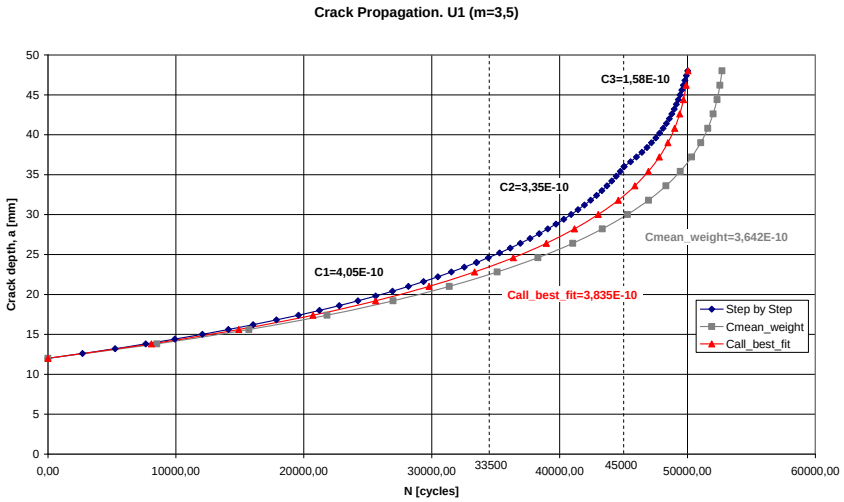

Figure A. 1. Crack propagation for specimen u1 (m=3.5)

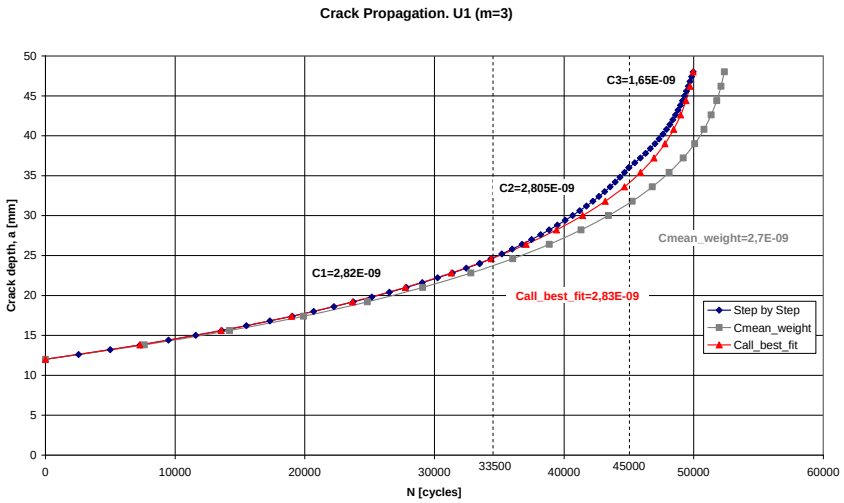

Figure A. 2. Crack propagation for specimen u1 (m=3.00)

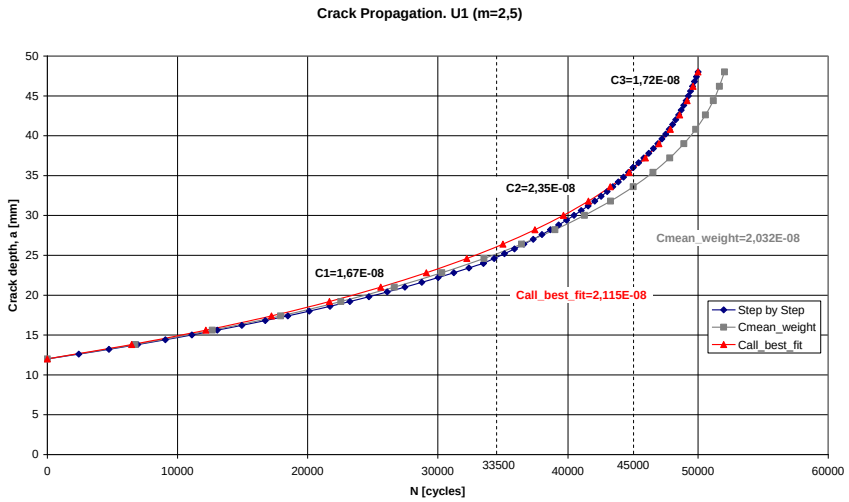

Figure A. 3. Crack propagation for specimen u1 (m=2.50)

Specimen u2 (left crack)

Table A. 2. Geometry of the crack and number of cycles during the propagation for specimen u2

beachmark	crack depth a [mm]	crack length c [mm]	Ntot	N
initial	5	20	0	-
1	28	38.5	44800	44800
2	37	51.5	54500	9700

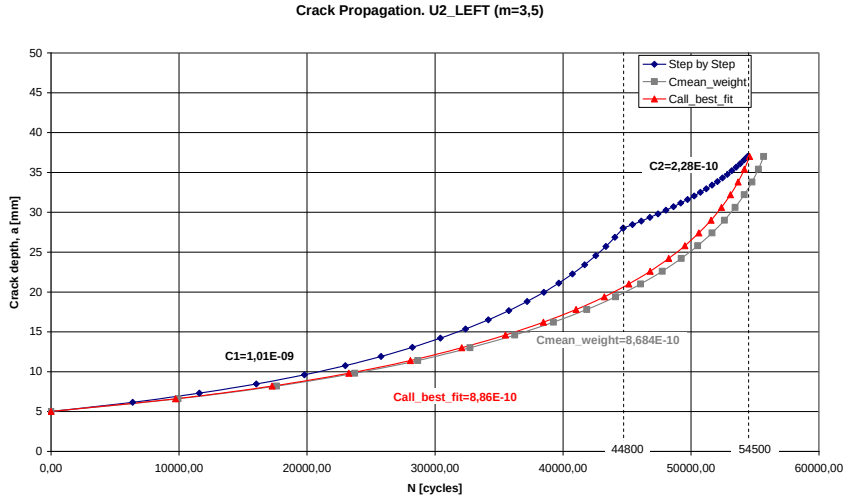

Figure A. 4. Crack propagation for specimen u1 (m=3.50)

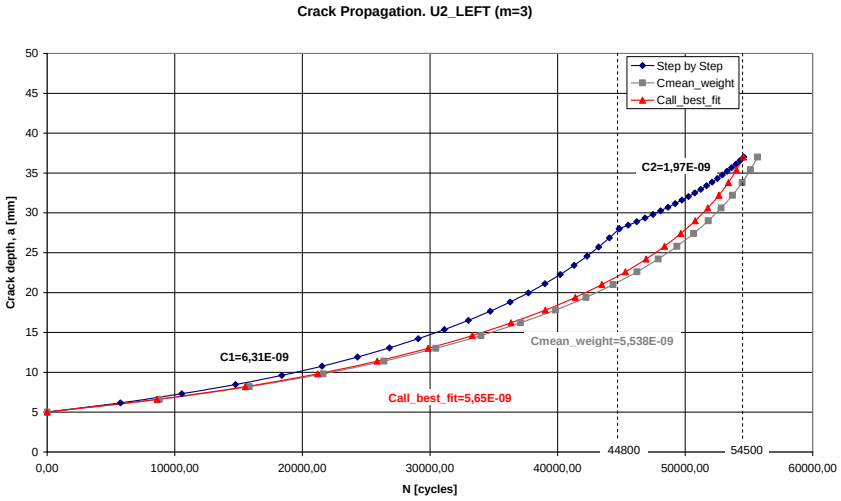

Figure A. 5. Crack propagation for specimen u1 (m=3.00)

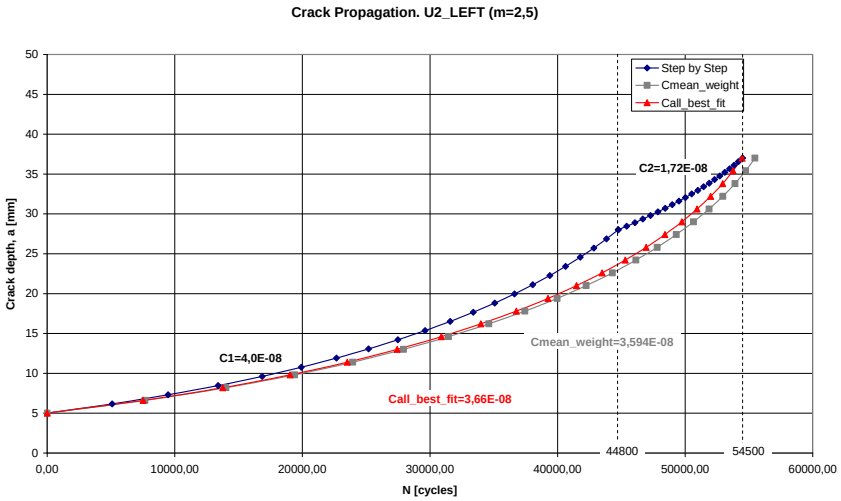

Figure A. 6. Crack propagation for specimen u1 (m=2.50)

Specimen u3

Table A. 3. Geometry of the crack and number of cycles during the propagation for specimen u3

beachmark	crack depth a [mm]	crack length c [mm]	Ntot	N
initial	4-8	29	0	-
1	13-15	36	25400	25400
2	20-22	44	39000	13600
3	29-31	62	53200	14200
4	40-41	77	59700	6500

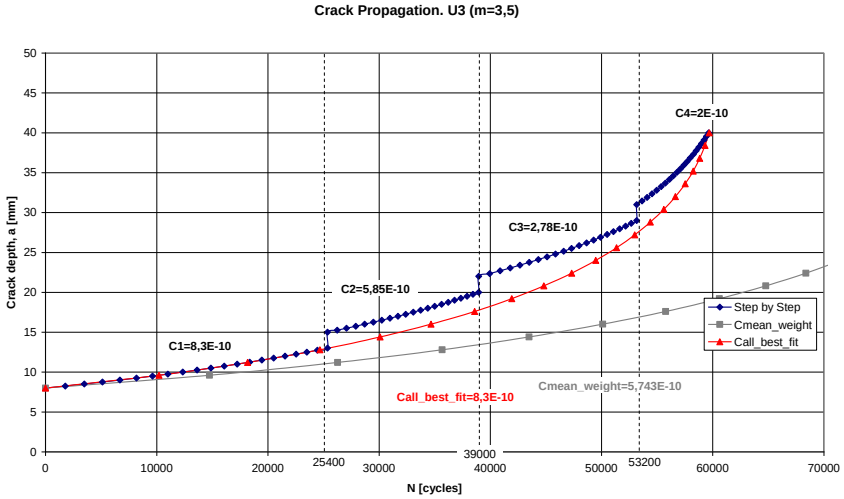

Figure A. 7. Crack propagation for specimen u3 (m=3.50)

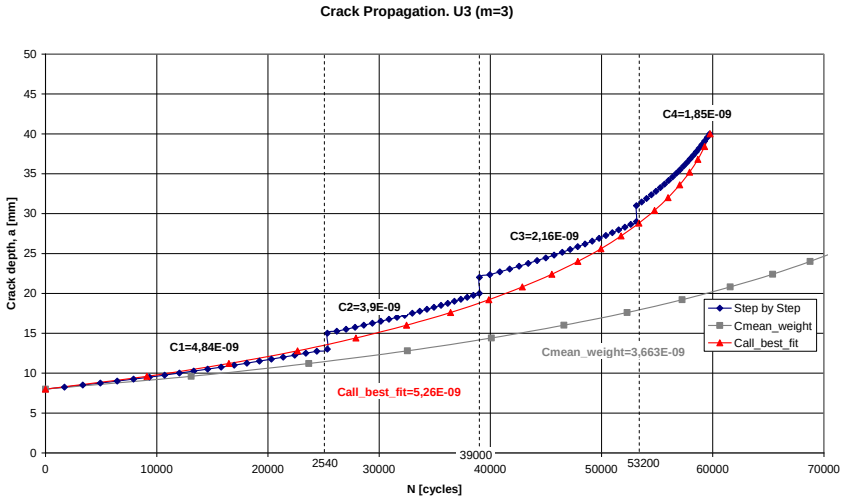

Figure A. 8. Crack propagation for specimen u3 (m=3.00)

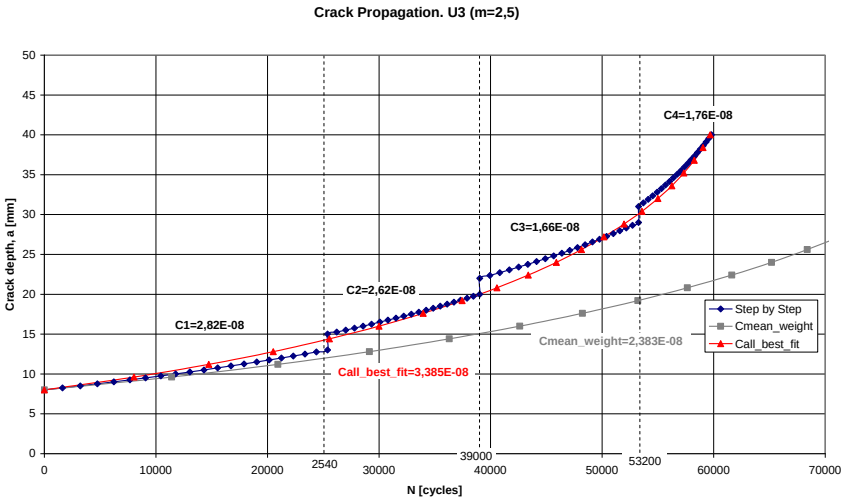

Figure A. 9. Crack propagation for specimen u3 (m=2.50)

Specimen u4

Table A. 4. Geometry of the crack and number of cycles during the propagation for specimen u4

beachmark	crack depth a [mm]	crack length c [mm]	Ntot	N
initial	24.5	39	0	0
1	29.5	43	7600	7600
2	35	46.5	15000	7400
3	42.5	52	23200	8200

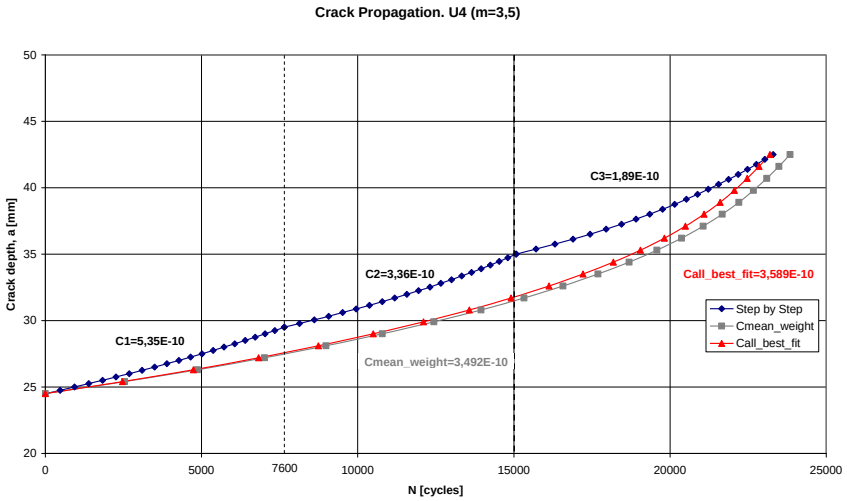

Figure A. 10. Crack propagation for specimen u4 (m=3.50)

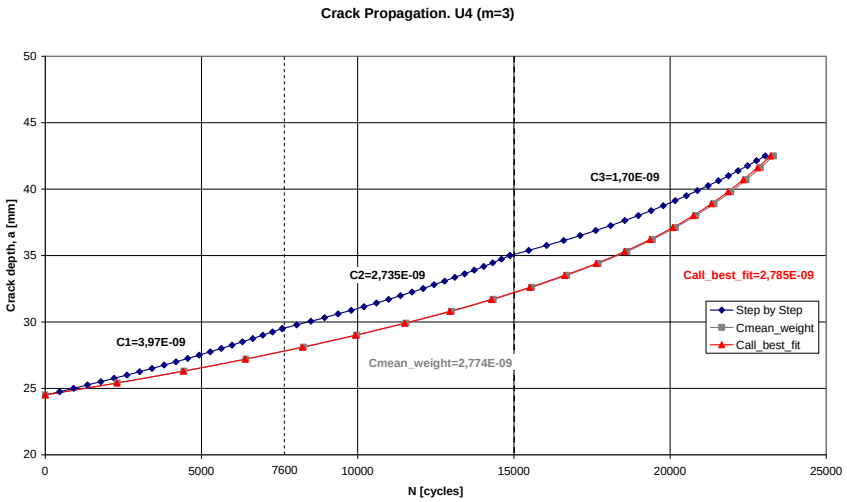

Figure A. 11. Crack propagation for specimen u4 (m=3.00)

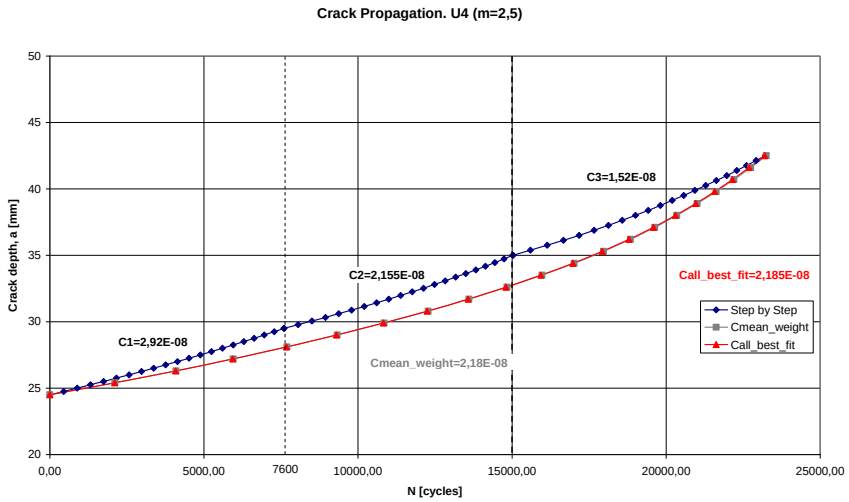

Figure A. 12. Crack propagation for specimen u4 (m=2.50)

Specimen u5

Table A. 5. Geometry of the crack and number of cycles during the propagation for specimen u5

beachmark	crack depth a [mm]	crack length c [mm]	Ntot	N
initial	10	23	0	0
1	13.5	27	12600	12600
2	17	29	19100	6500
3	23,5-24,5	32-32,5	28400	9300
4	30-31	34-35	35900	7500
5	46	54.5	45900	10000

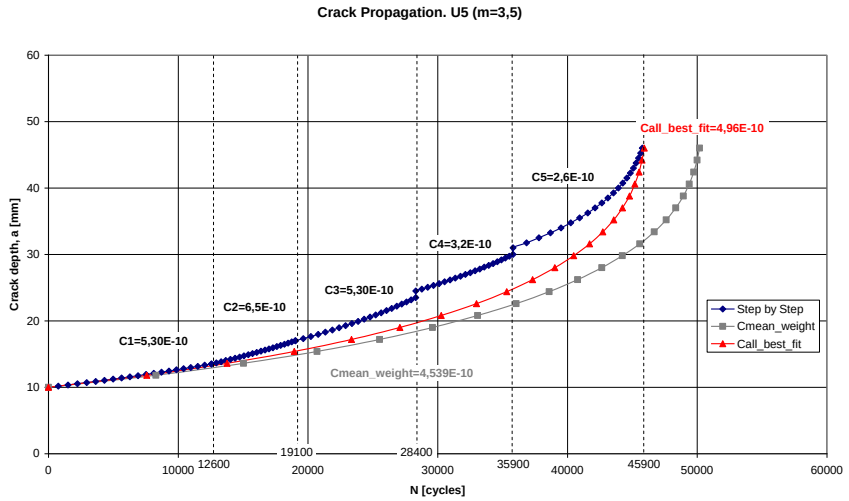

Figure A. 13. Crack propagation for specimen u5 (m=3.50)

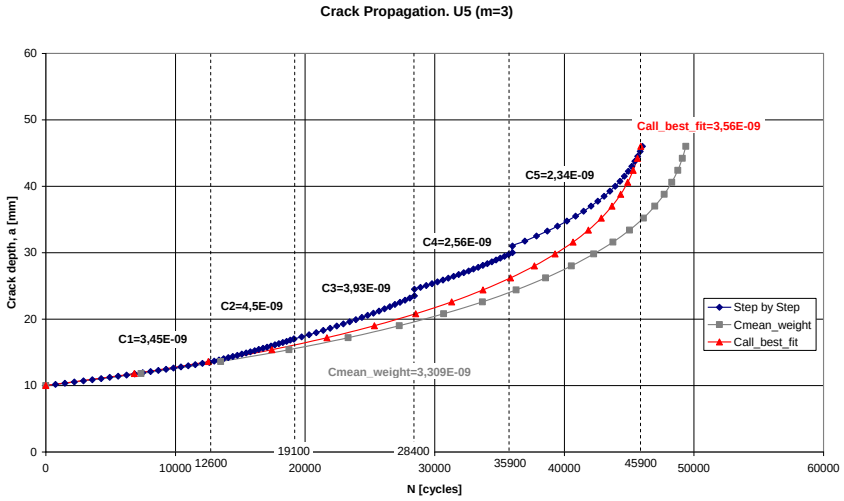

Figure A. 14. Crack propagation for specimen u5 (m=3.00)

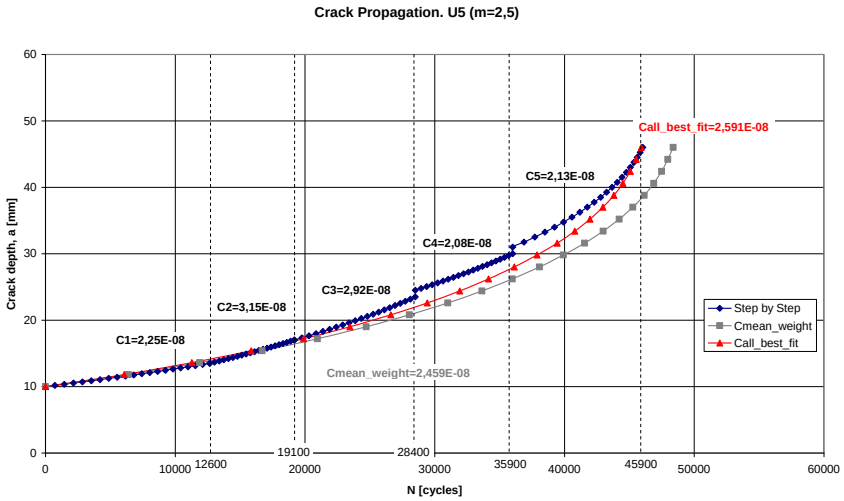

Figure A. 15. propagation for specimen u5 (m=2.50)

Specimen u8

Table A. 6. Geometry of the crack and number of cycles during the propagation for specimen u8

beachmark	crack depth a [mm]	crack length c [mm]	Ntot	N
initial	14	22	0	
1	21	27	24900	24900
2	39	42	50500	25600

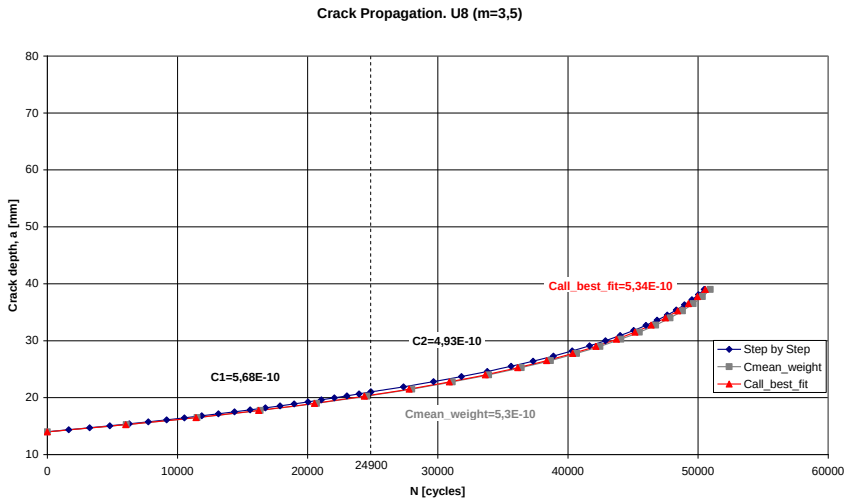

Figure A. 16. Crack propagation for specimen u8 (m=3.50)

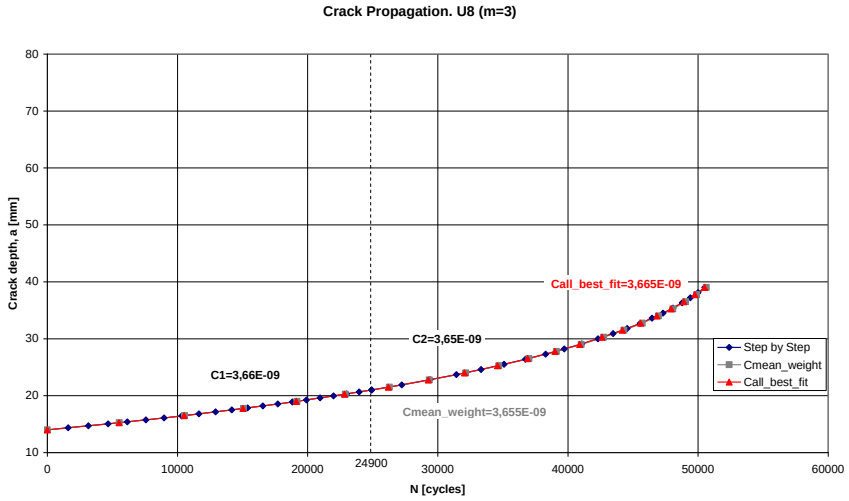

Figure A. 17. Crack propagation for specimen u8 (m=3.00)

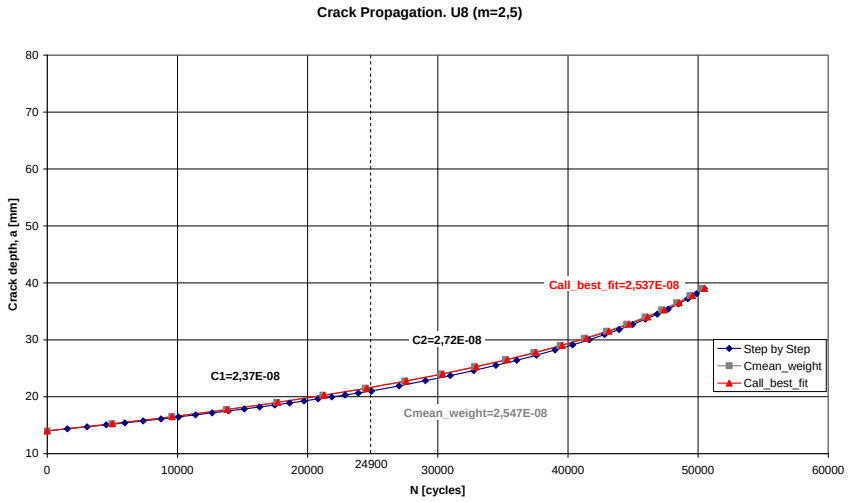

Figure A. 18. Crack propagation for specimen u8 (m=2.50)

Specimen up1

Table A. 7. Geometry of the crack and number of cycles during the propagation for specimen up1

beachmark	crack depth a [mm]	crack length c [mm]	Ntot	N
initial	30-34	43-45	0	-
1	39-41	50	3300	3300
2	47,5-52	56-60	6900	3600

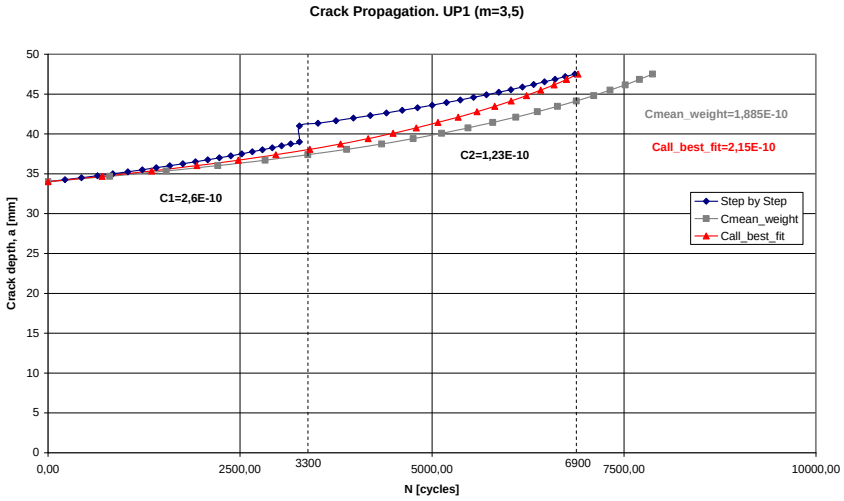

Figure A. 19. Crack propagation for specimen up1 (m=3.50)

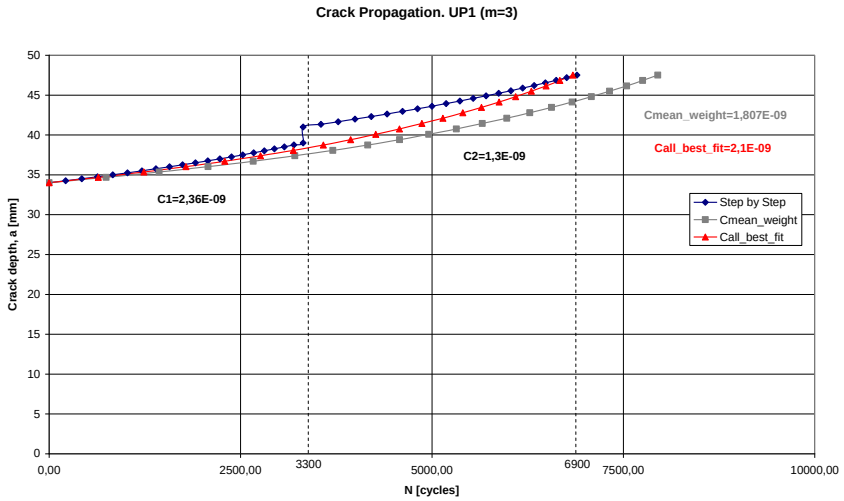

Figure A. 20. Crack propagation for specimen up1 (m=3.00)

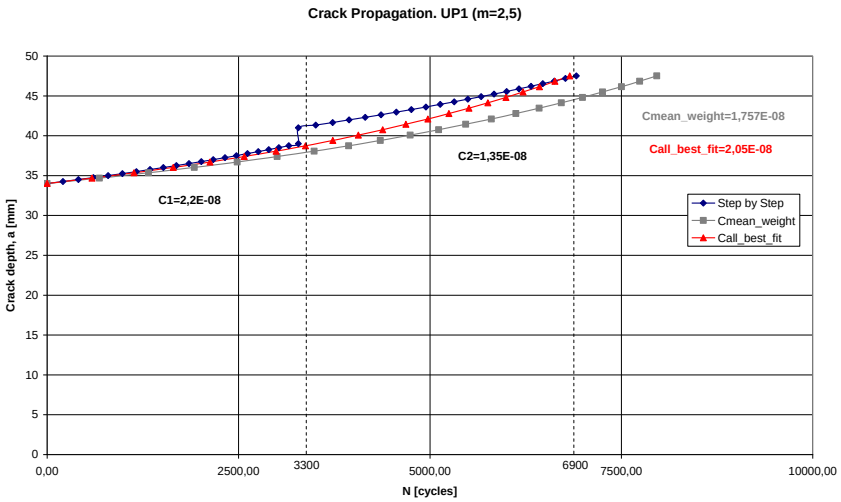

Figure A. 21. Crack propagation for specimen up1 (m=2.50)

Specimen up2

Table A. 8. Geometry of the crack and number of cycles during the propagation for specimen up2

beachmark	crack depth a [mm]	crack length c [mm]	Ntot	N
initial	11	18	0	-
1	16	21	8600	8600
2	19	27	15100	6500
3	25	33	22700	7600
4	32	41	28600	5900
5	40	48	32500	3900

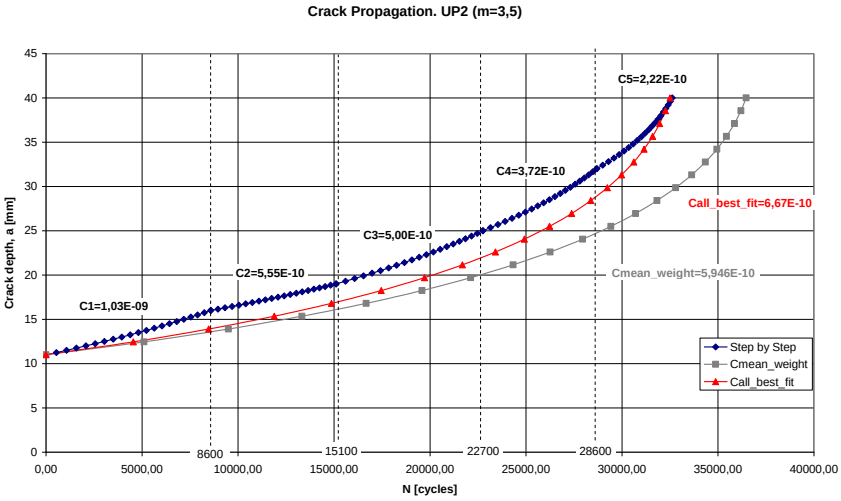

Figure A. 22. Crack propagation for specimen up2 (m=3.50)

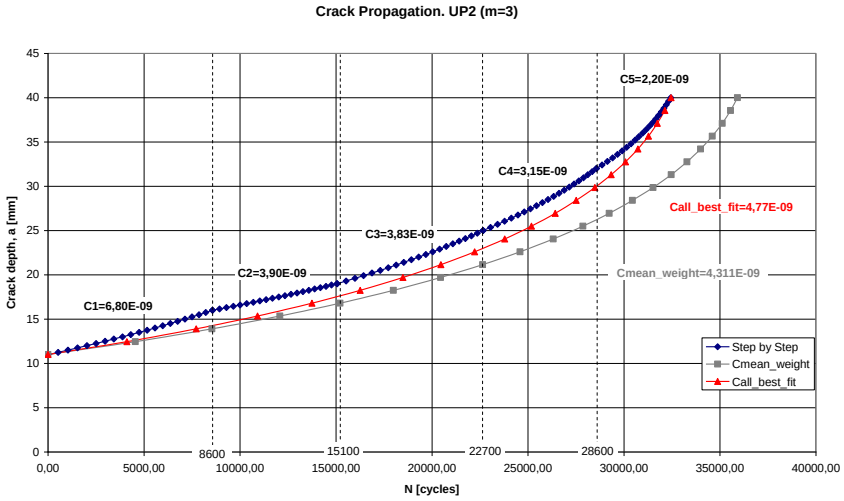

Figure A. 23. Crack propagation for specimen up2 (m=3.00)

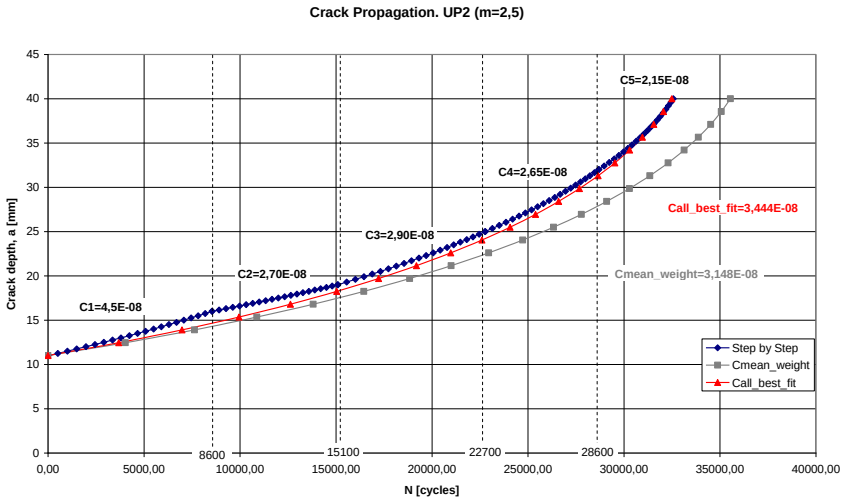

Figure A. 24. propagation for specimen up2 (m=2.50)

Specimen up3

Table A. 9. Geometry of the crack and number of cycles during the propagation for specimen up3

beachmark	crack depth a [mm]	crack length c [mm]	Ntot	N
initial	31	39	0	
1	34-37	42-44	4700	4700
2	41-43	47-49	8100	3400
3	50-53	55-57	12000	3900

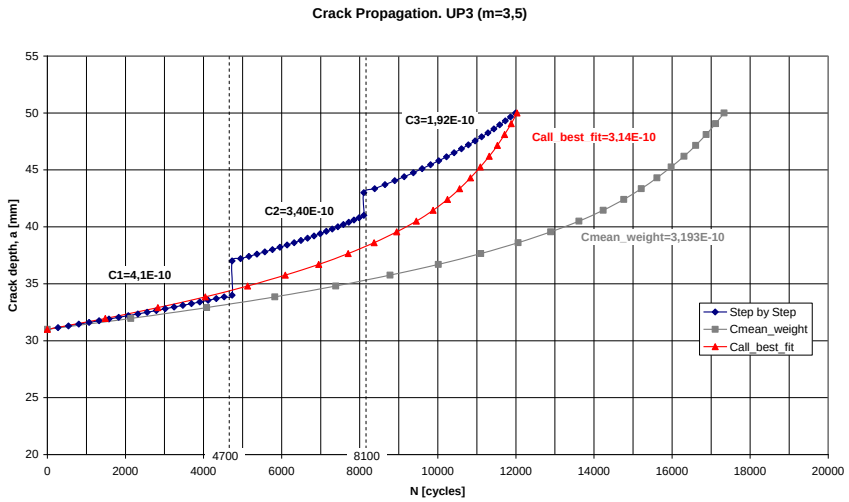

Figure A. 25. Crack propagation for specimen up3 (m=3.50)

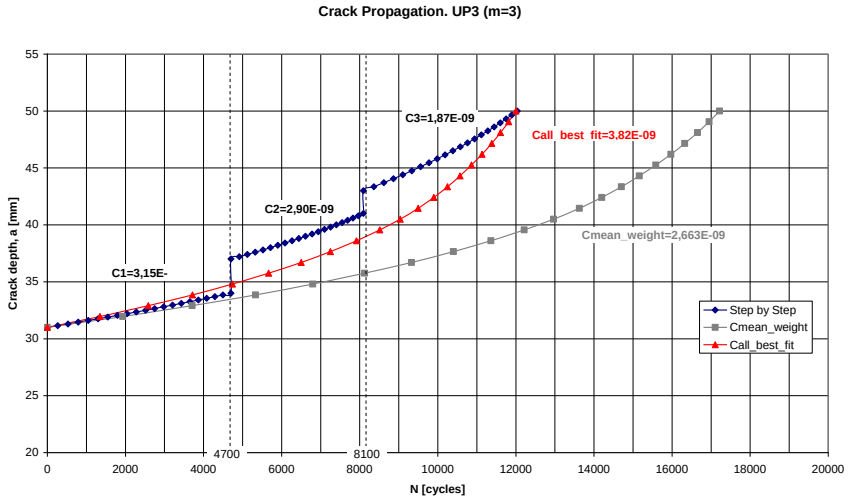

Figure A. 26. Crack propagation for specimen up3 (m=3.00)

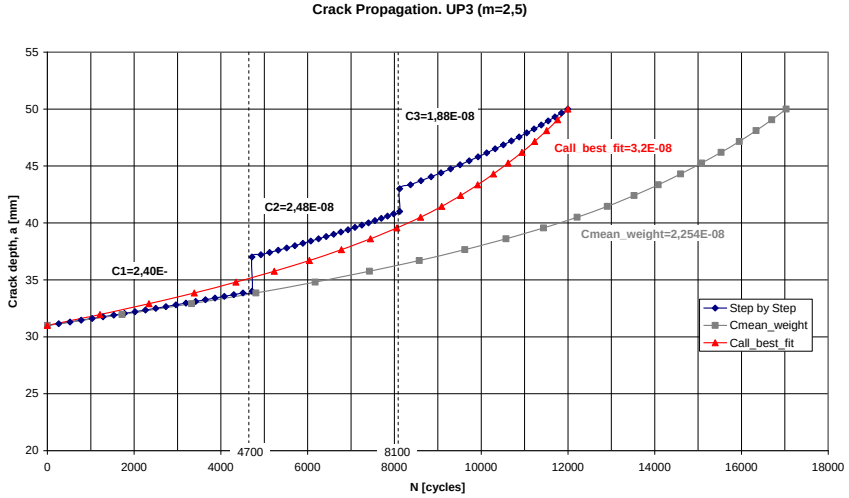

Figure A. 27. Crack propagation for specimen up3 (m=2.50)

Specimen up5

Table A. 10. Geometry of the crack and number of cycles during the propagation for specimen up3

beachmark	half crack depth a [mm]	half crack length c [mm]	ligament d [mm]	N
initial	2.25	21	22	
final	25-27,5	28	0	352800

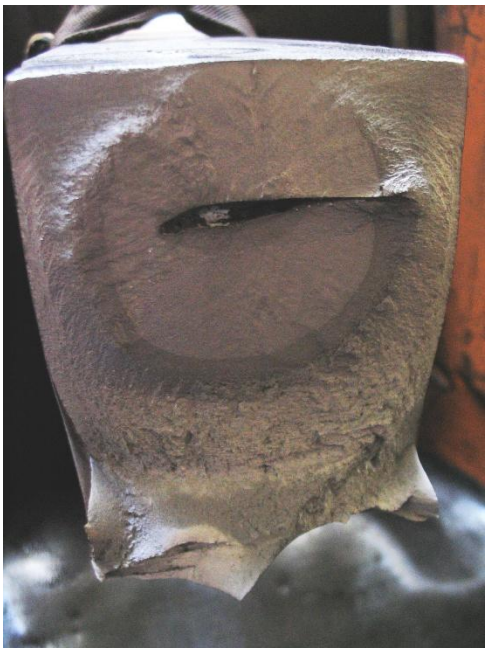

Figure A. 28. Fatigue crack surface of specimen up5 (elliptical embedded crack)

PPENDIX B – SOLUTION METHODS USED BY VERB

Plate with Quarter Elliptical Corner Crack

For the specific model the software uses the following empirical method to calculate the stress intensity factor, based on finite-element calculations (Newman, Raju, 1984):

$$K = (\sigma_m F_m + \sigma_b F_b)\sqrt{\frac{\pi a}{Q}}$$

$$F_m = \left[M_1 + M_2\left(\frac{a}{t}\right)^2 + M_3\left(\frac{a}{t}\right)^4\right] g_1 g_2 f_\varphi f_w$$

$$F_b = F_m[H_1 + (H_2 - H_1)sin^p\varphi] \qquad \text{(B-1)}$$

$$f_w = 1 - 0.2\lambda + 9.4\lambda^2 - 19.4\lambda^3 + 27.1\lambda^4, \lambda = \frac{c}{W}\sqrt{\frac{a}{t}}$$

At $a/c \leq 1$:

$$M_1 = 1.08 - 0.03\frac{a}{c}, M_2 = -0.44 + \frac{1.06}{0.3 + \frac{a}{c}}, M_3 = -0.5 + 0.25\frac{a}{c} + 14.8\left(1 - \frac{a}{c}\right)^{15}$$

$$g_1 = 1 + \left[0.08 + 0.4\left(\frac{a}{t}\right)^2\right](1 - sin\varphi)^3, g_2 = 1 + \left[0.08 + 0.15\left(\frac{a}{t}\right)^2\right](1 - cos\varphi)^3$$

$$Q = 1 + 1.464\left(\frac{a}{c}\right)^{1.65}, f_\varphi = \left(sin^2\varphi + \frac{a^2}{c^2}cos^2\varphi\right)^{1/4}$$

$$p = 0.2 + \frac{a}{c} + 0.6\frac{a}{t}$$

$$H_1 = 1 - 0.34\frac{a}{t} - 0.11\frac{a}{c}\frac{a}{t}$$

$$H_2 = 1 + \left(-1.22 - 0.12\frac{a}{c}\right)\frac{a}{t} + \left[0.64 - 1.05\left(\frac{a}{c}\right)^{0.75} + 0.47\left(\frac{a}{c}\right)^{1.5}\right]\left(\frac{a}{t}\right)^2$$

At $a/c > 1$:

$$M_1 = \sqrt{\frac{c}{a}}\left(1.08 - 0.03\frac{c}{a}\right), M_2 = 0.375\left(\frac{c}{a}\right)^2, M_3 = -0.25\left(\frac{c}{a}\right)^2$$

$$g_1 = 1 + \left[0.08 + 0.4\left(\frac{c}{a}\right)^2\left(\frac{a}{t}\right)^2\right](1 - sin\varphi)^3,$$

$$g_2 = 1 + \left[0.08 + 0.15\left(\frac{c}{a}\right)^2\left(\frac{a}{t}\right)^2\right](1 - cos\varphi)^3$$

$$Q = 1 + 1.464\left(\frac{c}{a}\right)^{1.65}, f_\varphi = \left(cos^2\varphi + \frac{c^2}{a^2}sin^2\varphi\right)^{1/4}$$

$$p = 0.2 + \frac{c}{a} + 0.6\frac{a}{t}$$

$$H_1 = 1 + \left(-0.04 - 0.41\frac{c}{a}\right)\frac{a}{t} + \left[0.55 - 1.93\left(\frac{c}{a}\right)^{0.75} + 1.38\left(\frac{c}{a}\right)^{1.5}\right]\left(\frac{a}{t}\right)^2$$

$$H_2 = 1 + \left(-2.11 - 0.77\frac{c}{a}\right)\frac{a}{t} + \left[0.64 - 0.72\left(\frac{c}{a}\right)^{0.75} + 0.14\left(\frac{c}{a}\right)^{1.5}\right]\left(\frac{a}{t}\right)^2$$

With:

K	linear-elastic stress intensity factor
σ_m/σ_b	membrane/bending stress
φ	parametric angle specifying location on the crack front
c/a	crack length/depth
t	thickness of the plate

Plate with Extended Surface Crack

The solution method used is the following weight function (Fett, T., Munz, D., 1997):

$$K = \int_0^a \sigma(x)h(x,a)dx$$

$$h = \sqrt{\frac{2}{\pi a}}\left(1 - \frac{x}{a}\right)^{-\frac{1}{2}}\left[1 + \sum_{n=0}^{2}\sum_{m=0}^{4} \frac{A_{nm}\xi^m}{(1-\xi)^{3/2}}\left(1 - \frac{x}{a}\right)^{n+1}\right] \qquad \text{(B-2)}$$

$$\xi = \frac{a}{t}$$

The coefficients A_{mn} are listed in the following table:

Table B 1. Approximating coefficients A_{mn} in the weight function

	$m = 0$	$m = 1$	$m = 2$	$m = 3$	$m = 4$
$n = 0$	0.4980	2.4463	0.0700	1.3187	-3.0670
$n = 1$	0.5416	-5.0806	24.3447	-32.7208	18.1214
$n = 2$	-0.19277	2.55863	-12.6415	19.7630	-10.9860